
Advanced State Transition Matrices

Computation Algorithms

Trabajo Fin de Máster

Máster Universitario en Ingeniería Aeronáutica

Escuela Técnica Superior de Ingeniería

Aeronáutica y del Espacio

Universidad Politécnica de Madrid



Autor: Rodrigo Fernández Matilla

Tutor profesional: Víctor Manuel Moreno Villa

Tutor académico: Manuel Pérez Cortés

Septiembre 2022

Contents

Nomenclature	vii
1 Relative dynamics around a near-circular unperturbed reference orbit.	1
1.1 Introduction.	1
1.2 Motion model: Hill equations.	1
1.2.1 Equations of motion of a spacecraft.	1
1.2.2 Forces in the spacecraft motion problem.	2
1.2.3 Two-body problem.	3
1.2.4 Three-body problem.	5
1.2.5 Differential equations of proximity relative motion.	5
1.2.6 Hill equations.	7
1.3 Solutions of Hill equations.	8
1.3.1 Direct numerical integration.	9
1.3.2 Clohessy-Wiltshire solution and STM.	9
1.3.3 State transition matrix propagation.	11
1.3.4 Jordan canonical decomposition.	12
1.3.5 Results: Comparison against High-Fidelity.	18
1.4 Orbit safety in near-circular orbits.	23
1.4.1 Orbit safety concept.	23
1.4.2 Eccentricity-inclination vector separation strategy.	24
2 Relative dynamics around elliptic reference orbits.	33
2.1 Introduction.	33
2.2 Motion model and STM.	34
2.2.1 Simplification of equations of motion: YA solution.	34
2.2.2 YA STM and integration constants.	37
2.2.3 Results: Comparison with HCW and Hi-Fi propagation.	41
2.3 Orbit safety in eccentric, unperturbed orbits.	47
2.3.1 Relative motion description in TAN frame.	47
2.3.2 General trajectories and safe orbits.	49

A Absolute and relative orbital element sets.	55
A.1 Introduction	55
A.2 Absolute element sets	55
A.2.1 Workflow for transformations between absolute element sets.	55
A.2.2 Element sets.	56
A.3 Relative sets.	60
A.3.1 Workflow for transformations between ROEs.	60
A.3.2 Element sets.	63
B Cartesian reference systems.	67
B.1 Introduction	67
B.1.1 Inertial and rotating reference frames.	67
B.1.2 Absolute and relative frames.	67
B.1.3 Time measurement.	67
B.2 Transformations between reference systems.	68
B.2.1 Direct analytical differentiation.	70
B.2.2 Classical motion composition.	71
B.3 Absolute reference systems.	72
B.3.1 Earth-Centered-Inertial reference system (ECI).	72
B.3.2 Earth-Centered, Earth-Fixed reference system (ECEF).	73
B.3.3 Perifocal (PQW) reference frame.	77
B.4 Relative reference systems.	80
B.4.1 RTN reference frame.	80
B.4.2 LVLH reference frame.	82
B.4.3 TAN reference frame.	85
B.5 Conversions from OEs to cartesian coordinates.	86
B.5.1 Keplerian OEs to ECI and vice versa.	86
B.5.2 Relative Keplerian OEs to RTN.	88
Bibliography	91
General	91
Eccentric Dynamics	92
Perturbations	93

MATLAB Exchange libraries	94
-------------------------------------	----

Nomenclature

Physical constants

γ	Coeficiente de dilatación adiabática de un gas	[—]
T_C	Temperatura del punto triple	[K]

Λ	Matriz de autovalores de un sistema de ecuaciones diferenciales
λ_i	Autovalor i -ésimo de la matriz del sistema
A	Matriz del sistema de una ecuación diferencial
$F(\mathbf{U})$	Vector de flujos de una ecuación diferencial
I	Matriz identidad
$K^{(i)}$	Autovector i -ésimo de la matriz del sistema
n	Vector normal exterior a una superficie
R	Vector de términos fuente de una ecuación diferencial
U	Vector de variables dependientes de un sistema de ecuaciones diferenciales
\mathbf{U}	Vector de variables dependientes de una ecuación diferencial
W	Vector de variables dependientes canónicas de un sistema de ecuaciones diferenciales
\mathbb{I}	Unidad imaginaria
$\mathcal{L}(\mathbf{U})$	Operador diferencial espacial de una ecuación diferencial en derivadas parciales
Ω	Volumen geométrico
$\partial\Omega$	Frontera del volumen Ω
ϕ	Superficie característica de una ecuación diferencial en derivadas parciales
Σ	Superficie geométrica

$d\gamma, d\sigma, d\omega$ Diferenciales de arco, superficie y volumen

s Parámetro de longitud de arco

Cartesian coordinates

\bar{u}_i^n Solución exacta de un esquema numérico

$\mathbf{F}_{i+1/2}$ Flujos numéricos en el extremo superior del volumen finito i -ésimo

\mathbf{Q} Vector de parámetros del método de Roe

$\mathbf{U}_{i+1/2}$ Solución computada en el extremo superior del volumen finito i -ésimo

$\Delta x, \Delta t$ Pasos espacial y temporal

ϵ_T Error de truncamiento de un esquema numérico

λ_j Longitud de onda del armónico j -ésimo

ω Relación de dispersión numérica

Ω_i Volumen de control i -ésimo

ϕ_j Fase del armónico j -ésimo

σ Número CFL

$\tilde{\mathbf{A}}$ Matriz promediada del sistema

$\tilde{\lambda}_i$ Autovalor i -ésimo de la matriz promediada del sistema

$\tilde{\omega}$ Relación de dispersión

$\tilde{\mathbf{K}}^{(i)}$ Autovector i -ésimo de la matriz promediada del sistema

\tilde{u}_i^n Solución exacta de un modelo matemático

G_j Factor de amplificación o ganancia del armónico j -ésimo

I_i Centroide del volumen finito i -ésimo

k_j Número de onda del armónico j -ésimo

$N(\bullet)$ Esquema numérico

S	Velocidad de propagación de una discontinuidad
S_{max}^n	Velocidad máxima de propagación de información en un problema de evolución discretizado
u_i^n	Solución computada de un esquema numérico
V_j^n	Amplitud del armónico j -ésimo en el instante n -ésimo
$x_{i+1/2}$	Extremo superior del volumen finito i -ésimo

Characteristic numbers

Fr	Número de Froude	$Fr = \frac{U_c}{\sqrt{g_0 L_c}}$
Nu	Número de Nusselt	$Nu = \frac{h_c L_c}{k}$
Pr	Número de Prandtl	$Pr = \frac{\nu}{\alpha}$
Re	Número de Reynolds	$Re = \frac{\rho_c U_c L_c}{\mu_c}$

Suffixes

∞	Variable en el infinito sin perturbar
c	Característica
d	Gota (<i>droplet</i>)
e	Borde de la capa límite (<i>edge</i>)
f	Película de agua (<i>water film</i>)
w	Agua (<i>water</i>)

Orbital elements

α	Difusividad térmica	$\left[\frac{m^2}{s} \right]$
α_w	Fracción volumétrica de agua en aire	$[- - -]$
\bar{U}	Vector velocidad de un cuerpo o fluido	$\left[\frac{m}{s} \right]$
\bar{u}	Vector velocidad adimensional de un cuerpo o fluido	$[- - -]$

β	Coeficiente de captación	[---]
\dot{m}	Flujo másico	$\left[\frac{kg}{s} \right]$
\dot{m}'	Flujo másico por unidad de área	$\left[\frac{kg}{s} \frac{1}{m^2} \right]$
\dot{Q}	Flujo de calor [W]	
\dot{q}	Flujo de calor por unidad de área	$\left[\frac{W}{m^2} \right]$
μ	Viscosidad dinámica de un fluido	[Pa · s]
ν	Viscosidad cinemática de un fluido	$\left[\frac{m^2}{s} \right]$
τ_{wall}	Esfuerzo viscoso de un fluido sobre una pared	[Pa]
\bar{c}_f	Coeficiente de fricción viscosa sobre una pared	[---]
ρ	Densidad de un fluido	$\left[\frac{kg}{m^3} \right]$
θ	Temperatura absoluta adimensionalizada con la del punto triple	[---]
\tilde{T}	Temperatura	[C]
C_D	Coeficiente de resistencia de un cuerpo	[---]
C_p	Calor específico a presión constante	$\left[\frac{J}{kg K} \right]$
d	Diámetro de las gotas	[μm]
f	Fracción de agua congelada	[---]
h	Espesor de una película de agua	[m]
h_c	Coeficiente de transferencia de calor por convección	$\left[\frac{W}{m^2 K} \right]$
k	Conductividad térmica de un fluido	$\left[\frac{W}{m K} \right]$
L	Calor latente de un fluido	$\left[\frac{J}{kg} \right]$
LWC	Contenido en agua líquida, <i>liquid water content</i>	$\left[\frac{kg}{m^3} \right]$
MVD	Tamaño volumétrico medio de las gotas, <i>median volumetric diameter</i>	[μm]

p	Presión de un fluido	[Pa]
$p_{v,sat}$	Presión de vapor de saturación	[Pa]
r	Factor de recuperación adiabática	[---]
T	Temperatura absoluta	[K]

List of Figures

1.1	Difference in relative distance between HCW methods and Hi-Fi (V-bar approach)	20
1.2	x-z trajectory comparison between STM propagation (HCW) and High-Fidelity	21
1.3	Difference in relative distance between HCW methods and Hi-Fi (R-bar approach)	22
1.4	x-z trajectory comparison between STM propagation (HCW) and High-Fidelity (R-bar approach)	23
1.5	Effect of δr and δu in radial and along-track distances.	25
1.6	Inclination vector and cross-track distance.	27
1.7	Relative motion in RTN frame for $\delta a = 0$ and a general $\delta e - \delta i$ alignment.	30
1.8	Relative motion for parallel and antiparallel $\delta e/\delta i$ vectors.	31
2.1	Workflow of the propagation with YA STM.	42
2.2	Scenario 1($e = 0.1$): Comparison between Hi-Fi, HCW and YA.	44
2.3	Scenario 2 ($e = 0.7$): Comparison between Hi-Fi, HCW and YA.	46
2.4	Safe orbit family: Scenario 1 ($C_1 = 0$).	52
2.5	Safe orbit family: Scenario 2 ($C_1 = C_m$).	52
2.6	Comparison between Peters-Noomen approach and High-Fidelity propagation.	54
A.1	Workflow for transforming between two arbitrary absolute element sets.	56
A.2	Frame rotation from inertial to perifocal frame.	57
A.3	Workflow for transforming any relative set into KOE.	62
A.4	Workflow for transforming RKOE into any other set.	63
A.5	Relative eccentricity & inclination vectors.	64
B.1	Sketch of the different time systems.	68
B.2	Absolute and relative frames.	69
B.3	ECI and ECEF reference frames.	74
B.4	Nutation and precession motion.	75
B.5	RTN frame [18].	81
B.6	Relative reference frames.	85

List of Tables

1.1	Testing scenarios for Hill equations validation [6].	19
1.2	Elapsed time for the computation of V-bar scenario through each HCW method.	21
1.3	Elapsed time for the computation of R-bar scenario through each HCW method.	23
2.1	Testing scenarios for YA STM [15].	42
2.2	Correspondence between QNS and C ROEs.	48
2.3	Parameters of an orbit family.	50
2.4	Testing scenarios for safe orbit implementation [16].	51

Relative dynamics around a near-circular unperturbed reference orbit.

1.1 Introduction.

Relative dynamics can involve different degrees of complexity, which depends basically on the considered model and the scenario to simulate. During this thesis, the approach will be to incrementally increase this complexity, starting from the simplest, less accurate models all the way to the more convoluted, realistic ones.

In this case, the least complicated scenario is the near-circular unperturbed reference orbit. This simplifies greatly the mathematical involvement, as it (a) neglects any perturbation and (b) yields a chief spacecraft with a constant velocity and orbital radius. It makes sense then that this was the first relative dynamics model ever created and hence used for rendez-vous and formation flying operations.

This chapter firstly focuses on the derivation of the linearized Hill equations, going from the most general form of the equations of motion of a spacecraft. Afterwards, some implementations of said equations are analyzed and compared with a High-Fidelity propagation. Lastly, the concept of orbit safety will be introduced, and safety strategies will be also studied.

1.2 Motion model: Hill equations.

1.2.1 Equations of motion of a spacecraft.

This section intends to briefly state the general equations of motion of a certain spacecraft. From these, several simplifications may follow. Any spacecraft is subject mainly to gravitational forces. Nonetheless, many other forces may be relevant, such as drag, solar radiation pressure or

thrust. Newton's equation, with its respective initial conditions, would then take the following form:

$$[P] \equiv \begin{cases} \text{Eq. } m_i \ddot{\underline{r}}_i = \underline{F}_{g,i} + \underline{T}_i + \underline{F}_{\text{other}, i} \\ \text{ICs } \begin{cases} \underline{r}_i(t = t_0) = \underline{r}_{i,0} \\ \dot{\underline{r}}_i(t = t_0) = \dot{\underline{r}}_{i,0} \end{cases} \end{cases} \quad (1.1)$$

where \underline{r}_i denotes the i^{th} spacecraft position vector with respect to an inertial frame. Obtaining an analytical solution for this problem is almost impossible for most of the cases, as forces may depend on the position, velocity and control variables of the spacecraft, as well as time. Numerical integration becomes an option, though it leads to barely no knowledge and a high computational cost. Our goal is then to find semi-analytical solutions, that is, analytical solutions of a modelled, simplified version of the problem. This does give an insight into the physical problem, allowing us to understand some aspects of it. These solutions can be implemented in an incremental way, namely, increasing in difficulty and incorporating elements progressively less relevant.

Let us now have a quick look at the forces that show up in equation (1.1).

1.2.2 Forces in the spacecraft motion problem.

I. Gravitational forces

This group includes the effect of the gravity generated by all the considered bodies. Generally, we will consider a primary body (much more massive than any other), the spacecraft set (of negligible gravitational effects) and possibly, third bodies, which fall in between the former (relevant effect but not close to the primary body).

The effect of each celestial body in the considered spacecraft can be modelled differently. For example, the Earth can be considered to be a perfect sphere (central body acceleration) or, in other modelizations, some of its shape irregularities can be taken into account. As we move further away from any celestial body, its gravity field tends that of a central body, which is why third bodies' fields are modelled as central bodies. In a latter section we will see how this asphericity is modelled and how it affects the dynamics of any given spacecraft.

We can then decompose the gravitational force on the spacecraft i as:

$$\underline{F}_{g,i} = \underline{F}_{\text{primary},i} + \underline{F}_{\text{third bodies},i} = \underline{F}_{\text{primary, CB}, i} + \underline{F}_{\text{primary, NSG}, i} + \underline{F}_{\text{third bodies},i}$$

where CB and NSG refer to Central Body and Non-Spherical Gravity, respectively.

II. Thrust

With the purpose of controlling the trajectory and attitude of the spacecraft, thrusters are usually installed and actuated. This has obviously to be taken into account when integrating the motion of any spacecraft, though in this thesis this will not be the case: only uncontrolled motion will be analyzed.

III. Other forces

Logically, interplanetary trajectories take place in a much different environment compared to Earth orbits. Hence, different perturbation forces must be taken into account in each case. For example, in the case of low Earth orbits (LEOs), tidal forces become relevant, as well as drag and even the solar albedo. Conversely, in a interplanetary transfer orbit, solar radiation pressure might be taken into account. The key here is to establish a threshold of which effects to take into account and then start modelling those which rise above it.

1.2.3 Two-body problem.

As we stated, semi-analytical solutions are to be found. The simplest and most widely studied simplification of equation (1.1) is the two-body problem. As the name suggests, it only considers a primary and a secondary body, and the goal is to obtain the latter's motion around the former.

The equations of motion of the Keplerian two-body problem are obtained under the following assumptions [1]:

- I. Gravity is the only internal or external force.
- II. Gravity fields come from spherical bodies.
- III. Gravitational forces are Newtonian.
- IV. There are no tidal forces.
- V. The mass of the primary body is much larger than the orbiting body's.

The equations of the two-body problem can be then written as:

$$[P] \equiv \begin{cases} \text{Eq.} & \ddot{\underline{r}} = -\frac{\mu \underline{r}}{r^3} \\ \text{ICs} & \begin{cases} \underline{r}(t = t_0) = \underline{r}_0 \\ \dot{\underline{r}}(t = t_0) = \dot{\underline{r}}_0 \end{cases} \end{cases} \quad (1.2)$$

The solution of (1.2) is known as Keplerian motion, and is universally known. There are many ways to obtain it, such as the one shown in [1], section 2.2. We merely quote that development, as it is not our goal to explain this solution.

1.2.3.1 Perturbed two-body problem.

With the two-body solution in mind, any problem can be modelled as a perturbed version of it. The Keplerian motion can then be seen as a *first order* solution of the problem at hand, from which the perturbed problem slightly deviates. This deviation may be approached through several ways [2].

A direct integration of the equation is again possible, though knowledge acquisition will again be null. Furthermore, many of the significant figures will simply reproduce the two-body solution, which is already known, leading to computational inefficiency. This is commonly referred to as Cowell's method.

Another numeric approach is to expand the perturbed solution around the original, thus integrating only the perturbation. Though this leads to a better computational efficiency, still no further understanding is gained.

The last main option is to integrate the Gauss Variational Equations (see **REFERENCE GVEs**). These equations actually provide some knowledge of the perturbed problem, and are quite computationally efficient. This fact is due to (a) the slow time-varying character of the OEs, allowing for a greater time-step and (b) the possibility of substituting the two-body problem solution in the right-side of the equations.

Whatever our approach is, the perturbed two-body problem can be written as:

$$[P] \equiv \begin{cases} \text{Eq.} & \ddot{\underline{r}} = -\frac{\mu \underline{r}}{r^3} + \underline{a}_P \\ \text{ICs} & \begin{cases} \underline{r}(t = t_0) = \underline{r}_0 \\ \dot{\underline{r}}(t = t_0) = \dot{\underline{r}}_0 \end{cases} \end{cases} \quad (1.3)$$

where \underline{a}_P is the perturbation acceleration.

1.2.4 Three-body problem.

The three-body problem considers the motion of three bodies: a primary and two secondaries. It can be understood as an extension of the two-body problem, where a third body appears and perturbs the motion of the pre-existing secondary body. This problem lacks a general, closed-form solution. Nonetheless, some approximations have been developed.

One approach to this problem is to consider the gravitational effect of the third body on the secondary body as a perturbation with respect to the two body problem. This approach is actually a particularization of the perturbed two-body problem, which is developed in detail in chapter ??.

1.2.4.1 Reduced three-body problem.

Another simplification of the three-body problem is obtained by assuming that the two secondary bodies do not cause a gravitational effects on each other. This is commonly referred to as the reduced three-body problem, being actually the set of equations that describe spacecraft formation flying. This and further simplifications will be analyzed in the following section.

1.2.5 Differential equations of proximity relative motion.

As the proximity assumption ($\|\underline{r}\| \ll \|\underline{R}\|$) is quite widely common and valid for a fair range of operations, it is interesting to describe them here briefly, following [Yamanaka·ankersen]. Let us then consider the motion of two spacecrafts, namely, chief and deputy. The general equations of motion for each of them can be written as:

$$\text{Chief} \Rightarrow \ddot{\underline{R}} = -\mu \frac{\underline{R}}{\|\underline{R}\|} + \underline{a}_{C,d} \quad (1.4)$$

$$\text{Deputy} \Rightarrow \ddot{\underline{R}} + \ddot{\underline{r}} = -\mu \frac{\underline{R} + \underline{r}}{\|\underline{R} + \underline{r}\|} + \underline{a}_{D,d} + \underline{a}_f \quad (1.5)$$

where \underline{R} and \underline{r} are the chief's absolute position vector and the deputy's relative position vector, respectively. $\underline{a}_{\bullet,d}$ is the disturbing acceleration on each spacecraft, while \underline{a}_f denotes the thrust vector of the deputy. In order to facilitate the linearization, let us rewrite the orbital radius of the deputy as:

$$\|\underline{R} + \underline{r}\| = [(\underline{R} + \underline{r})^T(\underline{R} + \underline{r})]^{1/2} = \|\underline{R}\| \left(1 + 2 \frac{\underline{R}^T \underline{r}}{\|\underline{R}\|^2} + \frac{\|\underline{r}\|^2}{\|\underline{R}\|^2} \right)^{1/2}$$

then, the effect of the gravity field on the deputy can be expressed as:

$$\frac{\underline{R} + \underline{r}}{\|\underline{R} + \underline{r}\|^3} = \frac{\underline{R} + \underline{r}}{\|\underline{R}\|^3} = \left(1 + 2\frac{\underline{R}^T \underline{r}}{\|\underline{R}\|^2} + \frac{\|\underline{r}\|^2}{\|\underline{R}\|^2}\right)^{-\frac{3}{2}}$$

Assuming that the relative distance is much smaller than the chief's orbital radius:

$$\frac{\underline{R} + \underline{r}}{\|\underline{R} + \underline{r}\|^3} \underset{\|\underline{r}\| \ll \|\underline{R}\|}{\approx} \frac{\underline{R} + \underline{r}}{\|\underline{R}\|^3} \left[1 - \frac{3}{2} \left(2\frac{\underline{R}^T \underline{r}}{\|\underline{R}\|^2} + \frac{\|\underline{r}\|^2}{\|\underline{R}\|^2}\right)\right] \approx \frac{1}{\|\underline{R}\|^3} \left(\underline{R} + \underline{r} - 3\frac{\underline{R}^T \underline{r}}{\|\underline{R}\|^2} \underline{R}\right) \quad (1.6)$$

If we now substitute (1.6) in the difference (1.5) minus (1.4), we arrive to:

$$\ddot{\underline{r}} = -\frac{\mu}{\|\underline{R}\|^3} \left(\underline{r} - 3\frac{\underline{R}^T \underline{r}}{\|\underline{R}\|^2} \underline{R}\right) + \underline{a}_f + \underline{a}_{D,d} - \underline{a}_{C,d} \quad (1.7)$$

Experience shows it is convenient to express equation (1.7) in a chief-centered frame, for example, the LVLH frame (see section B.4.2). This leads to the need of applying Coriolis' Theorem twice, so as to get the non-inertial effects derived from describing the motion in a rotating frame. The equations of motion take now the following form:

$$\ddot{\underline{r}} = -\frac{\mu}{\|\underline{R}\|^3} \left(\underline{r} - 3\frac{\underline{R}^T \underline{r}}{\|\underline{R}\|^2} \underline{R}\right) - 2\underline{\omega} \times \dot{\underline{r}} - \dot{\underline{\omega}} \times \underline{r} - \underline{\omega} \times (\underline{\omega} \times \underline{r}) + \underline{a}_f + \underline{a}_{D,d} - \underline{a}_{C,d} \quad (1.8)$$

where $\underline{\omega}$ is the target orbital rate. Let us now express each vector in the RTN frame:

$$\underline{\omega} = \begin{Bmatrix} 0 \\ -\omega \\ 0 \end{Bmatrix} \quad \underline{R} = \begin{Bmatrix} 0 \\ 0 \\ -R \end{Bmatrix} \quad \underline{r} = \begin{Bmatrix} x \\ y \\ z \end{Bmatrix} \quad (1.9)$$

leading to the next expressions for the terms in equation (1.8):

$$\begin{aligned} \underline{\omega} \times \dot{\underline{r}} &= \begin{Bmatrix} \omega \dot{z} \\ 0 \\ \omega \dot{x} \end{Bmatrix} & \dot{\underline{\omega}} \times \underline{r} &= \begin{Bmatrix} -\dot{\omega} z \\ 0 \\ \dot{\omega} x \end{Bmatrix} \\ \underline{\omega} \times (\underline{\omega} \times \underline{r}) &= \begin{Bmatrix} -\omega^2 x \\ 0 \\ -\omega^2 z \end{Bmatrix} & \underline{r} - 3\frac{\underline{R}^T \underline{r}}{\|\underline{R}\|^2} \underline{R} &= \begin{Bmatrix} x \\ y \\ -2z \end{Bmatrix} \end{aligned}$$

and introducing these results into (1.8), we arrive to:

$$\begin{Bmatrix} \ddot{x} \\ \ddot{y} \\ \ddot{z} \end{Bmatrix} = \begin{Bmatrix} -k\omega^{3/2}x + 2\omega\dot{z} + \dot{\omega}z + \omega^2x \\ -k\omega^{3/2}y \\ 2k\omega^{3/2}z - 2\omega\dot{x} - \dot{\omega}x + \omega^2z \end{Bmatrix} + \underline{a}_f + \underline{a}_{D,d} - \underline{a}_{C,d} \quad (1.10)$$

if we finally consider Keplerian motion:

$$\begin{Bmatrix} \ddot{x} \\ \ddot{y} \\ \ddot{z} \end{Bmatrix} = \begin{Bmatrix} -k\omega^{3/2}x + 2\omega\dot{z} + \dot{\omega}z + \omega^2x \\ -k\omega^{3/2}y \\ 2k\omega^{3/2}z - 2\omega\dot{x} - \dot{\omega}x + \omega^2z \end{Bmatrix} \quad (1.11)$$

where k is a constant defined by

$$\frac{\mu}{R^3} = \left(\frac{\mu}{h^{3/2}} \right) \equiv k\omega^{3/2} \Leftrightarrow k \equiv \frac{\mu}{h^{3/2}}$$

and $h = \omega R^2$ is the chief's angular momentum.

1.2.6 Hill equations.

Let us summarize the path followed up until now. We started with the equations of motion of a spacecraft, in which many effects appear. From there, we went to the perturbed two-body problem, which is actually a reformulation rather than a simplification. After that, the differential equations for relative motion between two spacecrafts were derived, which were finally simplified under the assumptions that motion was unperturbed and that the spacecrafts were in close proximity.

Now, it is turn to do the last simplification: the assumption of near-circular or circular orbits ($e \ll 1$). The derived equations are the so-called Hill equations, or, in some references, the Clohessy-Wiltshire equations (though these are presented in ??)

If the reference orbit is near-circular, the orbital radius and hence the velocity is constant along time. This leads to the angular rate ω to be constant, and equal to:

$$\omega = \sqrt{\frac{\mu}{a^3}}$$

hence:

$$k\omega^{3/2} = \frac{\mu}{a^3} = \omega^2 \quad (1.12)$$

The equations (1.11) simplify to:

$$\begin{Bmatrix} \ddot{x} \\ \ddot{y} \\ \ddot{z} \end{Bmatrix} = \begin{Bmatrix} 2\omega\dot{z} \\ -\omega^2 y \\ 3\omega^2 z - 2\omega\dot{x} \end{Bmatrix} \quad (1.13)$$

which can be expressed in a set of first-order ordinary differential equations:

$$\begin{Bmatrix} \dot{x} \\ \dot{y} \\ \dot{z} \\ \ddot{x} \\ \ddot{y} \\ \ddot{z} \end{Bmatrix} = \left[\begin{array}{ccc|ccc} 0 & 0 & 0 & 1 & 0 & 0 \\ 0 & 0 & 0 & 0 & 1 & 0 \\ 0 & 0 & 0 & 0 & 0 & 1 \\ \hline 0 & 0 & 0 & 0 & 0 & 2\omega \\ 0 & \omega^2 & 0 & 0 & 0 & 0 \\ 0 & 0 & 3\omega^2 & -2\omega & 0 & 0 \end{array} \right] \begin{Bmatrix} x \\ y \\ z \\ \dot{x} \\ \dot{y} \\ \dot{z} \end{Bmatrix} \quad (1.14)$$

Equation (1.14) are the said Hill equations, which can also be decoupled into in-plane ($x - z$) and out-of-plane motion (y). We can rewrite them in a more compact form through the coefficient matrix \mathbf{A} , as:

$$\begin{Bmatrix} \dot{x} \\ \dot{y} \\ \dot{z} \\ \ddot{x} \\ \ddot{y} \\ \ddot{z} \end{Bmatrix} = \left[\begin{array}{c|c} \mathbb{O}_{3x3} & \mathbb{I}_{3x3} \\ \hline \mathbf{G} & \boldsymbol{\Omega} \end{array} \right] \begin{Bmatrix} x \\ y \\ z \\ \dot{x} \\ \dot{y} \\ \dot{z} \end{Bmatrix} \quad (1.15)$$

$$\Rightarrow \mathbf{A} = \left[\begin{array}{c|c} \mathbb{O}_{3x3} & \mathbb{I}_{3x3} \\ \hline \mathbf{G} & \boldsymbol{\Omega} \end{array} \right] \quad (1.16)$$

1.3 Solutions of Hill equations.

Our goal now is to analyze which solution does this simplified set of equations lead to, which will be done through several methods. Once all of them have been presented, they will be compared between themselves and with respect to a high-fidelity solution for some circular orbit scenarios.

1.3.1 Direct numerical integration.

The first option that may come to mind is to simply numerically integrate equation (1.14), being somewhat efficient, as the coefficient matrix can be computed once for all iterations. In our case, the numerical integration was done using a four-step Runge-Kutta method, due to its good balance between performance, stability and complexity. A constant timestep of 10 seconds is imposed. No sensitivity analysis has been done to this respect, though results show that it is a good enough value.

This approach, as all computational approaches, does not yield any real knowledge: it is just “cranking the numbers”. That is why other methods are thereupon described.

1.3.2 Clohessy-Wiltshire solution and STM.

In order to get a reasonable insight into the behaviour of the relative dynamics, let us develop the Clohessy-Wiltshire (CW) solution [3]. Firstly, let us quickly recall the expression for Laplace transforms of derivatives:

$$\begin{aligned}\mathcal{L}(\dot{f}(t)) &= sF(s) - f(0_+) \\ \mathcal{L}(\ddot{f}(t)) &= s^2F(s) - sf(0_+) - \dot{f}(0_+)\end{aligned}$$

where $F(s) = \mathcal{L}(f(t))$. Taking that into consideration, the Laplace transform of the equations (1.13) becomes:

$$\begin{cases} s^2X(s) - sx_0 - \dot{x}_0 - 2\omega sZ(s) + 2\omega z_0 = 0 \end{cases} \quad (1.17a)$$

$$\begin{cases} s^2Y(s) - sy_0 - \dot{y}_0 + \omega^2 sY(s) = 0 \end{cases} \quad (1.17b)$$

$$\begin{cases} s^2Z(s) - sz_0 - \dot{z}_0 + 2\omega sX(s) - 2\omega x_0 - 3\omega^2 Z(s) = 0 \end{cases} \quad (1.17c)$$

Solving for $X(s)$, $Y(s)$ and $Z(s)$ in (1.17), we arrive to the solution in the Laplace domain:

$$\left\{ \begin{array}{l} X(s) = x_0 \frac{1}{s} + (\dot{x}_0 - 2\omega z_0) \frac{1}{s^2} + 2\omega z_0 \frac{1}{s^2 + \omega^2} + 2\omega \dot{z}_0 \frac{1}{s(s^2 + \omega^2)} \\ \quad + 2\omega (4\omega^2 z_0 - 2\omega \dot{x}_0) \frac{1}{s^2(s^2 + \omega^2)} \end{array} \right. \quad (1.18a)$$

$$\left\{ \begin{array}{l} Y(s) = y_0 \frac{s}{s^2 + \omega^2} + \dot{y}_0 \frac{1}{s^2 + \omega^2} \end{array} \right. \quad (1.18b)$$

$$\left\{ \begin{array}{l} Z(s) = z_0 \frac{s}{s^2 + \omega^2} + \dot{z}_0 \frac{1}{s^2 + \omega^2} + (4\omega^2 z_0 - 2\omega \dot{x}_0) \frac{1}{s(s^2 + \omega^2)} \end{array} \right. \quad (1.18c)$$

In order to obtain the time domain solution, the inverse Laplace transform is applied, leading to the Clohessy-Wiltshire (CW) solution:

$$\begin{cases} x(t) = \left(\frac{4\dot{x}_0}{\omega} - 6z_0 \right) \sin(\omega\tau) - \frac{2\dot{z}_0}{\omega} \cos(\omega\tau) + (6\omega z_0 - 3\dot{x}_0) \tau + \left(x_0 + \frac{2\dot{z}_0}{\omega} \right) \end{cases} \quad (1.19a)$$

$$\begin{cases} y(t) = y_0 \cos(\omega\tau) + \frac{\dot{y}_0}{\omega} \sin(\omega\tau) \end{cases} \quad (1.19b)$$

$$\begin{cases} z(t) = \left(\frac{2\dot{x}_0}{\omega} - 3z_0 \right) \cos(\omega\tau) + \frac{\dot{z}_0}{\omega} \sin(\omega\tau) + \left(4z_0 - \frac{2\dot{x}_0}{\omega} \right) \end{cases} \quad (1.19c)$$

1.3.2.1 Clohessy-Wiltshire STM.

Once the CW solution has been developed, we wish to derive an analog STM formulation. The expression we are looking for is:

$$\underline{y}(t) = \Phi(t, t_0) \underline{y}(t_0)$$

where $\underline{y}(t) = \{\underline{r}, \dot{\underline{r}}\}^T$ denotes the state vector of the deputy, expressed in the chief's LVLH frame. The computation of the STM $\Phi(t, t_0)$ can be carried out in two ways:

A. Differentiating (1.19) with respect to the initial state vector $\underline{y}(t_0) = \{x_0, y_0, z_0, \dot{x}_0, \dot{y}_0, \dot{z}_0\}^T$.

B. Using the general expression $\Phi(t, t_0) = \exp(\mathbf{A}(t - t_0))$.

As we have the actual explicit relationship $\underline{y}(t) = f(t, \underline{y}(t_0))$, we will proceed with the first approach. The second one will be developed in a latter section, following a Jordan Canonical Decomposition.

The CW STM takes then the following form:

$$\Phi(t, t_0) = \begin{bmatrix} 1 & 0 & 6(\omega\tau - \sin \omega\tau) & \frac{4}{\omega} \sin \omega\tau - 3\tau & 0 & \frac{2}{\omega}(1 - \cos \omega\tau) \\ 0 & \cos \omega\tau & 0 & 0 & \frac{1}{\omega} \sin \omega\tau & 0 \\ 0 & 0 & 4 - 3 \cos \omega\tau & \frac{2}{\omega}(\cos \omega\tau - 1) & 0 & \frac{1}{\omega} \sin \omega\tau \\ 0 & 0 & 6\omega(1 - \cos \omega\tau) & 4 \cos \omega\tau - 3 & 0 & 2 \sin \omega\tau \\ 0 & -\omega \sin \omega\tau & 0 & 0 & \cos \omega\tau & 0 \\ 0 & 0 & 3\omega \sin \omega\tau & -2 \sin \omega\tau & 0 & \cos \omega\tau \end{bmatrix} \quad (1.20)$$

where the gray shaded part of the matrix corresponds to the out-of-plane dynamics, which are completely decoupled from the in-plane (rest of the matrix). This shape suggests that, if reshaped, the matrix could show this decoupling in a more intuitive and visual manner. This will be somehow carried out later on with the Jordan Canonical decomposition.

Now we can easily calculate the state vector at a given epoch, being a function only of the elapsed time $\tau = t - t_0$ and the chief's semimajor axis a (through ω).

1.3.3 State transition matrix propagation.

Another alternative approach considers the propagation of the actual state transition matrix. Following Montenbruck [4, section 7.2.1], the initial value problem (IVP) for the state vector propagation can be written as:

$$[P] \equiv \begin{cases} \text{Eq. } \frac{d\underline{y}}{dt} = \underline{f}(t, \underline{y}) \\ \text{ICs } \underline{y}(t = t_0) = \underline{y}_0 \end{cases} \quad (1.21)$$

where $\underline{f} = \{\dot{\underline{r}}, \ddot{\underline{r}}\}$ is a generally non-linear function. Nonetheless, this problem can be linearized, arriving to:

$$[P] \equiv \begin{cases} \text{Eq. } \frac{d\underline{y}}{dt} = \mathbf{A}\underline{y} \\ \text{ICs } \underline{y}(t = t_0) = \underline{y}_0 \end{cases} \quad (1.22)$$

where $\mathbf{A} = \frac{\partial \underline{f}(t, \underline{y})}{\partial \underline{y}}$. This coefficient matrix A can be calculated as:

$$\mathbf{A} = \frac{\partial \{\dot{\underline{r}}, \ddot{\underline{r}}\}^T}{\partial \{\underline{r}, \dot{\underline{r}}\}^T} = \left[\begin{array}{c|c} \frac{\partial \dot{\underline{r}}}{\partial \underline{r}} & \frac{\partial \dot{\underline{r}}}{\partial \dot{\underline{r}}} \\ \hline \frac{\partial \ddot{\underline{r}}}{\partial \underline{r}} & \frac{\partial \ddot{\underline{r}}}{\partial \dot{\underline{r}}} \end{array} \right] = \left[\begin{array}{c|c} \mathbb{O}_{3x3} & \mathbb{I}_{3x3} \\ \hline \mathbf{G} & \mathbf{\Omega} \end{array} \right] \quad (1.23)$$

It is no coincidence that this \mathbf{A} matrix is (when under the Hill assumptions) identical to the one already defined in (1.16). The approach followed through equations (1.21), (1.22) and (1.23) is an equally valid way of obtaining the Hill equations. The procedure followed in section 1.2.6 starts from the already linearised differential equations for proximity relative motion, which are then simplified with Hill's assumptions. This leads to a constant-coefficient system of ODEs, in which the \mathbf{A} matrix can be deducted. The perspective outlined in this section develops a general, linearized form, in which the \mathbf{A} matrix is first defined and then simplified, in a more inductive fashion.

After this incise, let us transform a state vector IVP into a STM IVP. Firstly, let us take the derivative of (1.21) with respect to the initial state vector $\underline{y}(t_0)$. Manipulating the derivative of each

member of said equation, we arrive to:

$$\begin{aligned} \bullet \quad & \frac{\partial}{\partial \underline{y}(t_0)} \frac{d\underline{y}(t)}{dt} = \frac{d}{dt} \frac{\partial \underline{y}(t)}{\partial \underline{y}(t_0)} = \frac{d}{dt} \Phi(t, t_0) \\ \bullet \quad & \frac{\partial \underline{f}(t, \underline{y})}{\partial \underline{y}(t_0)} = \frac{\partial \underline{f}(t, \underline{y})}{\partial \underline{y}(t)} \frac{\partial \underline{y}}{\partial \underline{y}(t_0)} = \mathbf{A} \Phi(t, t_0) \\ \frac{\partial(1.21)}{\partial \underline{y}(t_0)} \Rightarrow [P] \equiv & \begin{cases} \text{Eq. } \frac{d}{dt} \Phi(t, t_0) = \mathbf{A} \Phi(t, t_0) \\ \text{ICs } \Phi(t, t_0)(t = t_0) = \mathbb{I}_{6 \times 6} \end{cases} \end{aligned} \quad (1.24)$$

We can then integrate the problem (1.24) and have the value of the STM at any time epoch. The state vector would be simply calculated through the STM definition, that is, $\underline{y}(t) = \Phi(t, t_0)\underline{y}(t_0)$.

1.3.4 Jordan canonical decomposition.

As we stated earlier, the most general way of obtaining the state transition matrix of a system involves calculating the exponential of the coefficient matrix \mathbf{A} . This can be easily derived from equation (1.22) as:

$$\begin{aligned} \frac{d\underline{y}}{dt} = \mathbf{A}\underline{y} \rightarrow \underline{y}(t) &= \exp \mathbf{A}(t - t_0)\underline{y}(t_0) \equiv \Phi(t, t_0)\underline{y}(t_0) \\ \Rightarrow \Phi(t, t_0) &= \exp \mathbf{A}(t - t_0) \end{aligned} \quad (1.25)$$

In order to compute the matrix exponential, a Jordan Canonical Decomposition will be performed. This procedure consists basically in applying eigenspace theory to decompose \mathbf{A} into elements whose exponential can be easily calculated. Firstly, a diagonal form of \mathbf{A} will be obtained, differencing between real diagonal and complex diagonal form. Once the desired shape has been achieved, the exponential of the diagonal matrix will be calculated. Finally, a rearrangement of the matrices will be done, and the meaning of each will be duly explained.

1.3.4.1 Jordan canonical forms of \mathbf{A} .

A. Complex Jordan form.

For the sake of simplicity, only the in-plane part of the matrix \mathbf{A} will be analyzed. The goal is to achieve the components of the following expression:

$$\mathbf{A} = VJV^{-1}$$

where V is the eigenvector matrix (*i.e.* each column is an eigenvector of \mathbf{A}) and J is the Jordan matrix. Let us first then compute the eigenvalues of \mathbf{A} , that is:

$$\det(\mathbf{A} - \lambda \mathbb{I}_{4 \times 4}) = \begin{vmatrix} -\lambda & 0 & 1 & 0 \\ 0 & -\lambda & 0 & 1 \\ 0 & 0 & -\lambda & 2\omega \\ 0 & 3\omega^2 & -2\omega & -\lambda \end{vmatrix} = 0 \Rightarrow \lambda^2(\lambda^2 + 1) = 0$$

$$\left\{ \begin{array}{ll} \lambda_1 = 0 & \Rightarrow \text{Double real eigenvalue} \\ \lambda_3 = \pm i\omega & \Rightarrow \text{Complex eigenvalue} \end{array} \right. \quad (1.26)$$

We have to check if the matrix can be diagonalized. For that to happen, the algebraic and geometric multiplicities of each eigenvalue must be equal, so that the nullspace of \mathbf{A} can be fully generated.

- Eigenvalue λ_1 :

$$\text{nullspace}(\mathbf{A} - \lambda_1 \mathbb{I}_{4 \times 4}) = \text{nullspace}(\mathbf{A}) = \mathcal{L} \left(\begin{Bmatrix} 1 \\ 0 \\ 0 \\ 0 \end{Bmatrix} \right)$$

As the nullspace of \mathbf{A} is generated by only one eigenvector, the geometric multiplicity of λ_1 is 1.

As the algebraic multiplicity is 2, the matrix cannot be diagonalized. In order to get the second eigenvector associated to λ_1 , let us calculate the nullspace of $(\mathbf{A} - \lambda_1 \mathbb{I}_{4 \times 4})^2$, that is:

$$\text{nullspace}(\mathbf{A} - \lambda_1 \mathbb{I}_{4 \times 4})^2 = \text{nullspace}(\mathbf{A}^2) = \mathcal{L} \left(\begin{Bmatrix} 1 \\ 0 \\ 0 \\ 0 \end{Bmatrix}, \begin{Bmatrix} 0 \\ \frac{2}{3\omega} \\ 1 \\ 0 \end{Bmatrix} \right)$$

The eigenvectors associated to λ_1 are then:

$$\begin{cases} \underline{v}_2 = \left\{ 0 \quad \frac{2}{3\omega} \quad 1 \quad 0 \right\}^T & \text{as } \underline{v}_2 \in \text{nullspace}(\mathbf{A}^2) \quad \text{and } \underline{v}_2 \notin \text{nullspace}(\mathbf{A}) \end{cases} \quad (1.27a)$$

$$\underline{v}_1 = \mathbf{A}\underline{v}_2 = \left\{ 1 \quad 0 \quad 0 \quad 0 \right\}^T \quad \text{as } \mathbf{A}^2\underline{v}_2 = 0 = \mathbf{A}(\mathbf{A}\underline{v}_2) \equiv \mathbf{A}\underline{v}_1 \quad (1.27b)$$

- Eigenvalue λ_3 :

$$\text{nullspace } (\mathbf{A} - \lambda_3 \mathbb{I}_{4x4}) = \mathcal{L} \left(\begin{Bmatrix} -\frac{2}{\omega} \\ \frac{i}{\omega} \\ 2i \\ 1 \end{Bmatrix} \right)$$

$$\text{nullspace } (\mathbf{A} - \lambda_4 \mathbb{I}_{4x4}) = \mathcal{L} \left(\begin{Bmatrix} -\frac{2}{\omega} \\ -\frac{i}{\omega} \\ -2i \\ 1 \end{Bmatrix} \right)$$

In this case, the algebraic and geometric multiplicity match, so no further calculations are to be made. The vectors \underline{v}_3 take then the following form:

$$\underline{v}_3 = \left\{ -\frac{2}{\omega}, \pm \frac{i}{\omega}, \pm 2i, 1 \right\}^T \quad (1.28)$$

Rescaling ($\times -3$) the eigenvectors (1.27) and merging with (1.28), we can construct the Jordan complex eigenvector matrix as:

$$V = \begin{bmatrix} -3 & 0 & -\frac{2}{\omega} & -\frac{2}{\omega} \\ 0 & -\frac{2}{\omega} & \frac{i}{\omega} & -\frac{i}{\omega} \\ 0 & -3 & 2i & -2i \\ 0 & 0 & 1 & 1 \end{bmatrix}$$

And the complex Jordan matrix J being:

$$J = V^{-1} \mathbf{A} V = \begin{bmatrix} 0 & 1 & 0 & 0 \\ 0 & 0 & 0 & 0 \\ 0 & 0 & -i\omega & 0 \\ 0 & 0 & 0 & i\omega \end{bmatrix} \quad (1.29)$$

B. Real Jordan form.

In order to get rid of the complex numbers from the matrices V and Λ , a complex-to-real diagonal form transformation can be performed. This consists in a modification of the eigenvector definition, and consequently, a reformulation of the eigenvalue matrix. In general, the transformation converts both matrices as [5]:

$$J|_{complex} = \begin{bmatrix} \lambda_1 & & & \\ & a + bi & & \\ & & a - bi & \\ & & & c + di \\ & & & c - di \\ & & & \dots \end{bmatrix} \xrightarrow{cdf2rdf} J|_{real} = \begin{bmatrix} \lambda_1 & & & \\ & a & b & \\ & -b & a & \\ & c & d & \\ & -d & c & \\ & & & \dots \end{bmatrix} \quad (1.30)$$

$$V|_{complex} = \left[\underline{v}_1 \mid Re(\underline{v}_2) + iIm(\underline{v}_2) \mid Re(\underline{v}_2) - iIm(\underline{v}_2) \mid Re(\underline{v}_3) + iIm(\underline{v}_3) \mid Re(\underline{v}_3) - iIm(\underline{v}_3) \mid \dots \right]$$

$$\xrightarrow{cdf2rdf} V|_{real} = \left[\underline{v}_1 \mid Re(\underline{v}_2) \mid Im(\underline{v}_2) \mid Re(\underline{v}_3) \mid Im(\underline{v}_3) \mid \dots \right] \quad (1.31)$$

This transformation is based in that the nullspace generated by the complex eigenvectors (\underline{v}_3 and \underline{v}_4 in this case) can also be generated by two linear combinations of both. For this case, the real eigenvector matrix becomes:

$$V = \begin{bmatrix} -3 & 0 & -\frac{2}{\omega} & 0 \\ 0 & -\frac{2}{\omega} & 0 & \frac{1}{\omega} \\ 0 & -3 & 0 & 2 \\ 0 & 0 & 1 & 1 \end{bmatrix} \quad (1.32)$$

The real Jordan matrix is computed again as:

$$J = \begin{bmatrix} 0 & 1 & 0 & 0 \\ 0 & 0 & 0 & 0 \\ 0 & 0 & 0 & \omega \\ 0 & 0 & -\omega & 0 \end{bmatrix} \quad (1.33)$$

1.3.4.2 Exponential of the Jordan matrix.

Up until now, we have decomposed the coefficient matrix \mathbf{A} into the following product:

$$\mathbf{A} = VJV^{-1}$$

where V and J are given by equations (1.32) and (1.33) respectively. Now it is turn to compute the exponential itself, which satisfies:

$$\exp(\mathbf{A}(t - t_0)) = V \exp(J(t - t_0)) V^{-1} \quad (1.34)$$

Our target is then to compute $\exp(J(t - t_0))$. Let us recall that the exponential of a matrix is calculated as:

$$\exp(A(t - t_0)) = \sum_{n=0}^{\infty} \frac{(t - t_0)^n A^n}{n!}$$

Due to the structure of J , the summation has a finite number of non-zero terms. Still, it is convenient to separate J in two components: the periodic part J_p and the time-proportional part J_t . These take the following form:

$$J_t = \begin{bmatrix} 0 & 1 & 0 & 0 \\ 0 & 0 & 0 & 0 \\ 0 & 0 & 0 & 0 \\ 0 & 0 & 0 & 0 \end{bmatrix} \quad (1.35a) \qquad J_p = \begin{bmatrix} 0 & 0 & 0 & 0 \\ 0 & 0 & 0 & 0 \\ 0 & 0 & 0 & \omega \\ 0 & 0 & -\omega & 0 \end{bmatrix} \quad (1.35b)$$

Now, the exponential of the Jordan matrix can be expressed as:

$$K \equiv \exp(J(t - t_0)) = K_p(t) K_t(t - t_0) (K_p(t_0))^{-1} \quad (1.36)$$

where:

$$K_p(t) = \exp J_p t \quad (1.37a)$$

$$K_t(t) = \exp J_t t \quad (1.37b)$$

The actual expressions for K , K_p and K_t are:

$$K_p(t) = \begin{bmatrix} 1 & 0 & 0 & 0 \\ 0 & 1 & 0 & 0 \\ 0 & 0 & C_{\omega t} & S_{\omega t} \\ 0 & 0 & -S_{\omega t} & C_{\omega t} \end{bmatrix} \quad (1.38a) \qquad K_t(t) = \begin{bmatrix} 1 & t & 0 & 0 \\ 0 & 1 & 0 & 0 \\ 0 & 0 & 1 & 0 \\ 0 & 0 & 0 & 1 \end{bmatrix} \quad (1.38b)$$

$$K(t) = \begin{bmatrix} 1 & t & 0 & 0 \\ 0 & 1 & 0 & 0 \\ 0 & 0 & C_{\omega t} & S_{\omega t} \\ 0 & 0 & -S_{\omega t} & C_{\omega t} \end{bmatrix} \quad (1.38c)$$

where $C_{\omega t} = \cos \omega t$ and $S_{\omega t} = \sin \omega t$.

III. Final expression of the in-plane motion STM.

Substituting (1.36) into (1.34), we arrive to:

$$\Phi(t, t_0) = \exp(\mathbf{A}(t - t_0)) = V K_p(t) K_t(t - t_0) (K_p(t_0))^{-1} V^{-1} \quad (1.39)$$

Equation (1.39) can be yet again reframed as:

$$\Phi(t, t_0) = B(t) \Phi_{E\lambda}(t, t_0) (B(t_0))^{-1} \quad (1.40)$$

where $B(t) = V K_p(t)$ and $\Phi_{E\lambda}(t, t_0) = K_t(t - t_0)$. The propagation can now be understood as the composition of three operations:

1st Conversion of the initial cartesian state vector to the eigenspace $E\lambda$.

2nd Propagation of the eigenspace state vector through the $\Phi_{E\lambda}(t, t_0)$ STM.

3rd Back-transformation of the eigenspace state vector at the final epoch to the cartesian space.

The matrices B and $\Phi_{E\lambda}$ can be calculated from (1.32),(1.38a) and (1.38b). The final result is:

$$\Phi_{IP}(t, t_0) = \begin{bmatrix} 1 & 6(\omega\tau - \sin \omega\tau) & \frac{4}{\omega} \sin \omega\tau - 3\tau & \frac{2}{\omega}(1 - \cos \omega\tau) \\ 0 & 4 - 3 \cos \omega\tau & \frac{2}{\omega}(\cos \omega\tau - 1) & \frac{1}{\omega} \sin \omega\tau \\ 0 & 6\omega(1 - \cos \omega\tau) & 4 \cos \omega\tau - 3 & 2 \sin \omega\tau \\ 0 & 3\omega \sin \omega\tau & -2 \sin \omega\tau & \cos \omega\tau \end{bmatrix} \quad (1.41)$$

Which is identical to the in-plane part of (1.20).

IV. Out-of-plane motion STM.

The out-of-plane counterpart can be equally calculated, but in this case, we will just show the results. The procedure is exactly the same as done with the in-plane, but with a simpler mathematical manipulation:

$$V_{complex} = \begin{bmatrix} \frac{i}{2n} & \frac{i}{2n} \\ \frac{1}{2} & \frac{1}{2} \end{bmatrix} \quad (1.42a)$$

$$V = \begin{bmatrix} 0 & \frac{1}{2} \\ \frac{n}{2} & 0 \end{bmatrix} \quad (1.42b)$$

$$K(t) = \begin{bmatrix} C_{\omega t} & S_{\omega t} \\ -S_{\omega t} & C_{\omega t} \end{bmatrix} \quad (1.42c) \quad K_p(t) = \begin{bmatrix} C_{\omega t} & S_{\omega t} \\ -S_{\omega t} & C_{\omega t} \end{bmatrix} \quad (1.42d) \quad K_t(t) = \begin{bmatrix} 1 & S_{\omega t} \\ -S_{\omega t} & 1 \end{bmatrix} \quad (1.42e)$$

$$\Phi_{OOP}(t, t_0) = \begin{bmatrix} \cos \omega(t - t_0) & \frac{\sin \omega(t - t_0)}{\omega} \\ -\omega \sin \omega(t - t_0) & \cos \omega(t - t_0) \end{bmatrix} \quad (1.43)$$

The combination of (1.41) and (1.43) lead to the exact same expression as (1.20). Alternatively, the Jordan Canonical Decomposition could be carried out for the full system, though it would be of more cumbersome manipulation.

1.3.5 Results: Comparison against High-Fidelity.

Once all these methods have been duly developed, it is time to test them between themselves and against the High-Fidelity propagation. This will be done for two simple, very typical scenarios: V-bar and R-bar approach, both provided in [6], page 367. The V-bar approach is an along-track approach, which means that the orbital rate is equal for both spacecrafts. The R-bar approach is a radial approach, in which the deputy, who is in a lower orbit, features a higher orbital rate.

Wakker [6] only specifies the orbit height, which is not a problem for the Hill equations propagation. Conversely, the Hi-Fi propagator requires the whole set of the Keplerian OEs, which is why the rest of them are set to zero (for pure simplicity). Table 1.1 shows the full setup of the scenario. Without further ado, let us analyze the results.

Parameter	Value
Chief's orbit	
Height	$h = 400 \text{ km}$
Deputy's relative state (LVLH frame)	
Scenario 1) V-bar approach.	
Initial position	$(x, y, z) = (-200, 0, 0) \text{ m}$
Initial velocity	$(\dot{x}, \dot{y}, \dot{z}) = (0.2, 0, 0) \text{ m/s}$
Scenario 2) R-bar approach.	
Initial position	$(x, y, z) = (0, 0, -200) \text{ m}$
Initial velocity	$(\dot{x}, \dot{y}, \dot{z}) = (0, 0, 0.2) \text{ m/s}$
Propagation parameters	
Propagation time	$N_{\text{orbits}} = 10$

Table 1.1: Testing scenarios for Hill equations validation [6].

1.3.5.1 Scenario 1: V-Bar approach.

Figure 1.1(a) shows the relative error of the described Hill equations approaches with respect to High-Fidelity in relative distance, for the V-Bar approach. This allows us to select the most accurate method, which turns out to be the STM propagation. The error is nonetheless quite close in all surveyed methods. We can now compare every other method with STM integration, which is shown in figure 1.1(b). As it could be expected, direct integration and STM propagation yield really similar results, as they are two completely equivalent formulations. On the other hand, CW solution and Jordan Decomposition yield also the same result, as again, they use exactly the same STM (decomposed or not).

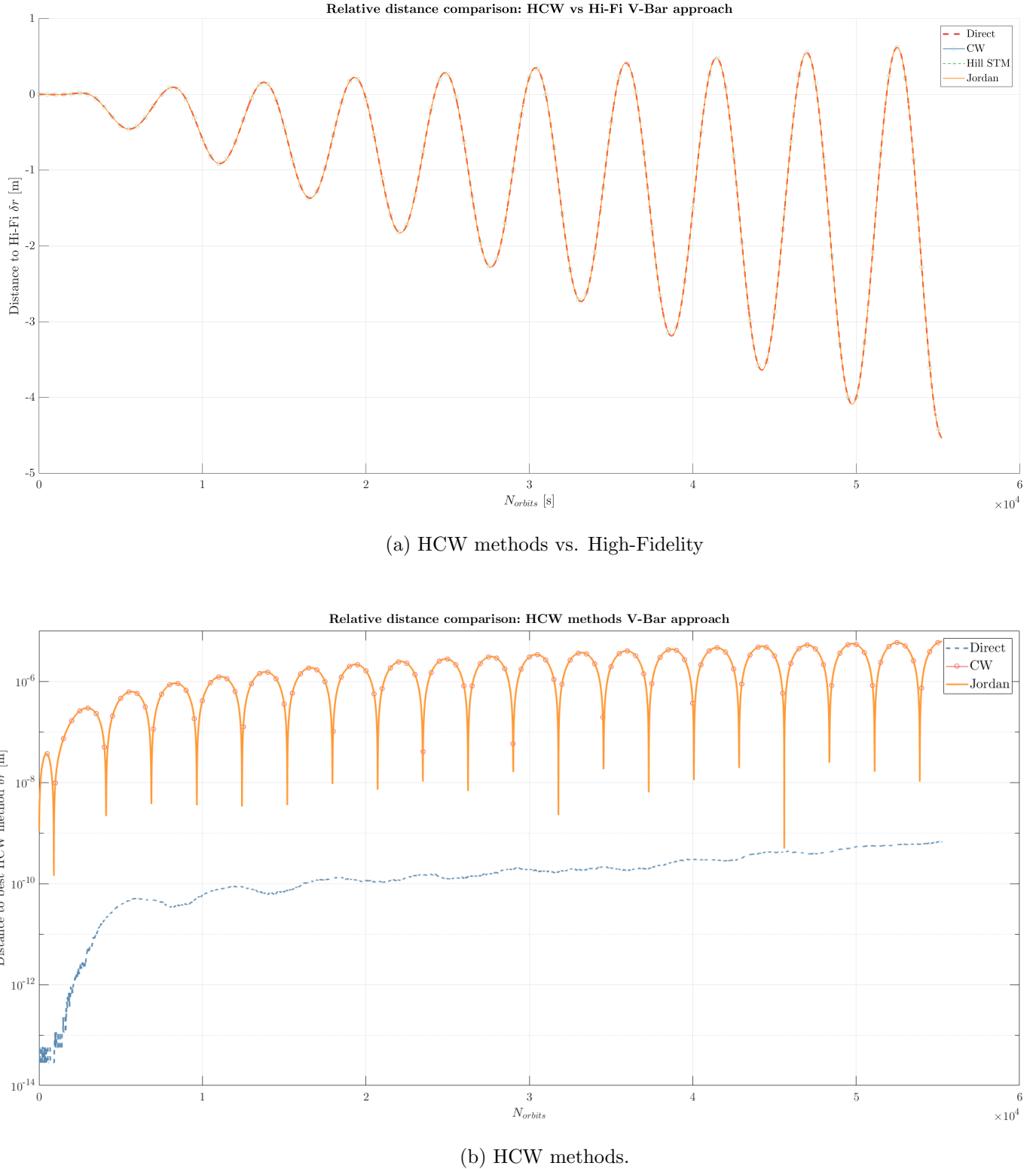


Figure 1.1: Difference in relative distance between HCW methods and Hi-Fi (V-bar approach).

This is only one side of the sword. Besides accuracy, we can also analyze computational efficiency through the elapsed time. Table 1.2 represents these results, which show a big difference between the two numerical methods and the analytical ones (around one order of magnitude). As a scale, the time required for High-Fidelity propagation is also provided, which doubles any of the HCW methods.

Method	Direct integration	CW solution	STM propagation	Jordan Decomposition	High-Fidelity
Elapsed time [s]	1.8697	0.1407	2.1526	0.2881	3.9657

Table 1.2: Elapsed time for the computation of V-bar scenario through each HCW method.

Finally, let us physically see the difference between Hill equations and the Hi-Fi results. Figure 1.2 shows the in-plane motion for this scenario. A drift in radial direction is seen as the main difference between them, which is due to Hill assumptions and the close-proximity simplification.

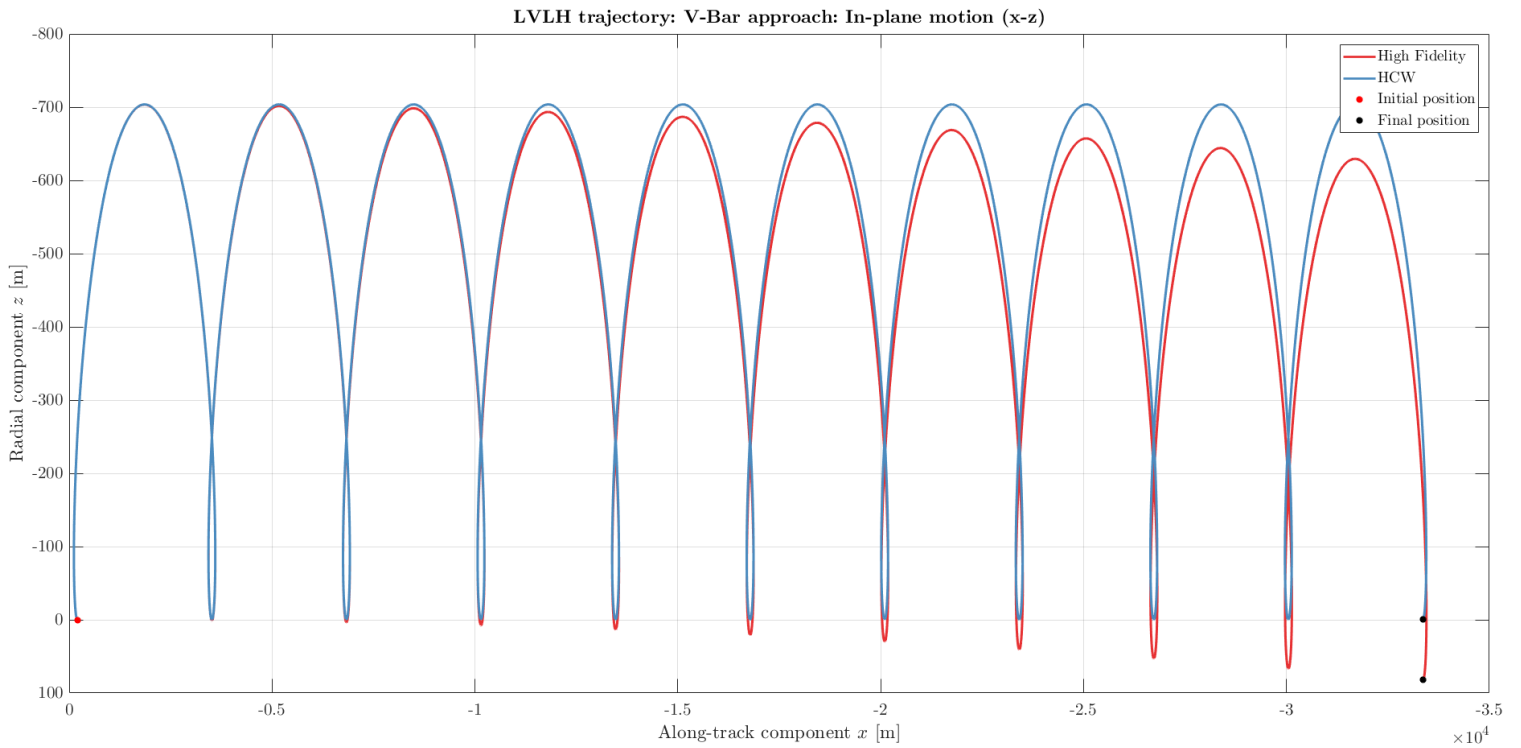


Figure 1.2: x-z trajectory comparison between STM propagation (HCW) and High-Fidelity.

1.3.5.2 Scenario 2: R-Bar approach.

The same procedure is here reproduced for the R-bar approach. No further comments are to be made, as the same behaviour is repeated: STM propagation is the most accurate, numerical methods are much more expensive and a similar drift in radial coordinate is again present.

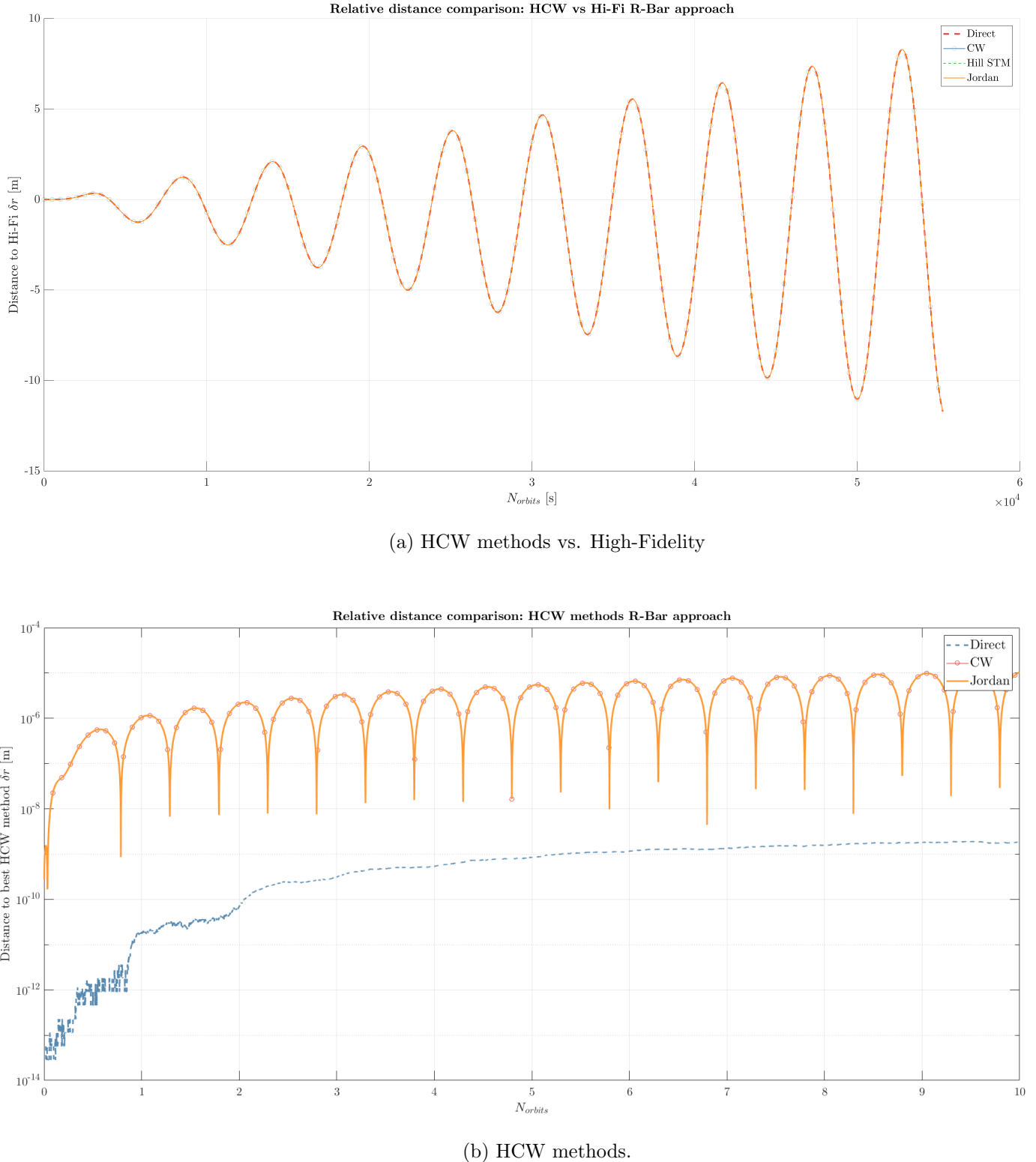


Figure 1.3: Difference in relative distance between HCW methods and Hi-Fi (R-bar approach).

Method	Direct integration	CW solution	STM propagation	Jordan Decomposition	High-Fidelity
Elapsed time [s]	1.9224	0.1486	2.2159	0.2984	4.1314

Table 1.3: Elapsed time for the computation of R-bar scenario through each HCW method.

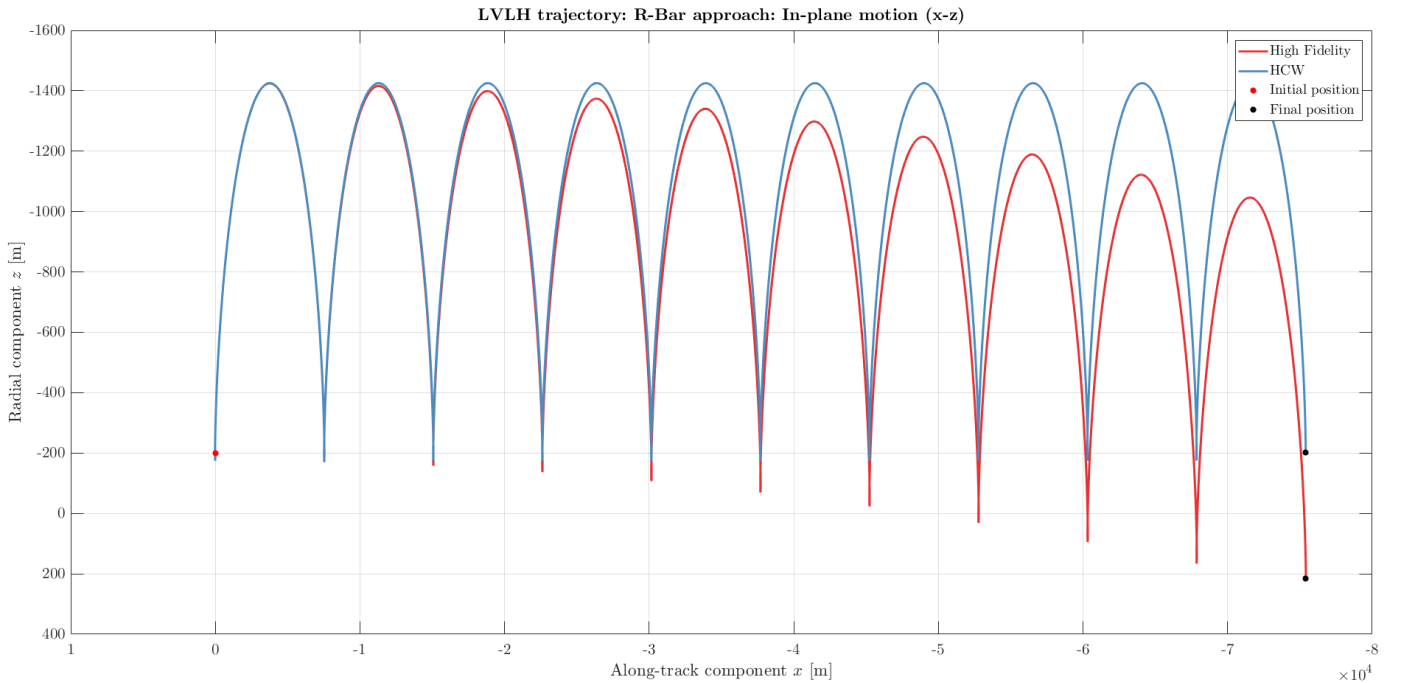


Figure 1.4: x-z trajectory comparison between STM propagation (HCW) and High-Fidelity (R-bar approach).

1.4 Orbit safety in near-circular orbits.

1.4.1 Orbit safety concept.

Orbit or trajectory safety can be understood as how protected from danger or risk a spacecraft formation is. It is essentially a kinematic condition, being closely related to the notions of relative position and velocity, and how these vary over time. Both branches of relative motion (*i.e.* rendez-vous and formation flying) are subject to this concept.

One of the biggest concerns about orbit safety is trajectory uncertainty. If we knew the exact position of each spacecraft, safety margins could be lowered down to almost zero, but unfortunately, that is not the case. For this reason, distance margins have to be established. As we have seen, there are three basic components in relative motion: radial, along-track and cross-track. The most susceptible one to estimation errors is the along-track component, due to the high influence of the semimajor axis on the angular rate, thus on the angular position [7]. Hence, along-track uncertainty

will always tend to be much higher than either radial or cross-track.

With this fact in mind, it seems logical to try and separate the spacecrafts in radial or cross-track components, as motion can be more accurately predicted in those directions. It is here where the eccentricity/inclination vector separation concept raises, as an approach to describe the periodic relative motion that takes place in said components. In the following section, its grounds and applications will be discussed, both in general terms and applied to near-circular reference orbits.

1.4.2 Eccentricity-inclination vector separation strategy.

1.4.2.1 Eccentricity and inclination vectors.

The eccentricity and inclination vectors constitute an interesting way to parametrize relative motion. This description was firstly introduced by Eckstein [7], aimed at geostationary orbits. Later on, it was extended to proximity LEO operations [8], which is today's main scope of application.

This approach to orbit safety will be treated recurrently along the thesis, being progressively extended as the orbits grow in complexity. In this section, the basics of this concept will be described, starting with the parametrization of proximity relative motion in terms of the eccentricity and inclination vectors (see section A.3.2.1). After that, the two feasible setups of δ_e and δ_i are discussed.

1.4.2.2 Linearized equations of relative motion in terms of δ_e and δ_i .

Our target is to obtain an expression which relates the eccentricity and inclination vector components to the radial, along-track and cross-track distances. This can be done by applying some transformations to the already available Keplerian OE set to RTN (see B.5.2), or through a geometric analysis of the motion. As the first one is almost trivial (considered said section), let us proceed with the second one, explained in more detail in [9]:

I. Effect of relative eccentricity vector δ_e .

The relative eccentricity vector accounts for the variation in the eccentricity value and the argument of perigee. Assuming no other variation in any element, it can be projected on the chief's orbital plane, leading to:

$$\underline{e} = \begin{Bmatrix} e_x \\ e_y \end{Bmatrix} = e \begin{Bmatrix} \cos \omega \\ \sin \omega \end{Bmatrix} \Rightarrow \delta\underline{e} = \begin{Bmatrix} \delta e_x \\ \delta e_y \end{Bmatrix} = \delta e \begin{Bmatrix} \cos \varphi \\ \sin \varphi \end{Bmatrix}$$

The relative eccentricity has an effect on the in-plane motion. That is to say, on the radial and along-track components. In order to get these, we must first derive some expressions for the orbital radius r and the difference $\theta - M$.

The orbital radius for near-circular orbits ($e \ll 1$) can be expressed as:

$$\begin{aligned} \frac{r}{a} &= 1 - e \cos E \underset{e \ll 1}{\approx} 1 - e \cos M = 1 - e \cos(\lambda - \omega) = 1 - e \cos \omega \cos \lambda + e \sin \lambda \sin \omega \\ &\Rightarrow \frac{r}{a} \approx 1 - e_x \cos \lambda - e_y \sin \lambda \end{aligned} \quad (1.44)$$

where λ is the mean argument of latitude, which embodies the time-varying element of the E/I element set. The second auxiliary expression $\theta - M$ can be obtained in many handbooks, by looking for the series expansion of the mean anomaly in terms of the true [10]:

$$M = \theta + 2 \sum_{n=1}^{\infty} (-1)^n \left(\frac{1}{n} + \sqrt{1-e^2} \right) \beta^n \sin n\theta \underset{e \ll 1}{\approx} \theta - 2e \sin \theta$$

$$\Rightarrow \theta - M = 2e \sin M = 2e \sin(\lambda - \omega) = 2e (\sin \lambda \cos \omega - \cos \lambda \sin \omega) = 2e_x \sin \lambda - 2e_y \cos \lambda \quad (1.45)$$

Assuming that both spacecrafts have the same mean argument of latitude and semimajor axis, the radial and along-track distance (δr_R , δr_T) between chief and deputy are due to (a) the difference in orbital radius δr and (b) the difference in true argument of latitude $\delta u = \delta\theta + \delta\omega$. With this in mind, let us construct a graphical representation of the situation, shown in 1.5. The angle α

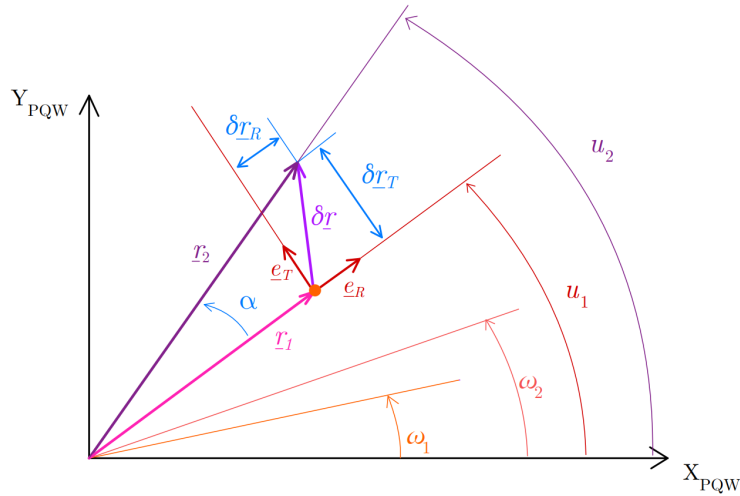


Figure 1.5: Effect of δr and δu in radial and along-track distances.

can be developed in terms of known magnitudes, that is:

$$\begin{aligned}\alpha = u_2 - u_1 &= (\lambda_2 - \lambda_1) + (\theta_2 - M_2) - (\theta_1 - M_1) = \\ 0 + 2e_2 \sin M_2 - 2e_1 \sin M_1 &= 2\delta e_x \sin \lambda - 2\delta e_y \cos \lambda = \mathcal{O}(\delta e) \sim 10^{-3}\end{aligned}\quad (1.46)$$

I.A. Effect of $\underline{\delta e}$ in δr_R .

Radial distance can be derived from figure 1.5 as:

$$\delta r_R = r_2 \cos \alpha - r_1 \approx r_2 - r_1 = \delta r$$

In virtue of equation (1.44):

$$\begin{aligned}\delta r_R &= \delta r = a(e_1 \cos M_1 - e_2 \cos M_2) \\ \frac{\delta r_R}{a} &= e_1(\cos \lambda \cos \omega_1 - \sin \lambda \sin \omega_1) - e_2(\cos \lambda \cos \omega_2 - \sin \lambda \sin \omega_2) = \\ &= \cos \lambda(e_{x1} - e_{x2}) - \sin \lambda(e_{y1} - e_{y2}) \\ \Rightarrow \frac{\delta r_R}{a} \Big|_{\delta e} &\approx -\delta e_y \sin \lambda - \delta e_x \cos \lambda\end{aligned}\quad (1.47)$$

I.B. Effect of $\underline{\delta e}$ in δr_T .

The along-track distance can be computed in a similar manner, neglecting terms of order $e \delta e$ and higher:

$$\begin{aligned}\delta r_T &= r_2 \sin \alpha \underset{|\alpha| << 1}{\approx} a(1 - e_2 \cos M_2) \alpha \underset{|e \delta e| << \delta e}{\approx} a \alpha \\ \Rightarrow \frac{\delta r_T}{a} \Big|_{\delta e} &\approx \alpha = 2\delta e_x \sin \lambda - 2\delta e_y \cos \lambda\end{aligned}\quad (1.48)$$

II. Effect of relative inclination vector $\underline{\delta i}$.

As presented in section A.3.2.1, the relative inclination vector takes the following form:

$$\delta \underline{i} = \sin \delta i \begin{Bmatrix} \cos \psi \\ \sin \psi \end{Bmatrix} \approx \begin{Bmatrix} \delta i \\ \sin i \delta \Omega \end{Bmatrix}$$

Its effect on the cross-track distance can be derived from the spherical triangle in figure 1.6, applying the law of sines as:

$$\frac{\sin(u_2 - \psi)}{\sin \frac{\pi}{2}} = \frac{\sin \frac{\delta r_N}{a}}{\sin \delta i} \Rightarrow \sin \frac{\delta r_N}{a} \underset{\delta r_N \ll a}{\approx} \frac{\delta r_N}{a} = \sin \delta i \sin(u_2 - \psi) \quad (1.49)$$

However, we need an expression with the mean argument of latitude instead of the true one. As we look to retain only first-order terms:

$$\begin{aligned} \sin(u - \psi) &= \sin[(\lambda - \psi) + (u - \lambda)] = \sin(\lambda - \psi) \cos(u - \lambda) + \cos(\lambda - \psi) \sin(u - \lambda) = \\ &= \sin(\lambda - \psi) \cos(2e \sin \theta) + \cos(\lambda - \psi) \sin(2e \sin \theta) \\ \sin(u - \psi) &\underset{|2e \sin \theta| \ll 1}{\approx} \sin(\lambda - \psi) \left(1 - \frac{(2e \sin \theta)^2}{2}\right) + \cos(\lambda - \psi) 2e \sin \theta = \sin(\lambda - \psi) + \mathcal{O}(e) \end{aligned} \quad (1.50)$$

Substituting (1.50) into (1.49):

$$\begin{aligned} \frac{\delta r_N}{a} &\approx \sin \delta i \sin(\lambda - \psi) = \sin \delta i \cos \psi \sin \lambda - \sin \delta i \sin \theta \cos \lambda \\ \Rightarrow \frac{\delta r_N}{a} \Big|_{\delta i} &\approx \delta i_x \sin \lambda - \delta i_y \cos \lambda \end{aligned} \quad (1.51)$$

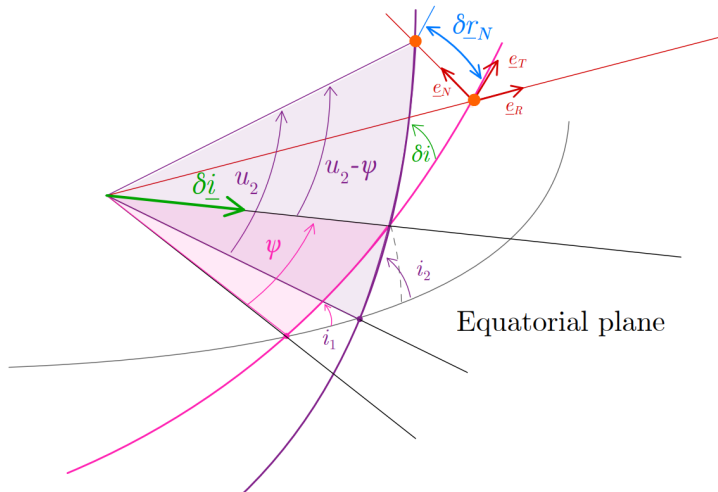


Figure 1.6: Inclination vector and cross-track distance.

III. Effect of relative semimajor axis and mean argument of latitude $\delta a, \delta \lambda$.

As previously stated, the relative semimajor axis has a crucial influence on the relative dynamics, as it varies the angular rate of the orbit, leading to an unbounded along-track drift. Consequently, let us estimate, to first order, the effect of a relative semimajor axis δa in the angular rate $\dot{\lambda}$:

$$\begin{aligned}
 \dot{\lambda}(a) &= \dot{\omega} + \dot{M}(a) = \dot{M}(a) = n = \sqrt{\frac{\mu}{a^3}} \\
 \Rightarrow \delta \dot{\lambda}_{\delta a} &= \dot{\lambda}(a + \delta a) - \dot{\lambda}(a) = \sqrt{\frac{\mu}{(a + \delta a)^3}} - \sqrt{\frac{\mu}{a^3}} \\
 \Rightarrow \delta \dot{\lambda}_{\delta a} &= \sqrt{\frac{\mu}{a^3}} \left[\frac{1}{(1 + \frac{\delta a}{a})^{3/2}} - 1 \right] \underset{|\frac{\delta a}{a}| \ll 1}{\approx} -\frac{3}{2} \frac{\delta a}{a} n \\
 \delta \lambda|_{\delta a} &= \int_{t_0}^t \delta \dot{\lambda} dt = -\frac{3}{2} \frac{\delta a}{a} n(t - t_0) = -\frac{3}{2} \frac{\delta a}{a} (M - M_0) = -\frac{3}{2} \frac{\delta a}{a} (\lambda - \lambda_0)
 \end{aligned} \tag{1.52}$$

III.A. Effect of $\delta a, \delta \lambda$ in δr_R .

The expression for the radial distance induced by δa is, assuming a constant mean argument of latitude λ and argument of perigee ω :

$$\begin{aligned}
 \delta r_R &\approx r_2 - r_1 \approx (a + \delta a)(1 - e_2 \cos M_2) - a(1 - e_1 \cos M_1) \approx \delta a \\
 \Rightarrow \frac{\delta r_R}{a} \Big|_{\delta a} &\approx \frac{\delta a}{a}
 \end{aligned} \tag{1.53}$$

where it is assumed that the relative mean argument of latitude has no effect on it.

III.B. Effect of $\delta a, \delta \lambda$ in δr_T .

The effect in along-track distance is due to both δa and $\delta \lambda$, as λ is intrinsically affected by δa (see eq. (1.52)). Without further ado:

$$\begin{aligned}
 \delta r_T &= r_2 \sin(u_2 - u_1) \underset{(1.52)}{\approx} r_2 \sin(\lambda_2 - \lambda_1) \underset{|\lambda_2 - \lambda_1| \ll 1}{\approx} (a + \delta a) (1 - e_2 \cos M_2) (\lambda_2 - \lambda_1) \\
 &\rightarrow \delta r_T \underset{e \ll 1}{\approx} (a + \delta a) \left[\delta \lambda - \frac{3}{2} \frac{\delta a}{a} (\lambda - \lambda_0) \right] \\
 \Rightarrow \frac{\delta r_T}{a} \Big|_{\delta a \delta \lambda} &\approx \delta \lambda - \frac{3}{2} \frac{\delta a}{a} (\lambda - \lambda_0)
 \end{aligned} \tag{1.54}$$

IV. Final set of linearized equations.

Now, considering all the previous effects, we can reach a compact set of equations [8]:

$$\begin{Bmatrix} \delta r_R \\ \delta r_T \\ \delta r_N \end{Bmatrix} = \begin{Bmatrix} \delta a \\ \delta \lambda - \frac{3}{2} \frac{\delta a}{a} (\lambda - \lambda_0) \\ 0 \end{Bmatrix} + a \delta e \begin{Bmatrix} -\cos(\lambda - \varphi) \\ 2 \sin(\lambda - \varphi) \\ 0 \end{Bmatrix} + a \delta i \begin{Bmatrix} 0 \\ 0 \\ \sin(\lambda - \psi) \end{Bmatrix} \quad (1.55)$$

$$\Leftrightarrow \begin{Bmatrix} \delta r_R \\ \delta r_T \\ \delta r_N \end{Bmatrix} = \begin{bmatrix} \delta a/a & 0 & -\delta e_x & -\delta e_y \\ \delta \lambda & -\frac{3}{2} \delta a/a & -2\delta e_y & 2\delta e_x \\ 0 & 0 & -\delta i_y & \delta i_x \end{bmatrix} \begin{Bmatrix} 1 \\ \lambda - \lambda_0 \\ \cos \lambda \\ \sin \lambda \end{Bmatrix} \quad (1.56)$$

A comparison of 1.56 and the analytical solution of the HCW equations show a complete correspondence of individual terms, hence proving the mathematical equivalence of both formulations. This equation can also be understood as a linearized approach to the Gauss Variational Equations, and finally, as an alternative to the mapping provided in B.5.2.

1.4.2.3 Collision avoidance for bounded trajectories: $\delta e/\delta i$ separation.

Let us now particularize the previous equations for the bounded trajectory case. This means that there is no mutual drift, hence relative semimajor axis drops to zero. The equations for the relative distances between both spacecrafts can be expressed as:

$$\begin{cases} \frac{\delta r_R}{a} = -\delta e \cos(\lambda - \varphi) \end{cases} \quad (1.57a)$$

$$\begin{cases} \frac{\delta r_T}{a} = 2\delta e \sin(\lambda - \varphi) \end{cases} \quad (1.57b)$$

$$\begin{cases} \frac{\delta r_N}{a} = \delta i \sin(\lambda - \psi) \end{cases} \quad (1.57c)$$

This formulation eases facilitates the safety analysis, as we will later see. In order to avoid collision hazard, considering along-track position uncertainties, a proper separation in radial and cross-track components must be set up. As shown in [11], two possible strategies to achieve this are (a) a parallel alignment of δe and δi and (b) an antiparallel (orthogonal) arrangement.

Before discussing these alternatives, let us do a quick analysis of the relevant positions that may arise from (1.57). If $\lambda = \varphi$, tangential distance vanishes, that is, the deputy is right below the chief (at a certain cross-track distance). Conversely, if $\lambda = \varphi + \frac{\pi}{2}$, radial distance vanishes, and the deputy comes just in front of the chief. Similar statements can be made with the out-of-plane motion. A

graphical representation of the mentioned geometry is shown in figure 1.7.

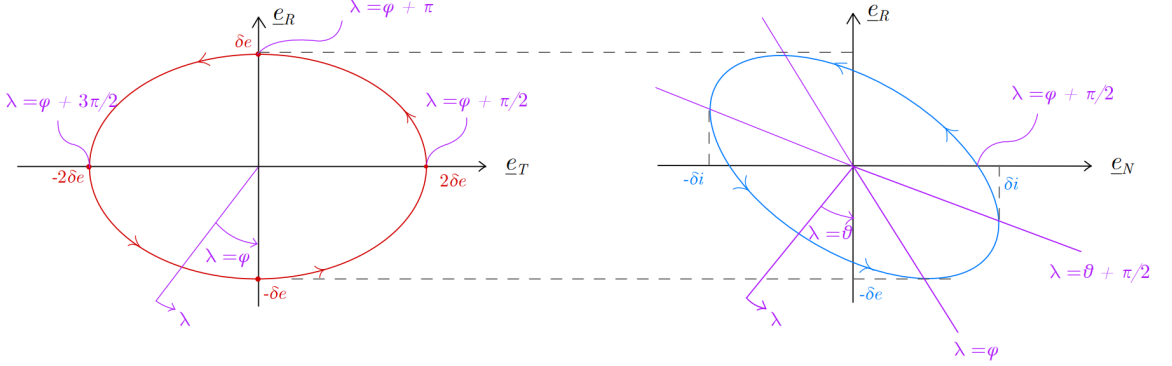


Figure 1.7: Relative motion in RTN frame for $\delta a = 0$ and a general $\underline{\delta e} - \underline{\delta i}$ alignment.

A. Parallel configuration.

If the relative eccentricity and inclination vectors are parallel, then we can write:

$$\underline{\delta e} \parallel \underline{\delta i} \Rightarrow \underline{\delta e} \cdot \underline{\delta i} = \delta e \delta i \begin{Bmatrix} \cos \varphi & \sin \varphi \end{Bmatrix} \begin{Bmatrix} \cos \psi \\ \sin \psi \end{Bmatrix} = \delta e \delta i \cos(\varphi - \psi) \xrightarrow{\underline{\delta e} \parallel \underline{\delta i}} 1$$

$$\implies \varphi = \psi + 2\pi k, \quad k \in \mathbb{Z} \quad (1.58)$$

For this configuration, the radial and cross-track distances never drop to zero simultaneously. In fact, if $\delta r_R = 0$, then δr_N is maximum, and viceversa. Hence, minimum separation satisfies:

$$\text{mod } \delta r \geq \min(a \delta e, a \delta i)$$

In conclusion, separation between the spacecrafts is ensured, even if tangential distance is null.

A graphical representation of this configuration can be seen in figure 1.8(a).

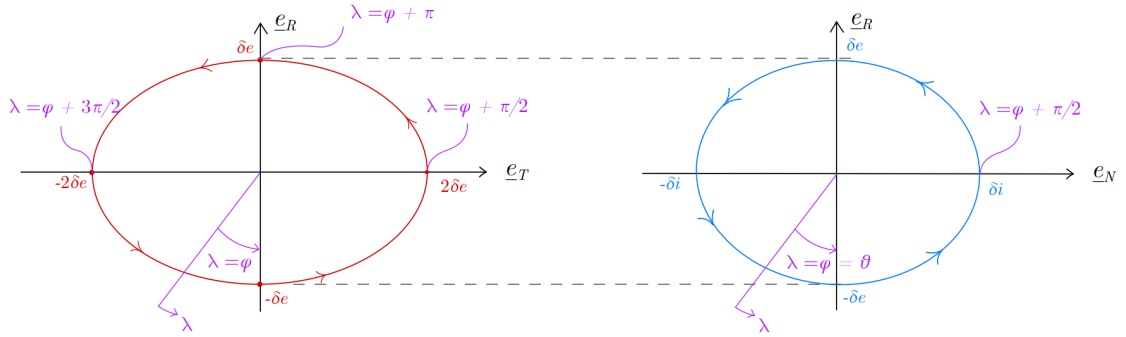
B. Antiparallel configuration.

The condition for antiparallel configuration can be expressed as:

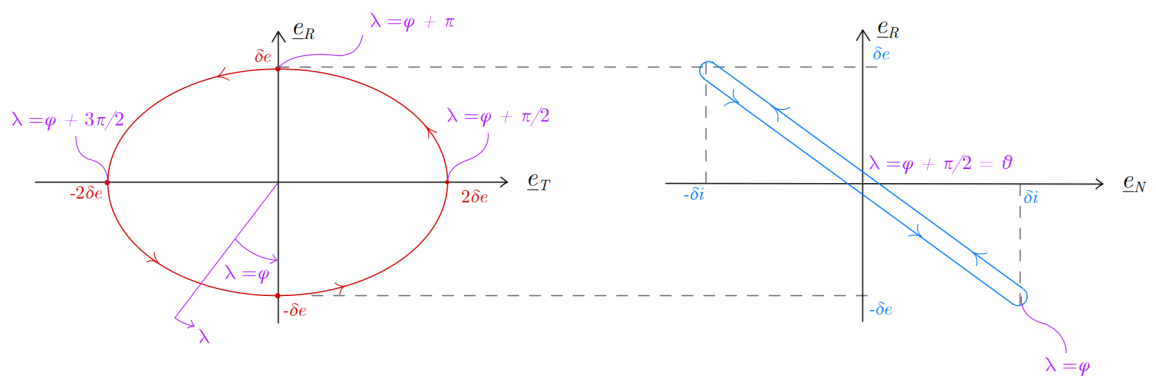
$$\underline{\delta e} \perp \underline{\delta i} \Rightarrow \underline{\delta e} \cdot \underline{\delta i} = \delta e \delta i \begin{Bmatrix} \cos \varphi & \sin \varphi \end{Bmatrix} \begin{Bmatrix} \cos \psi \\ \sin \psi \end{Bmatrix} = \delta e \delta i \cos(\varphi - \psi) \xrightarrow{\underline{\delta e} \perp \underline{\delta i}} 0$$

$$\implies \varphi = \psi + (2k+1)\frac{\pi}{2}, \quad k \in \mathbb{Z} \quad (1.59)$$

This configuration can also be seen in 1.8(b).



(a) Parallel configuration.



(b) Antiparallel configuration.

Figure 1.8: Relative motion for parallel and antiparallel $\underline{\delta e}/\underline{\delta i}$ vectors.

Relative dynamics around elliptic reference orbits.

2.1 Introduction.

In the previous chapter, the Clohessy-Wiltshire set of equations of motion has been analyzed. Getting them from Newton's law required the fulfillment of two assumptions. Firstly, the distance between deputy and chief must be negligible compared to either spacecraft's orbital radius. This is usually the case when dealing both with formation flying and rendez-vous maneuvers. The second assumption is that both orbits are near-circular ($e \ll 1$), which is not as acceptable as the first one. This is specially relevant on formation flying, as the timescale is usually large enough to experience sensible deviations.

Conceptually, there are some obvious differences between near-circular and eccentric orbits. First of all, orbital radius varies over time, which means that, at every point, the spacecraft is radially closing or moving away from the central body (*i.e.* the Earth). But more importantly, the angular velocity is no longer constant, which means that the non-inertial effects when analyzing the relative motion are not constant. That will surely make it harder to get analytical expressions, though through some simplifications, it may be done.

For this reason, several motion models for elliptic orbits have been developed [12]. Both linear and nonlinear models are present in the literature, though the first ones are the most usually employed. Tschauner and Hempel [13] developed a linear, first-order model via the truncation of the Taylor series expansion of the differential gravity. The so-called Tschauner-Hempel equations were widely used at the time, as they are consistent with the Hill/Clohessy-Wiltshire (HCW) model. Nonetheless, they were subsequently improved, due to the existence of singularities in the in-plane motion. Carter [14] provides a non-singular solution for this issue.

Instead of these solutions, the motion model used for elliptic, unperturbed orbits in this thesis is one developed by Yamanaka and Ankersen [15] (YA onwards). It results in a fairly simpler STM,

which is generally considered the state-of-the-art solution for linear propagation of the relative position and velocity in eccentric orbits. It will actually be used in the PROBA-3 mission, which flies in a highly elliptical orbit.

During this chapter, we will firstly develop YA's approach for the motion model and their proposed solution for it. This enables in turn to develop the YA STM, which will be duly tested with their own scenarios. Lastly, orbit safety concerns will be approached, extending the prior knowledge from near-circular orbits to arbitrarily elliptical, as done by Peters and Noomen [16].

2.2 Motion model and STM.

2.2.1 Simplification of equations of motion: YA solution.

As developed in section 1.2.5, the differential equations for proximity relative motion are:

$$\begin{Bmatrix} \ddot{x} \\ \ddot{y} \\ \ddot{z} \end{Bmatrix} = \begin{Bmatrix} -k\omega^{3/2}x + 2\omega\dot{z} + \dot{\omega}z + \omega^2x \\ -k\omega^{3/2}y \\ 2k\omega^{3/2}z - 2\omega\dot{x} - \dot{\omega}x + \omega^2z \end{Bmatrix} + \underline{a}_f + \underline{a}_{D,d} - \underline{a}_{C,d} \quad (2.1)$$

In this chapter, we will focus solely on the unperturbed version of this problem, that is, $\underline{a}_f = \underline{a}_{D,d} = \underline{a}_{C,d} = 0$. A slightly more general approach is to assume that, if dealing with perturbed motion, the perturbation acceleration is equal on either body. The main difference now with respect to Hill equations (CITE HILL EQUATIONS) is that the angular rate ω is now time-varying, whereas before it was constant ($\omega = n = \text{const.}$). This fact completely changes the character of the mathematical problem: the coefficient matrix is no longer constant.

It is here where Yamanaka and Ankersen, following Carter's approach, implement two changes. Firstly, chief's true anomaly θ is adopted as the independent variable instead of time. That changes the derivative definition, and for a certain variable ξ , the conversion from time to true anomaly derivatives is as follows:

$$\frac{d\xi}{dt} = \frac{d\xi}{d\theta} \frac{d\theta}{dt} = \omega \frac{d\xi}{d\theta} \Rightarrow \dot{\xi} = \omega \xi' \quad (2.2a)$$

$$\frac{d^2\xi}{dt^2} = \frac{d}{dt} \left(\frac{d\xi}{dt} \right) = \omega \frac{d\omega}{d\theta} \frac{d\xi}{d\theta} + \omega^2 \frac{d^2\xi}{d\theta^2} \Rightarrow \ddot{\xi} = \omega^2 \xi'' + \omega \omega' \xi' \quad (2.2b)$$

where ω' is calculated by simply using the angular momentum definition:

$$\omega = \frac{h}{R^2} = \frac{h}{p^2} (1 + e \cos \theta)^2 = k^2 \rho^2 \Rightarrow \omega t = 2k^2 \rho \rho' = -2k^2 e \sin \theta \rho \quad (2.3)$$

Substituting (2.2a), (2.2b) and (2.3) into (2.1) yields:

$$\begin{cases} \rho x'' - 2e \sin \theta x' - e \cos \theta x = 2\rho z' - 2e \sin \theta z \\ \rho y'' - 2e \sin \theta y' = -y \end{cases} \quad (2.4a)$$

$$\begin{cases} \rho z'' - 2e \sin \theta z' - (3 + e \cos \theta)z = -2\rho x' + 2e \sin \theta x \end{cases} \quad (2.4b)$$

$$\begin{cases} \rho z'' - 2e \sin \theta z' - (3 + e \cos \theta)z = -2\rho x' + 2e \sin \theta x \end{cases} \quad (2.4c)$$

Once this change of variable has been applied, the following transformation is performed:

$$\begin{Bmatrix} \tilde{x} \\ \tilde{y} \\ \tilde{z} \end{Bmatrix} = (1 + e \cos \theta) \begin{Bmatrix} x \\ y \\ z \end{Bmatrix} \quad (2.5)$$

which, if substituted in (2.6), lead to the rather simple following set of equations:

$$\begin{cases} \tilde{x}'' = 2\tilde{z}' \\ \tilde{y}'' = -\tilde{y} \end{cases} \quad (2.6a)$$

$$\begin{cases} \tilde{y}'' = -\tilde{y} \\ \tilde{z}'' = 3\frac{\tilde{z}}{\rho} - 2\tilde{x}' \end{cases} \quad (2.6b)$$

$$\begin{cases} \tilde{z}'' = 3\frac{\tilde{z}}{\rho} - 2\tilde{x}' \end{cases} \quad (2.6c)$$

The initial conditions that complete the initial value problem (IVP) can be written as:

$$\begin{Bmatrix} \tilde{x} \\ \tilde{y} \\ \tilde{z} \end{Bmatrix}(\theta_0) = \begin{Bmatrix} \tilde{x}_0 \\ \tilde{y}_0 \\ \tilde{z}_0 \end{Bmatrix} = (1 + e \cos \theta_0) \begin{Bmatrix} x_0 \\ y_0 \\ z_0 \end{Bmatrix}$$

Solution of the simplified set of equations.

It is rather obvious that equations (2.6a), (2.6b), (2.6c) feature a decoupling between in-plane components (x-z) and out-of-plane (y). The latter can easily be solved as:

$$\tilde{y} = K_{y1} \sin \theta + K_{y2} \cos \theta \quad (2.7)$$

while for the in-plane motion, equation (2.6a) must be first integrated, then introduced into (2.6c), yielding:

$$\tilde{z}'' + \left(4 - \frac{3}{\rho}\right) \tilde{z} = -2K_{x1} \quad (2.8)$$

with \tilde{x} is calculated from \tilde{z} as:

$$\tilde{z}' = 2\tilde{z} + K_{x1} \quad (2.9)$$

where K_i is the set of integration constants, derived from the prescribed initial conditions. The relation between them will be later described.

The task at hand now is to solve (2.8). Yamanaka and Ankersen propose a new solution to it, whose mathematical development is explained in [15]. Bottom line is that, the solution for \tilde{z} is:

$$\tilde{z} = K_{z1}\rho \sin \theta + \left(K_{z2} - \frac{K_{x1}}{e} \right) \rho \cos \theta - K_{z2}e (2 - 3e\rho \sin \theta J) \quad (2.10)$$

where:

$$J = k^2(t - t_0)$$

Substituting into (2.9) and integrating:

$$\tilde{x} = K_{x2} - K_{z1} \cos \theta (\rho + 1) + \left(K_{z2} - \frac{K_{x1}}{e} \right) \sin \theta (\rho + 1) - 3K_{z2}e\rho^2 J \quad (2.11)$$

Redefining the integral constants for simplicity as:

$$K_1 \equiv K_{x2} \quad K_2 \equiv K_{z1} \quad K_3 = \left(K_{z2} - \frac{K_{x1}}{e} \right) \quad K_4 = -K_{z2}e$$

and using the following simplified notation

$$s = \rho \sin \theta \quad c = \rho \cos \theta$$

the solution of the in-plane dynamics turns fairly simpler:

$$\begin{cases} \tilde{x} = K_1 - K_2c \left(1 + \frac{1}{\rho} \right) + K_3s \left(1 + \frac{1}{\rho} \right) + 3K_4\rho^2 J \\ \tilde{z} = K_2s + K_3c + K_4(2 - 3esJ) \end{cases} \quad (2.12a)$$

$$(2.12b)$$

By simply differentiating the latter equations, we can obtain the in-plane velocity components. Considering both position and velocity, a simple matrix form can be achieved:

$$\begin{Bmatrix} \tilde{x} \\ \tilde{z} \\ \tilde{v}_x \\ \tilde{v}_z \end{Bmatrix} = \begin{bmatrix} 1 & -c(1 + \rho^{-1}) & s(1 + \rho^{-1}) & 3\rho^2 J \\ 0 & s & c & (2 - 3esJ) \\ 0 & 2s & 2c - e & 3(1 - 2esJ) \\ 0 & s' & c' & -3e(s'J + s/\rho^2) \end{bmatrix} \begin{Bmatrix} K_1 \\ K_2 \\ K_3 \\ K_4 \end{Bmatrix} \equiv \Phi_\theta|_{IP} \underline{K}_{IP} \quad (2.13)$$

where:

$$s' = \cos \theta + e \cos 2\theta \quad c' = -(\sin \theta + e \sin 2\theta)$$

The out-of-plane problem can be expressed in this form as well:

$$\begin{Bmatrix} \tilde{y} \\ \tilde{v}_y \end{Bmatrix} = \begin{bmatrix} \cos \theta & \sin \theta \\ -\sin \theta & \cos \theta \end{bmatrix} \begin{Bmatrix} \tilde{y}_0 \\ \tilde{v}_{y0} \end{Bmatrix} \equiv \Phi_\theta|_{OOP} \underline{K}_{OOP} \quad (2.14)$$

2.2.2 YA STM and integration constants.

Our target is to obtain a state transition matrix, that is, a matrix which when fed a state vector at a given time, returns the state vector at a latter epoch. Generally speaking, said entity is built as:

$$\Phi_{\theta_0}^\theta = \Phi_\theta \Phi_{\theta_0}^{-1} \Rightarrow \underline{x}(\theta) = \Phi_{\theta_0}^\theta \underline{x}(\theta_0)$$

where θ can be substituted by any independent variable, such as time. Yamanaka and Ankersen propose to merge the second part of the STM and the initial state vector, leading to the so-called pseudoinitital state vector, defined by:

$$\bar{\underline{x}}_0 = \Phi_{\theta_0}^\theta \underline{x}(\theta_0)$$

which is also called the YA element set. With this in mind, our target now is to obtain both matrices, which in fact can be built from the in- and out-of-plane parts, previously defined in (2.13) and (2.14).

2.2.2.1 In-plane motion.

The first component Φ_θ was already defined as (2.13):

$$\Phi_\theta|_{IP} = \begin{bmatrix} 1 & -c(1 + \rho^{-1}) & s(1 + \rho^{-1}) & 3\rho^2 J \\ 0 & s & c & (2 - 3esJ) \\ 0 & 2s & 2c - e & 3(1 - 2esJ) \\ 0 & s' & c' & -3e(s'J + s/\rho^2) \end{bmatrix} \quad (2.15)$$

In order to get $\Phi_{\theta_0}|_{IP}^{-1}$, let us note that $J(\theta_0) = J(t_0) = 0$. Once applied that, the inverse is not so hard to compute, namely:

$$\Phi_{\theta_0}|_{IP}^{-1} = \frac{1}{1 - e^2} \begin{bmatrix} 1 - e^2 & 3e(s/\rho)(1 + \rho^{-1}) & -es(1 + \rho^{-1}) & 2 - ec \\ 0 & -3(s/\rho)(1 + e^2/\rho) & s(1 + \rho^{-1}) & c - 2e \\ 0 & -3(e + c/\rho) & c(1 + \rho^{-1}) + e & -s \\ 0 & 3\rho + e^2 - 1 & -\rho^2 & es \end{bmatrix}_{\theta_0} \quad (2.16)$$

2.2.2.2 Out-of-plane motion.

The out-of-plane equations require a less cumbersome manipulation. As we already have the full STM in (2.14), we have to first divide it into the two subcomponents by substituting θ for $\theta - \theta_0$. Then, using trigonometric relations for the sum of sines and cosines, it is easy to pull both matrices apart as:

$$\Phi_{\theta_0}^\theta = \begin{bmatrix} \cos(\theta - \theta_0) & \sin(\theta - \theta_0) \\ -\sin(\theta - \theta_0) & \cos(\theta - \theta_0) \end{bmatrix} = \begin{bmatrix} \cos \theta & \sin \theta \\ -\sin \theta & \cos \theta \end{bmatrix} \begin{bmatrix} \cos \theta_0 & -\sin \theta_0 \\ \sin \theta_0 & \cos \theta_0 \end{bmatrix} \equiv \Phi_\theta \Phi_{\theta_0}^{-1} \quad (2.17)$$

This expression could have also been reached similarly to the in-plane counterpart.

2.2.2.3 Full matrices.

By simply but carefully placing the elements of (2.15), (2.16), and (2.17) in a 6x6 matrix, we can finally reach the full matrices as:

$$\Phi_\theta = \begin{bmatrix} 1 & 0 & -c(1 + \rho^{-1}) & s(1 + \rho^{-1}) & 0 & 3\rho^2 J \\ 0 & \cos \theta & 0 & 0 & \sin \theta & 0 \\ 0 & 0 & s & c & 0 & 2 - 3esJ \\ 0 & 0 & 2s & 2c - e & 0 & 3(1 - 2esJ) \\ 0 & -\sin \theta & 0 & 0 & \cos \theta & 0 \\ 0 & 0 & s' & c' & 0 & -3e(s'J + s/\rho^2) \end{bmatrix} \quad (2.18a)$$

$$\Phi_{\theta_0}^{-1} = \frac{1}{1 - e^2} \times \begin{bmatrix} 1 - e^2 & 0 & 3e(s/\rho)(1 + \rho^{-1}) & -es(1 + \rho^{-1}) & 0 & 2 - ec \\ 0 & (1 - e^2)\cos \theta & 0 & 0 & -(1 - e^2)\sin \theta & 0 \\ 0 & 0 & -3(s/\rho)(1 + e^2/\rho) & s(1 + \rho^{-1}) & 0 & c - 2e \\ 0 & 0 & -3(c/\rho + e) & c(1 + \rho^{-1}) + e & 0 & -s \\ 0 & (1 - e^2)\sin \theta & 0 & 0 & (1 - e^2)\cos \theta & 0 \\ 0 & 0 & 3\rho + e^2 - 1 & -\rho^2 & 0 & es \end{bmatrix} \quad (2.18b)$$

2.2.2.4 Pseudo-initial state vector.

Finally, let us compute the so-called pseudoinitial conditions as defined before, namely:

$$\left\{ \begin{array}{c} \bar{x}_0 \\ \bar{y}_0 \\ \bar{z}_0 \\ \bar{v}_{x0} \\ \bar{v}_{y0} \\ \bar{v}_{z0} \end{array} \right\} = \Phi_{\theta_0}^{-1} \tilde{\underline{x}}_0 = \frac{1}{1 - e^2} \times$$

$$\left[\begin{array}{cccccc} 1 - e^2 & 0 & 3e(s/\rho)(1 + \rho^{-1}) & -es(1 + \rho^{-1}) & 0 & 2 - ec \\ 0 & (1 - e^2)C\theta & 0 & 0 & -(1 - e^2)S\theta & 0 \\ 0 & 0 & -3(s/\rho)(1 + e^2/\rho) & s(1 + \rho^{-1}) & 0 & c - 2e \\ 0 & 0 & -3(c/\rho + e) & c(1 + \rho^{-1}) + e & 0 & -s \\ 0 & (1 - e^2)S\theta & 0 & 0 & (1 - e^2)C\theta & 0 \\ 0 & 0 & 3\rho + e^2 - 1 & -\rho^2 & 0 & es \end{array} \right] \left\{ \begin{array}{c} \tilde{x}_0 \\ \tilde{y}_0 \\ \tilde{z}_0 \\ \tilde{v}_{x0} \\ \tilde{v}_{y0} \\ \tilde{v}_{z0} \end{array} \right\} \quad (2.19)$$

where $C = \cos$ and $S = \sin$. Nonetheless, the right hand side vector $\tilde{\underline{x}}_0$ is actually a transformation of a genuine LVLH state vector (see (2.5)), which is the true inputs of our relative dynamics problem. For that reason, it is necessary to map the transformed state vector $\tilde{\underline{x}}$ from and to the original one \underline{x} . This is done through the matrix T_θ as follows:

$$\tilde{\underline{x}} = T_\theta \underline{x} \Rightarrow \left\{ \begin{array}{c} \tilde{r} \\ \tilde{v} \end{array} \right\} = \left[\begin{array}{cc} \rho \mathbb{I}_{3 \times 3} & \mathbb{O}_{3 \times 3} \\ -e \sin \theta \mathbb{I}_{3 \times 3} & \frac{1}{k^2 \rho} \mathbb{I}_{3 \times 3} \end{array} \right] \left\{ \begin{array}{c} r \\ v \end{array} \right\} \quad (2.20)$$

The combination of (2.19) and (2.20) lead to a transformation between a LVLH state vector and the so-called Yamanaka-Ankersen element set, through the transformation matrix $T_{LVLH \rightarrow YA}$:

$$\bar{\underline{x}} \equiv \underline{x}_{YA} = \Phi_{\theta_0}^{-1} T_{\theta} \underline{x}_{LVLH} = \frac{1}{1 - e^2} \times$$

$$\left[\begin{array}{ccccccc} 1 - e^2 & 0 & 3e(s/\rho)(1 + \rho^{-1}) & -es(1 + \rho^{-1}) & 0 & 2 - ec \\ 0 & (1 - e^2)\cos\theta & 0 & 0 & -(1 - e^2)\sin\theta & 0 \\ 0 & 0 & -3(s/\rho)(1 + e^2/\rho) & s(1 + \rho^{-1}) & 0 & c - 2e \\ 0 & 0 & -3(c/\rho + e) & c(1 + \rho^{-1}) + e & 0 & -s \\ 0 & (1 - e^2)\sin\theta & 0 & 0 & (1 - e^2)\cos\theta & 0 \\ 0 & 0 & 3\rho + e^2 - 1 & -\rho^2 & 0 & es \end{array} \right] \times$$

$$\left[\begin{array}{ccccc} \rho & 0 & 0 & & \\ 0 & \rho & 0 & \mathbb{O}_{3 \times 3} & \\ 0 & 0 & \rho & & \\ -e\sin\theta & 0 & 0 & \frac{1}{k^2\rho} & 0 \\ 0 & -e\sin\theta & 0 & 0 & \frac{1}{k^2\rho} \\ 0 & 0 & -e\sin\theta & 0 & 0 \end{array} \right] \underline{x}_{LVLH} \quad (2.21)$$

2.2.2.5 Solution scheme.

The target is to compute the relative state vector at a certain time epoch, given the following inputs:

- $\underline{x}_{LVLH}|_0$: Initial LVLH relative state vector (see section B.4.2).
- $KOE_C|_0$: Initial chief's Keplerian OE set (see section A.2.2.1).
- t : Time elapsed from the initial time epoch to the desired one.

This is, as explained in appendix ??, the usual workflow for orbit propagation. With all the operations and transformations previously described, this process is graphically described in 2.1.

2.2.3 Results: Comparison with HCW and Hi-Fi propagation.

Once we have defined the complete model for orbit propagation, it is turn to discuss how does it compare with respect to the previous solution (HCW) and the High-Fidelity propagation. The workflows for both of these approach are available at **REF HCW DIAGRAM** and **REF HIFI**

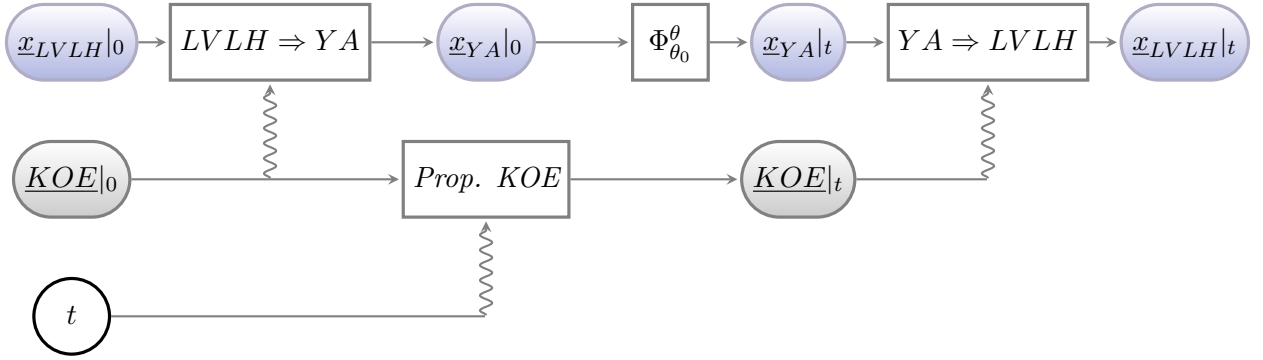


Figure 2.1: Workflow of the propagation with YA STM.

DIAGRAM.

Now, let us define (rather cite) a scenario to test this method. In order to be able to compare the results with the method source, we will use the scenarios defined by Yamanaka and Ankersen [15]. As we know, if no body-dependent perturbations are considered, a scenario is completely defined by:

- Chief's reference orbit (Keplerian OEs)
- Deputy's relative position and velocity with respect to chief (LVLH frame)
- Propagation values: Time elapsed and numerical method for high-fidelity propagation(algorithm, timestep ...)

In this case, Yamanaka and Ankersen define them as:

Parameter	Value
Chief's orbit	
Eccentricity	$e_1 = 0.1, e_2 = 0.7$
Perigee height	$h_p = 500 \text{ km}$
Inclination	$i = 30^\circ$
RAAN	$\Omega = 0^\circ$
Argument of perigee	$\omega = 0^\circ$
True anomaly at $t = 0$	$\theta = 45^\circ$
Deputy's relative position (LVLH frame)	
Initial position	$\{x, y, z\} = [100, 10, 10] \text{ m}$
Initial velocity	$\{\dot{x}, \dot{y}, \dot{z}\} = [0.1, 0.1, 0.1] \text{ m/s}$
Propagation parameters	
Propagation time	$N_{\text{orbits}} = 2$
Numerical method	Fourth order Runge-Kutta

Table 2.1: Testing scenarios for YA STM [15].

Nonetheless, we must get the set of Keplerian OEs as defined in A.2.2.1. Firstly, let us compute the semimajor axis from the perigee height h_p as:

$$h_p = a(1 - e) \Rightarrow a = \frac{h_p}{1 - e}$$

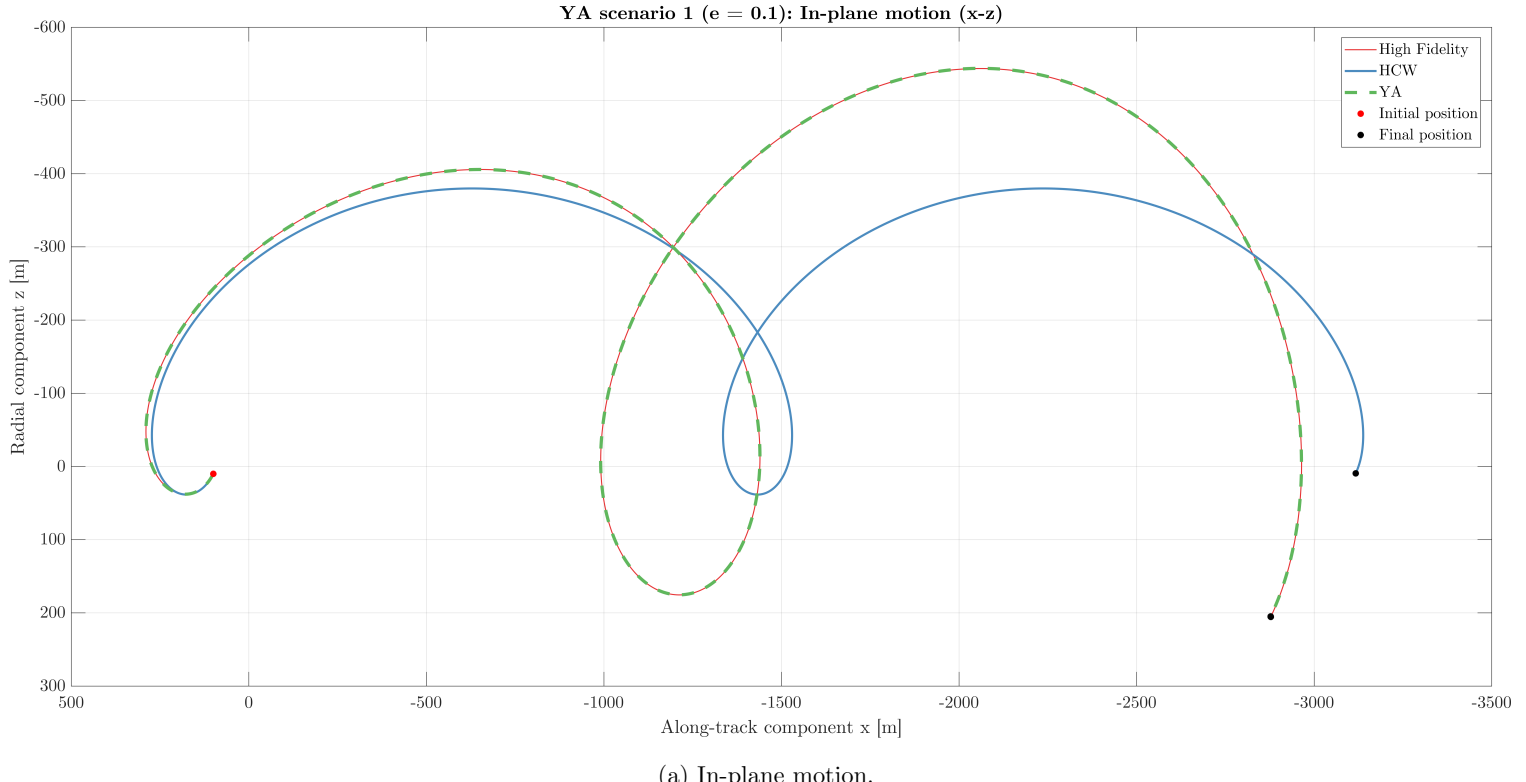
Secondly, the mean anomaly is computed from the true anomaly and the eccentricity, as explained in **REF MEAN2TRUE**. Then, the Keplerian OEs for both scenarios are:

$$\begin{cases} KOE_1 = (7.61861333 \cdot 10^6, 0.1, \pi/6, 0, 0, 0.65125326) & [\text{m}, -, \text{rad}, \text{rad}, \text{rad}, \text{rad}] \\ KOE_2 = (2.28558400 \cdot 10^7, 0.7, \pi/6, 0, 0, 0.10811191) & [\text{m}, -, \text{rad}, \text{rad}, \text{rad}, \text{rad}] \end{cases} \quad (2.22a)$$

$$(2.22b)$$

Let us now proceed with the result evaluation.

2.2.3.1 Scenario 1: $e = 0.1$.



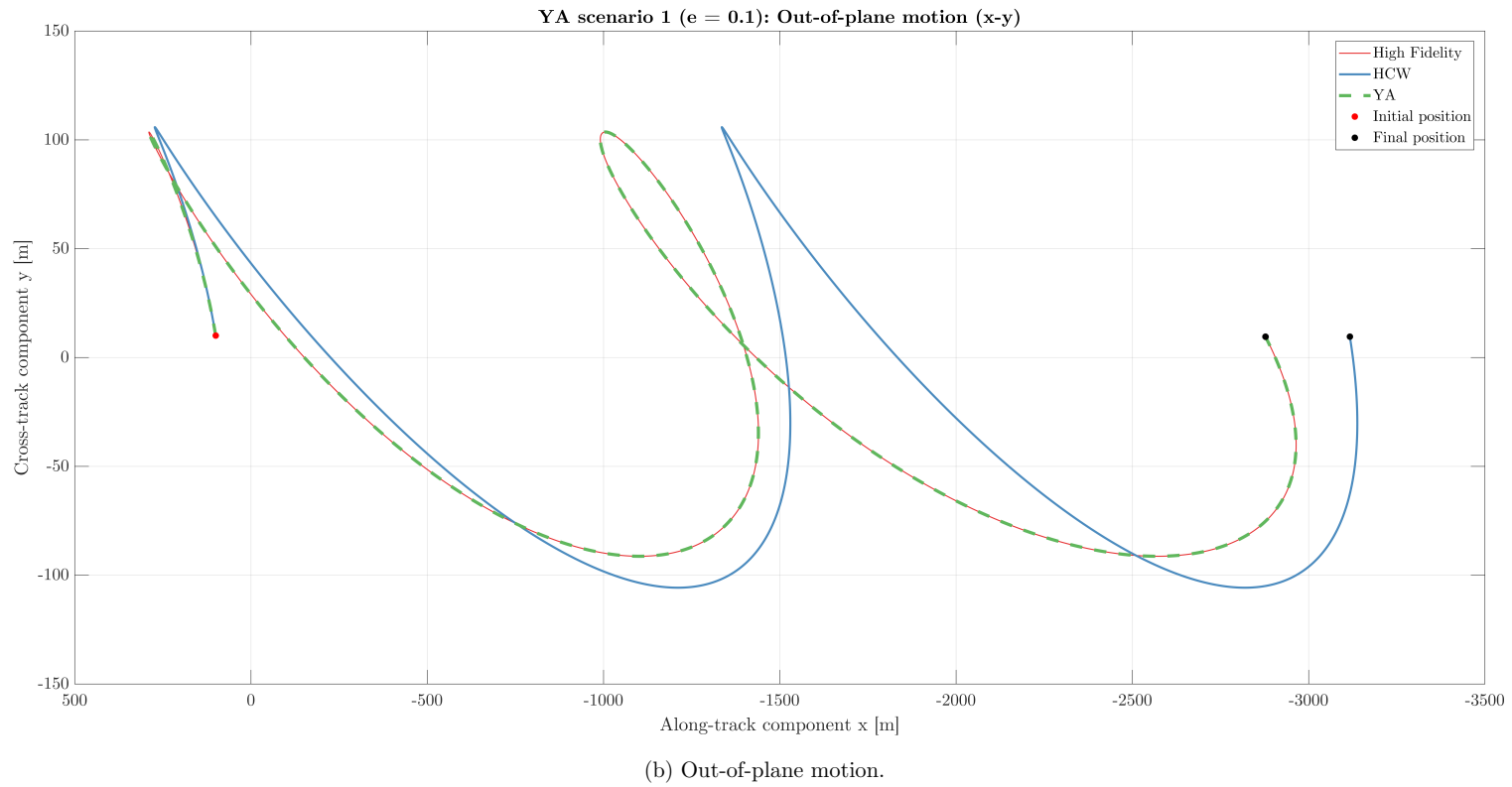
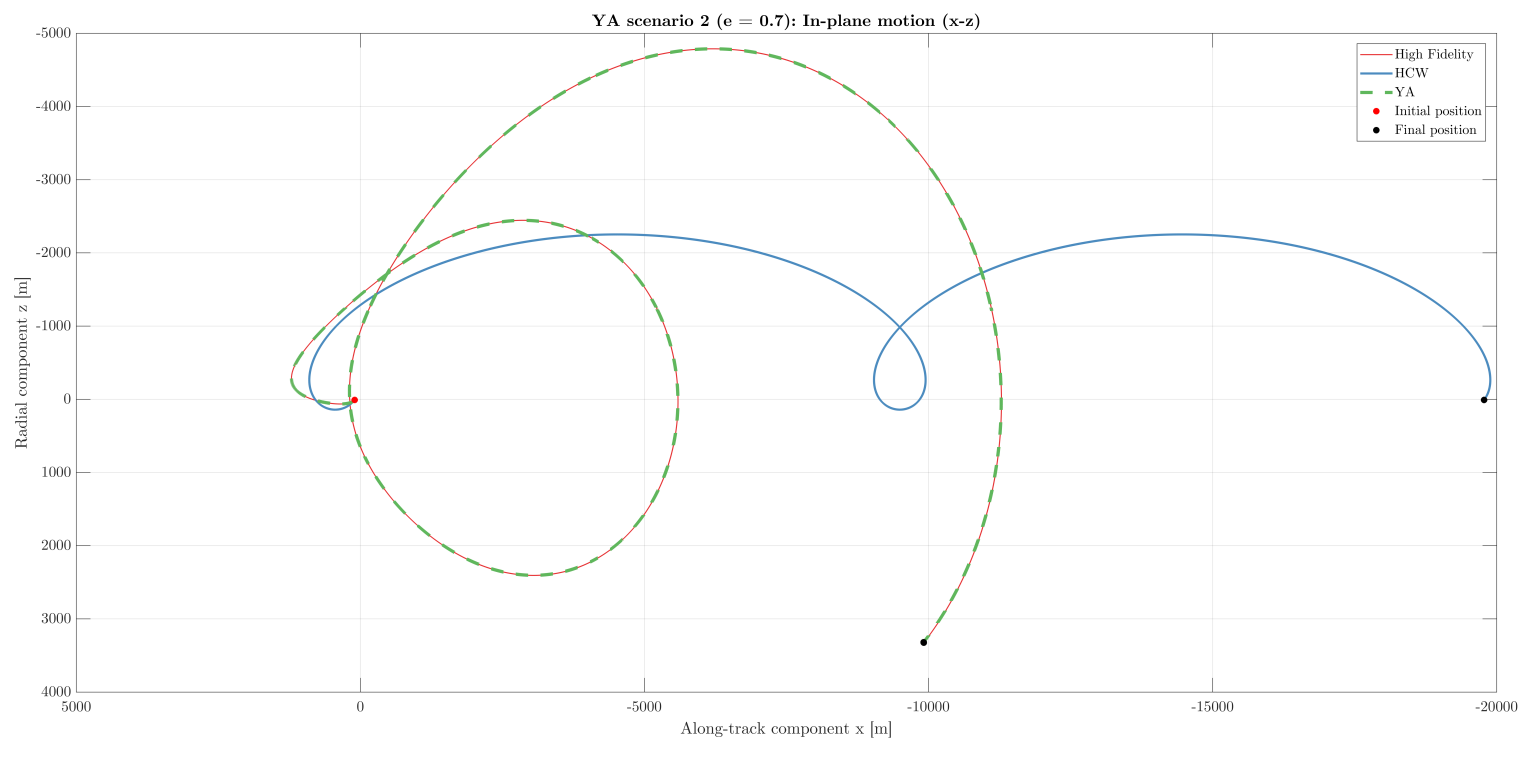


Figure 2.2: Scenario 1($e = 0.1$): Comparison between Hi-Fi, HCW and YA.

2.2.3.2 Scenario 2: $e = 0.7$.



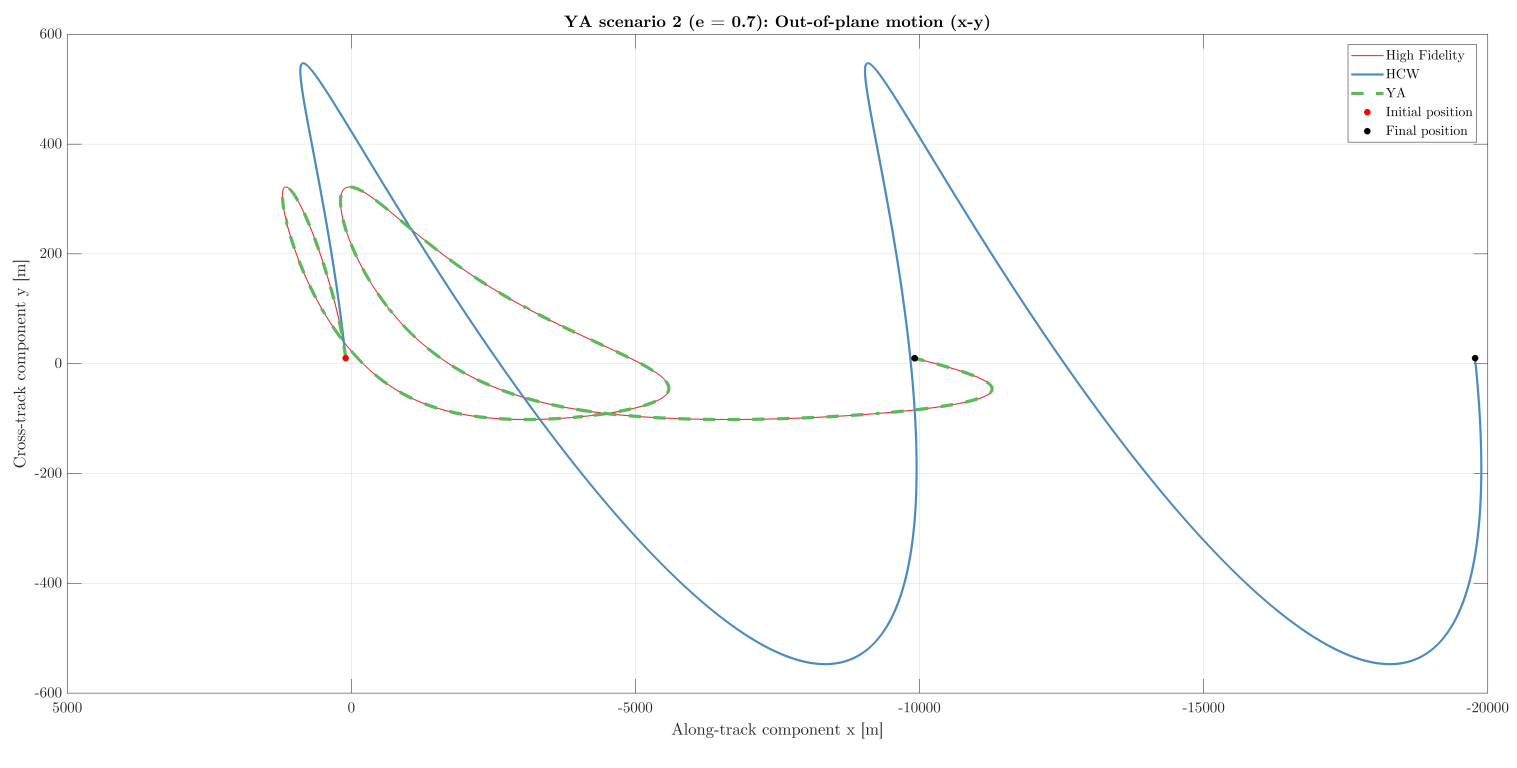


Figure 2.3: Scenario 2 ($e = 0.7$): Comparison between Hi-Fi, HCW and YA.

2.3 Orbit safety in eccentric, unperturbed orbits.

As orbit safety has already been introduced in section 1.4.1, we just need to extend it to eccentric orbits. This is neatly presented in [16], whose main concern is linear cotangential transfers. As a quick summary, trajectory safety is tightly related to the notions of relative position, looking for avoiding collision by maintaining a certain distance and orientation between the spacecrafts.

One substantial fact that differentiates eccentric and circular orbits is that orbital radius is no longer constant. As a consequence, orbital velocity is also time-varying. This two facts lead to the definition of the TAN frame (see B.4.3), which embodies a set of characteristics that allow for a much simpler description of the relative motion. That is to say, as for near-circular orbits we used the LVLH frame, we will now use the TAN frame for describing the relative motion. Later on, said advantages will be duly looked at.

This section starts by giving a brief description of the parametrization of the relative motion in the TAN frame. Secondly, general relative trajectories for eccentric reference orbits will be discussed, and finally, safe orbit families will be defined and represented, extending as well the eccentricity-inclination vector separation strategy.

2.3.1 Relative motion description in TAN frame.

In order to properly follow the herewith developed relations, it is recommended to first understand sections A.3.2.2 and B.4.3. As already explained, we analyze the radial and cross-track coordinates to ensure orbit safety, as along-track uncertainty is much larger. Our target is then to describe the relative motion in TAN frame, that is, to have a description of (y_{TAN}, z_{TAN}) in terms of some relative orbital elements, in a somewhat analog manner compared to 1.4.1.

The QNS relative OE set is quite useful in near-circular orbits, greatly simplifying the relative motion description. Nonetheless, this simplicity fades away for elliptic reference orbits. This is where the C relative OE set becomes useful. The elements C_1 , C_2 and C_3 will somehow describe the radial coordinate, while C_4 is associated with the along-track position. Finally, C_5 and C_6 describe the cross-track relative motion. We can then draft a one-to-one relation between the QNS ROEs and the C ROEs, as shown in table 2.2.

	Near-circular (RQNSOE)		Elliptic (C ROE)
Radial	δa	$\xrightarrow[\text{corresponds to}]{} \quad$	C_1
	δe_x	$\xrightarrow[\text{corresponds to}]{} \quad$	C_2
	δe_y	$\xrightarrow[\text{corresponds to}]{} \quad$	C_3
Along-track	$\delta \lambda$	$\xrightarrow[\text{corresponds to}]{} \quad$	C_4
Cross-track	δi_x	$\xrightarrow[\text{corresponds to}]{} \quad$	C_5
	δi_y	$\xrightarrow[\text{corresponds to}]{} \quad$	C_6

Table 2.2: Correspondence between QNS and C ROEs.

I. Parameter reformulation.

The description we arrived at in 1.4.1 (see equation 1.57) depended on the relative inclination and eccentricity δi and δe and the angles φ and θ . The complete $y - z$ motion in LVLH frame was then determined by four parameters: The amplitude of two oscillations and their respective phase angles. A similar formulation can be developed here for the C ROE set. Let us start by converting C_2 and C_3 into a radial amplitude C_m and a radial phase angle α as [16]:

$$\left\{ \begin{array}{l} C_m = \sqrt{C_2^2 + C_3^2} \\ \alpha = \text{atan2}(C_3, C_2) \end{array} \right. \quad (2.23a)$$

$$\left\{ \begin{array}{l} C_2 = C_m \cos \alpha \\ C_3 = C_m \sin \alpha \end{array} \right. \quad (2.23b)$$

that is,

$$\left\{ \begin{array}{l} C_2 = C_m \cos \alpha \end{array} \right. \quad (2.24a)$$

$$\left\{ \begin{array}{l} C_3 = C_m \sin \alpha \end{array} \right. \quad (2.24b)$$

Now it is turn to do the same for the cross-track component. The cross-track amplitude is defined by the ratio Λ , hand in hand with the cross-track phase β :

$$\left\{ \begin{array}{l} \Lambda C_m = \sqrt{C_5^2 + C_6^2} \end{array} \right. \quad (2.25a)$$

$$\left\{ \begin{array}{l} \beta = \text{atan2}(C_6, C_5) \end{array} \right. \quad (2.25b)$$

that is,

$$\begin{cases} C_5 = \Lambda C_m \cos \beta \\ C_6 = \Lambda C_m \sin \beta \end{cases} \quad (2.26a)$$

$$(2.26b)$$

With these expressions at hand, the description turns easier and parallel to the developed for near-circular orbits.

II. Radial and cross-track coordinates. The TAN coordinates can be easily obtained from the C ROE set and the true anomaly of the chief θ as [16, appendix B]:

$$\begin{cases} \hat{y}_{TAN} = \rho y_{TAN} = C_5 \sin \theta - C_6 \cos \theta \\ \hat{z}_{TAN} = \rho \Theta z_{TAN} = -(C_1 + C_2 \cos \theta + C_3 \sin \theta) \end{cases} \quad (2.27a)$$

$$(2.27b)$$

where the variables with a hat denote the scaled variables (unlike the regular, unscaled ones). ρ (defined as before) and $\Theta = \sqrt{2\rho - \text{eta}^2}$ are the scaling factors. Substituting (2.24) and (2.26) into (2.27) and applying trigonometric relations, we arrive to:

$$\begin{cases} \hat{y}_{TAN} = \Lambda C_m \sin(\tau - \tau_0) \\ \hat{z}_{TAN} = C_m \cos \tau - C_1 \end{cases} \quad (2.28a)$$

$$(2.28b)$$

where $\tau = \theta - \alpha$ is the radial phase referred to the maximum radial separation and $\tau_0 = \beta - \alpha$ is the relative phase between radial and cross-track motion. Now we have arrived to a very similar expression compared to (1.57), especially considering that, for bounded trajectories, $C_1 = 0$. From a very primitive analysis, we see that τ_0 will determine the shape of the $y - z$ motion, similarly to what $\varphi - \psi$ did in near-circular orbits.

2.3.2 General trajectories and safe orbits.

2.3.2.1 Orbit families.

In this context, an orbit family is a set of relative orbits who share most of the defining elements (in particular, C_1 , C_m , e and τ_0), being differenced just by the phase angle α (anomaly at which radial distance is maximum). Scaled variables are actually independent of α , conversely to the unscaled ones. This will be later graphically portrayed. As a summary, table 2.3 shows the different elements

which define an orbit family.

	Parameter	Meaning	Units
Fixed for each family	e	Chief's orbit eccentricity	[–]
	C_1	Relative radial offset	[m]
	C_m	Radial motion amplitude	[m]
	Λ	Cross-track/radial amplitude ratio	[–]
	τ_0	Cross-track/radial relative phase	[rad]
Member parameter	α	Radial motion phase	[rad]
Propagation parameter	θ	Chief's true anomaly	[rad]

Table 2.3: Parameters of an orbit family.

2.3.2.2 Eccentricity/inclination vector separation in eccentric orbits.

By simply looking at equation (2.28), it is clear that τ_0 will determine the eccentricity/inclination vector relative orientation. As for the near-circular case, the parallel configuration takes place when both phases have the same value, that is:

$$\beta = \alpha \Rightarrow \tau_0 = 0$$

In that case, the scaled coordinates behave as:

$$\begin{cases} \hat{y}_{TAN} = \Lambda C_m \sin \tau \\ \hat{z}_{TAN} = C_m \cos \tau - C_1 \end{cases} \quad (2.29a)$$

$$\begin{cases} \hat{y}_{TAN} = \Lambda C_m \sin \tau \\ \hat{z}_{TAN} = C_m \cos \tau - C_1 \end{cases} \quad (2.29b)$$

which is the equation of an ellipse with center at $(0, -C_1)$, a semimajor axis C_m and semiminor axis ΛC_m . An antiparallel configuration is obtained if $\tau_0 = \pi$, exactly as for near-circular reference orbits. Nonetheless, the useful configuration is the parallel one, and that is why we will now analyze a safe orbit family with that characteristic.

I. Scenario definition.

Our goal is to propagate a family of safe orbits, which as we know, is defined by (a) the chief's orbit and (b) the amplitudes and phase angles of the radial and cross-track components. In fact, only the eccentricity of the chief's orbit is required. Table 2.4 shows the two scenarios that have been chosen for this validation, as well as the different values of α within each family.

Parameter	Value
Chief's orbit	
Eccentricity	$e = 0.1$
Deputy's relative position (LVLH frame)	
Radial amplitude	$C_m = 10 \text{ m}$
Radial phase	$\alpha = \frac{i}{4}2\pi, \quad i = 0, 1, 2, 3, 4$
Radial offset	$C_1 _1 = 0, \quad C_1 _2 = C_m = 10 \text{ m}$
Amplitude ratio	$\Lambda = 1$
Relative phase	$\tau_0 = \beta - \alpha = 0$
Propagation parameters	
Propagation time	$N_{\text{orbits}} = 1$

Table 2.4: Testing scenarios for safe orbit implementation [16].

II. A. Bounded trajectory case ($C_1 = 0$).

Figure 2.4 shows the scaled coordinates, the unscaled coordinates (one for each α value) and the lower and upper boundaries of the relative motion. They can be easily obtained from the scaled variables by applying the maximum and minimum scaling factors, respectively. That is:

$$\begin{cases} y_{TAN,LB} = \frac{1}{\rho(\theta=0)} \Lambda C_m \sin \tau & = \frac{\Lambda C_m}{1+e} \sin \tau \\ z_{TAN,LB} = \frac{1}{\rho(\theta=0)\Theta(\theta=0)} C_m \cos \tau & = \frac{C_m}{(1+e)^2} \cos \tau \end{cases} \quad (2.30)$$

$$\begin{cases} y_{TAN,UB} = \frac{1}{\rho(\theta=\pi)} \Lambda C_m \sin \tau & = \frac{\Lambda C_m}{1-e} \sin \tau \\ z_{TAN,UB} = \frac{1}{\rho(\theta=\pi)\Theta(\theta=\pi)} C_m \cos \tau & = \frac{C_m}{(1-e)^2} \cos \tau \end{cases} \quad (2.31)$$

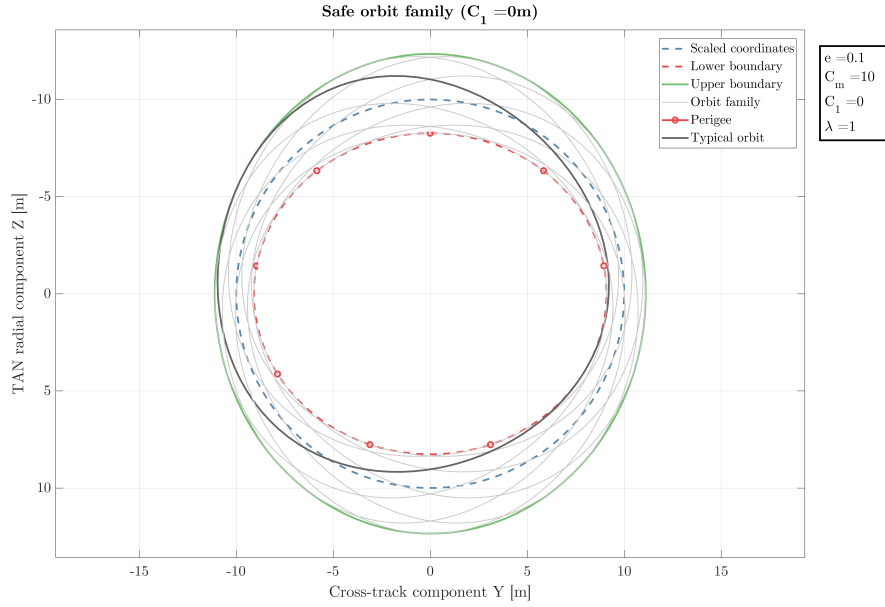


Figure 2.4: Safe orbit family: Scenario 1 ($C_1 = 0$).

As $C_1 = 0$, the every member of the family is an ellipse is centered at the origin.

II. B. Unbounded trajectory case ($C_1 = 0$).

The orbit family for this second case is shown in figure 2.5. The main difference now is that every orbit passes through the origin, as both boundaries collapse there.

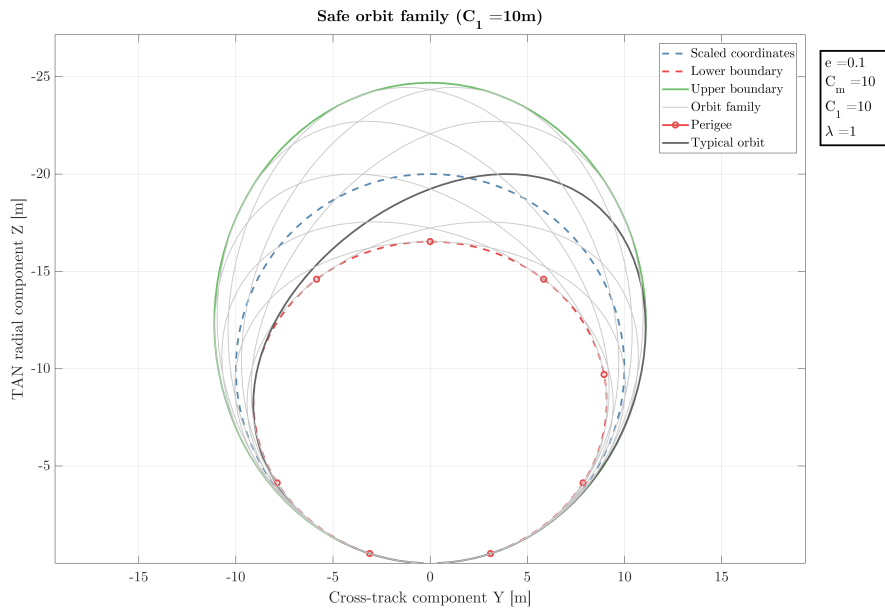
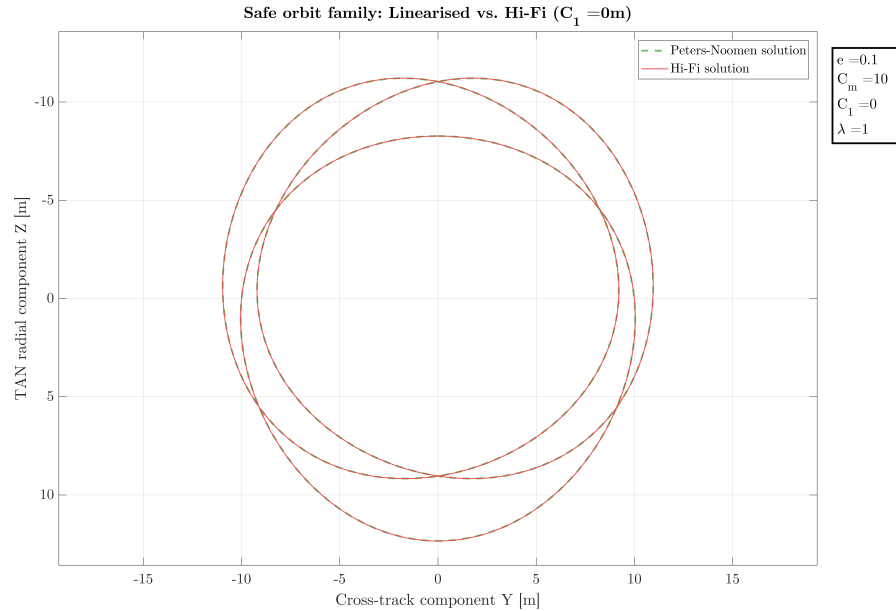


Figure 2.5: Safe orbit family: Scenario 2 ($C_1 = C_m$).

Besides analyzing the results by themselves, we can additionally compare them to a truth model

(High-Fidelity). For this to be done, we have to (a) convert the C ROEs into Keplerian and (b) define some dummy values of the chief's orbit. An example of this can be seen in figure 2.6, where some members of the previously graphed families are shown. The chief's orbit is defined by the first case specified in 2.1.



(a) Scenario 1: No offset ($C_1 = 0\text{m}$).

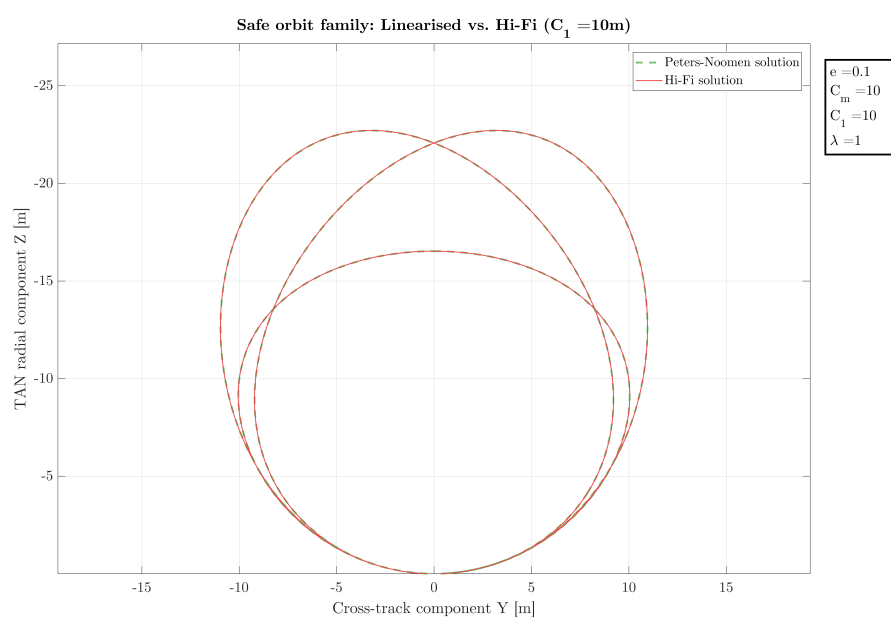
(b) Scenario 2: Offset ($C_1 = C_m = 10\text{m}$).

Figure 2.6: Comparison between Peters-Noomen approach and High-Fidelity propagation.

Absolute and relative orbital element sets.

A.1 Introduction.

The description of a spacecraft's state is done via a **state vector**. While it can include several variables with other purposes (*e.g.* filtering), its only information throughout this thesis is the position and velocity. There are two main ways to describe them:

- A. Through **cartesian coordinates**
- B. Through **orbital elements**

While the first option yields a very explicit and graphic-ready description, the second one usually has two advantages over it. Firstly, orbital elements are generally more intuitive about both the orbit and the position on it. Secondly, as orbital elements are generally slow-varying, they allow for a bigger integration timestep without losing accuracy. This is quite clear when studying keplerian motion, as most of the elements remain constant. Variational formulation and Hamilton-Jacobi theory (with the notion of changing variables as the full solution of a problem) relate to this fact.

Throughout this thesis, several sets of orbital elements have been used. The goal of this appendix is to clarify on the definition and differences between them. Absolute orbital elements (OEs) will be described first, followed by relative OEs (ROEs).

A.2 Absolute element sets.

A.2.1 Workflow for transformations between absolute element sets.

Consider two different sets of OEs, denoted by \underline{OE} and \widetilde{OE} . The transformation function $G_{OE \rightarrow \widetilde{OE}}$ between them is defined by:

$$\widetilde{OE} = G_{OE \rightarrow \widetilde{OE}}(\underline{OE}) \quad (\text{A.1})$$

A numerous amount of element sets have been historically defined. Nevertheless, some of them are much more commonly used than others. Although we will restrain ourselves to a short number of sets (say n), the number of transformations becomes arduously large as n increases ($n(n - 1)$).

In order to reduce the number of transformation functions \mathbf{G} , let us use the later defined Keplerian OEs (KOE) as a pivot, that is, building only transformations to and from KOEs. This will in turn reduce the number of required functions to $2n$. The Keplerian set also has a further advantage: as it is the classical element set, almost every other set is defined explicitly in terms of it, so that transformations to and from them can easily be derived. A simple, graphical explanation of this is shown in figure A.1.



Figure A.1: Workflow for transforming between two arbitrary absolute element sets.

A.2.2 Element sets.

A.2.2.1 Keplerian orbital elements (KOE).

The Keplerian set of OEs (KOE) is one of the most widely used and classic options. While the last element may change from author to author, an usual definition is the following:

$$\left\{ \begin{array}{lll} a & \equiv & \text{Semimajor axis} & [L] \\ e & \equiv & \text{Eccentricity} & [-] \\ i & \equiv & \text{Inclination} & [\text{rad}] \\ \Omega \text{ or } RAAN & \equiv & \text{Right ascension of the ascending node} & [\text{rad}] \\ \omega & \equiv & \text{Argument of periapsis} & [\text{rad}] \\ M & \equiv & \text{Mean anomaly} & [\text{rad}] \end{array} \right. \quad (\text{A.2})$$

The last element commonly varies across literature, being substituted by the true anomaly θ ; or, when tackling the variation of orbital parameters, by the mean anomaly at $t = 0$ (M_0) or the perigee time T_0 [2]. Mean anomaly is used due to the simplicity of its unperturbed variational equation, as it has a constant rate (denoted by n). The geometrical meaning and definition of these elements is out from the scope of this thesis. Nonetheless, figure A.2 shows a simple geometrical drawing of the involved angles.

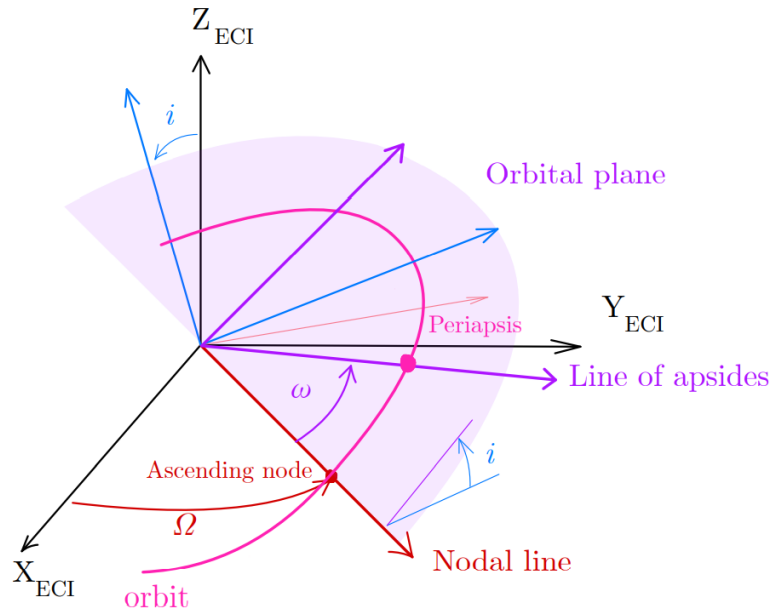


Figure A.2: Frame rotation from inertial to perifocal frame.

As it is seen in the figure before, the Keplerian elements become singular in two cases:

- A. If the **inclination** is null, the orbital plane is coincident with the inertial reference (ECI x-y) plane. The ascending node is hence undefined in this case.
- B. If the **eccentricity** is null, the periapsis is not defined, as it is the nearest point of the orbit around the central body. Thus, there is no angle defining its position, making the argument of periapsis nonsingular.

These singularities are unfortunately quite common in orbit design. They correspond respectively with equatorial and circular orbits. In order to avoid this behaviour, many different elements sets have been defined. Wiesel [2] shows an intuitive approach in chapter 2.10, solving either problem with a graphic approach.

A.2.2.2 Eccentricity/inclination vectors orbital elements (EIOE).

This set, originally defined for geostationary orbits in absolute terms [7], is used mainly as a relative OE set. Though it is actually not used along this thesis, its definition is helpful for introducing the common relative counterpart. In any case, let us proceed with the eccentricity and inclination vectors concept.

Eccentricity vector

The notion of the eccentricity vector is quite basic, as it is, when in unperturbed motion, a constant of the dynamic system. It is defined as the eccentricity-sized vector pointing towards the perigee. Nonetheless, for this purpose, the eccentricity vector is defined as [DAmico · montenbruck]:

$$\underline{e} = \begin{Bmatrix} e_x \\ e_y \end{Bmatrix} = e \begin{Bmatrix} \cos \varpi \\ \sin \varpi \end{Bmatrix} \quad (\text{A.3})$$

where the argument of perigee ω might be substituted with the sum $\omega + \Omega$ [as in 7]. A graphical representation can be seen later in the relative definition A.5(a). As it arises from (A.3), it substitutes the eccentricity and argument of perigee from the Keplerian OE set.

Inclination vector

The inclination vector is perpendicular to the orbital plane, similarly to the angular momentum, but inclination-sized. It is defined by its components as [7]:

$$\underline{i} = \begin{Bmatrix} i_x \\ i_y \end{Bmatrix} = i \begin{Bmatrix} \cos \Omega \\ \sin \Omega \end{Bmatrix}$$

The graphical interpretation is not as straightforward as for the eccentricity vector. Nonetheless, we are only interested in the definition itself. It is clear that this components substitute the out-of-plane related elements i and Ω .

Element set

The EI orbital element set is then composed of:

$$\left\{ \begin{array}{lcl} a & \equiv & \text{Semimajor axis} & [L] \\ e_x = e \cos \omega & \equiv & \text{x-projection of } \underline{e} & [-] \\ e_y = e \sin \omega & \equiv & \text{y-projection of } \underline{e} & [-] \\ i_x & \equiv & \text{x-component of } \underline{i} & [-] \\ i_y & \equiv & \text{y-component of } \underline{i} & [-] \\ \lambda = \omega + M & \equiv & \text{Mean argument of latitude} & [\text{rad}] \end{array} \right. \quad (\text{A.4})$$

A.2.2.3 Quasi-nonsingular orbital elements (QNSOE).

The quasi-nonsingular (QNS) orbital element set tackles the singularity existing in circular orbits [17], [18] [19]. It is quite similar to the formerly defined EI set, as it uses again the components of the eccentricity vector to substitute e and ω . The set is then defined as:

$$\left\{ \begin{array}{lcl} a & \equiv & \text{Semimajor axis} & [L] \\ q_1 = e \cos \omega & \equiv & \text{x-projection of } \underline{e} & [--] \\ q_2 = e \sin \omega & \equiv & \text{y-projection of } \underline{e} & [--] \\ i & \equiv & \text{Inclination} & [\text{rad}] \\ \Omega & \equiv & \text{Right ascension of the ascending node} & [\text{rad}] \\ u = \omega + \theta & \equiv & \text{True argument of latitude} & [\text{rad}] \end{array} \right. \quad (\text{A.5})$$

Though some authors use a different order, this is the one used in this thesis, so as to keep the time-varying element on the last place.

A.2.2.4 Equinoctial orbital elements (EOE).

The QNS set of elements only solved half of the singularity problem. To solve both, thus enabling the description of equatorial and polar orbits, the equinoctial set of elements is defined as:

$$\left\{ \begin{array}{lcl} a & \equiv & \text{Semimajor axis} & [L] \\ P_1 = e \cos \varpi & \equiv & \text{unclear physical meaning, similar to } e_x & [--] \\ P_2 = e \sin \varpi & \equiv & \text{unclear physical meaning, similar to } e_y & [--] \\ Q_1 = \tan \frac{i}{2} \cos \Omega & \equiv & \text{unclear physical meaning, similar to } i_x & [--] \\ Q_2 = \tan \frac{i}{2} \sin \Omega & \equiv & \text{unclear physical meaning, similar to } i_y & [--] \\ L = \Omega + \omega + \theta & \equiv & \text{True longitude} & [\text{rad}] \end{array} \right. \quad (\text{A.6})$$

Not only does the order does change depending on the author, but also the symbols to refer to them. An example of its use is [17].

A.2.2.5 Delaunay orbital elements (DOE).

Delaunay elements arise when formulating the two-body problem through analytical mechanics. All of the previous element sets are clearly non-canonical (*i.e.* they do not satisfy Hamilton's equations). Starting from the canonical set of elements (see appendix ??), Delaunay elements are reached

after performing a canonical transformation, leading to the following definition:

$$\left\{ \begin{array}{lll} L = \sqrt{\mu a} & \equiv & \text{unclear physical meaning} & [L^{1/2}] \\ G = L\sqrt{1-e^2} & \equiv & \text{Angular momentum} & [L^{1/2}] \\ H = G \cos i & \equiv & \text{Polar component of angular momentum} & [L^{1/2}] \\ l = M & \equiv & \text{Mean anomaly} & [\text{rad}] \\ g = \omega & \equiv & \text{Argument of perigee} & [\text{rad}] \\ h = \Omega & \equiv & \text{Right ascension of ascending node} & [\text{rad}] \end{array} \right. \quad (\text{A.7})$$

This set is mainly used in the context of perturbations, as it yields a very convenient expression for the perturbed Hamiltonian (see section **PUT SECTION HERE**).

A.3 Relative sets.

Relative elements are at the deepest roots of spacecraft relative motion, offering several advantages over cartesian relative states. First and foremost, they are more intuitive, but they also lead to a reduction of linearisation errors when expanding the deputy's movement around the chief's orbit [20]. In general, relative elements are defined as:

$$\delta \underline{OE} = \mathbf{f} (\underline{OE}_C, \underline{OE}_D) \quad (\text{A.8})$$

which is usually simplified by just taking the arithmetic difference between them, namely

$$\delta \underline{OE} = \underline{OE}_D - \underline{OE}_C \quad (\text{A.9})$$

where the subscripts denote respectively the deputy and chief spacecraft. The question now is, how do transformations between ROEs work.

A.3.1 Workflow for transformations between ROEs.

As for the absolute elements, Keplerian elements will be used as a pivot point. That means that only the transformations from and to RKOEs must be implemented. There are then two types of transformations:

A) From any ROE set to RKOE

While authors provide with scenarios expressed in their own ROE set, the element choice for our simulator is the Keplerian set. That leads us to the need of implementing a transformation from the former set to the latter. Let us assume then the following inputs and outputs:

- **Inputs:**

- $\widetilde{\underline{ROE}} = \delta\widetilde{\underline{OE}}$: Different type of ROEs, whose absolute equivalents are known as a function of the KOEs ($\widetilde{\underline{OE}} = \mathbf{f}(\underline{KOE})$)
- \underline{KOE}_C : Chief spacecraft/reference orbit KOEs

- **Output:**

- $\underline{RKOE} = \delta\underline{KOE}$: Keplerian ROEs

Taking equation (A.9) and particularizing it for KOEs:

$$\delta\underline{KOE} = \underline{KOE}_D - \underline{KOE}_C \quad (\text{A.10})$$

while the second term is known (input), the second one must be calculated through a certain process:

1. Calculate chief's OEs in the source phase space (*i.e.* $\widetilde{\underline{OE}}_C$)

$$\widetilde{\underline{OE}}_C = \mathbf{G}_{KOE \rightarrow \widetilde{OE}}(\underline{KOE}_C)$$

2. Compute deputy's OEs by direct addition

$$\widetilde{\underline{OE}}_D = \widetilde{\underline{OE}}_C + \delta\widetilde{\underline{OE}}$$

3. Compute deputy's KOEs by back-transformation

$$\underline{KOE}_D = \mathbf{G}_{\widetilde{OE} \rightarrow KOE}(\underline{OE}_D)$$

4. Subtract chief's KOEs from deputy's

$$\delta\underline{KOE} = \underline{KOE}_D - \underline{KOE}_C$$

See graphic A.3 for a more visual explanation.

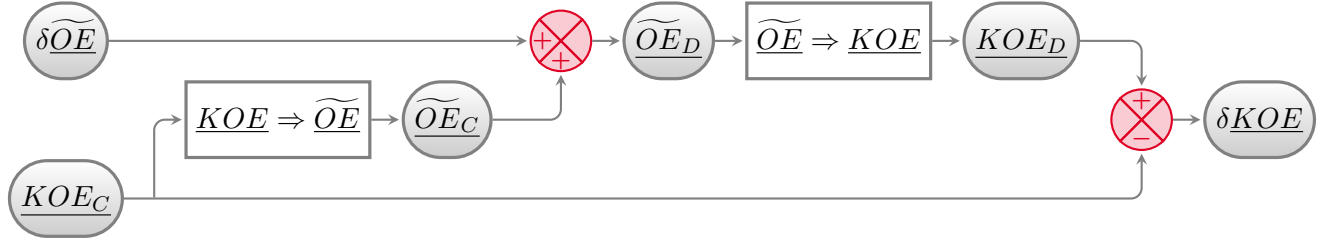


Figure A.3: Workflow for transforming any relative set into KOE.

B) From RKOE to any ROE set

In this case, let us assume the next inputs and outputs:

- **Inputs:**

- $\underline{RKOE} = \delta\underline{KOE}$: Keplerian ROEs
- \underline{KOE}_C : Chief KOEs

- **Output:**

- $\underline{ROE} = \delta\underline{OE}$: Different type of ROEs, whose absolute equivalents are known as a function of the KOEs ($\underline{OE} = f(\underline{KOE})$)

For this transformation, the equation A.8 particularized for this case acquires the following shape:

$$\delta\underline{OE} = \underline{OE}_D - \underline{OE}_C \quad (\text{A.11})$$

Equation A.11 can be tackled in two main ways:

- A. Using the pertinent transformations, compute the absolute elements for both spacecrafts \underline{OE}_D , \underline{OE}_C , and then calculate the arithmetic difference (in a A.3.1). See graphic A.4.
- B. Expand the deputy absolute OEs (*i.e.* \underline{OE}_D) around the chief via a Taylor series expansion with respect to the Keplerian set of elements, retaining terms up to first order, achieving a linearised expression for the transformation. Mathematically:

$$\underline{OE}_D = \underline{OE}(KOE_D) = \underline{OE}(KOE_C + \delta\underline{KOE}) = \underline{OE}_C + \frac{\partial \underline{OE}}{\partial \underline{KOE}} \delta\underline{KOE} + \mathcal{O}(\delta\underline{KOE}^2)$$

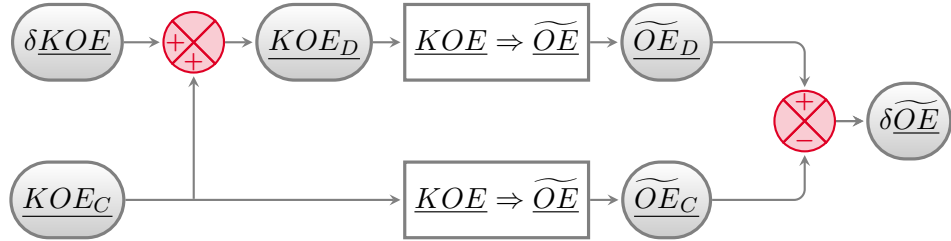


Figure A.4: Workflow for transforming RKOE into any other set.

hence,

$$\delta\widetilde{OE} \approx \widetilde{OE}_C + \frac{\partial\widetilde{OE}}{\partial\underline{KOE}}\delta\underline{KOE} - \widetilde{OE}_C = \frac{\partial\widetilde{OE}}{\partial\underline{KOE}}\delta\underline{KOE} \quad (\text{A.12})$$

where the Jacobian matrix is generally simple, as it usually only implies polynomic or trigonometric functions. Equation (A.12) is then a first order approximation of (A.11). Its validity is then reduced to a close proximity between both spacecrafts, which should be assessed.

A.3.2 Element sets.

Besides the ones derived directly from its absolute counterparts, a couple of additional ROE sets will be herewith defined and explained. This is due to one of two reasons. The first one is that some ROE sets are only defined in relative terms, lacking any absolute equivalent. The second one is that it might be interesting to dive in the meaning of the relative sets, deriving interesting relations that would otherwise be overlooked.

A.3.2.1 Relative eccentricity/inclination vectors orbital elements (REIOE).

This ROE set is the counterpart of the EI set (see A.2.2.2). It is nonetheless interesting to see the meaning and shape of it, as it is quite widely used in literature [DAmico'montenbruck, 18, 19]. Let us first define its elements, to later analyze the meaning behind them:

$$\left\{ \begin{array}{lcl} \delta a & \equiv & \text{Relative semimajor axis} & [L] \\ \delta e_x & \equiv & \text{Relative x-component of } \underline{e} & [-] \\ \delta e_y & \equiv & \text{Relative y-component of } \underline{e} & [-] \\ \delta i_x & \equiv & \text{Relative x-component of } \underline{i} & [-] \\ \delta i_y & \equiv & \text{Relative y-component of } \underline{i} & [-] \\ \delta \lambda & \equiv & \text{Relative mean argument of latitude} & [\text{rad}] \end{array} \right. \quad (\text{A.13})$$

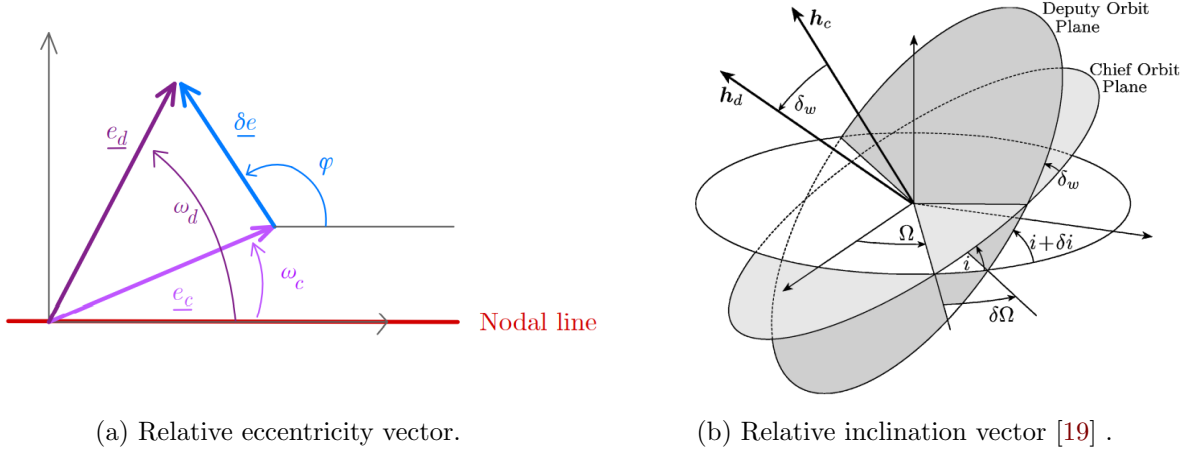


Figure A.5: Relative eccentricity & inclination vectors.

Concept & meaning

The relative eccentricity vector components substitute the relative eccentricity and the relative argument of perigee. It is based on the eccentricity vector definition (A.3), and a graphical representation can be seen in figure A.5(a). Mathematically:

$$\underline{\delta e} = \begin{Bmatrix} \delta e_x \\ \delta e_y \end{Bmatrix} = \delta e \begin{Bmatrix} \cos \varphi \\ \sin \varphi \end{Bmatrix}$$

which rules the in-plane relative motion (hand in hand with δa and $\delta \lambda$). As we know, there are two ways of tackling the transformation from RKOE to this set (see A.3.1). Though the nonlinear form is exact, let us analyze the linear version. If we assume that the difference in the eccentricity vector is due to that of the eccentricity and argument of perigee (δe , $\delta \omega$), we arrive to:

$$\underline{\delta e} \approx \begin{bmatrix} \cos \omega & -e \sin \omega \\ \sin \omega & e \cos \omega \end{bmatrix} \begin{Bmatrix} \delta e \\ \delta \omega \end{Bmatrix} \quad (\text{A.14})$$

where we have neglected terms of second order and higher. The relative inclination vector is defined in an alternative way [DAmico & montenbruck] (comparing with the absolute counterpart). Mathe-

matically:

$$\delta \underline{i} = \sin \delta i \begin{Bmatrix} \cos \theta \\ \sin \theta \end{Bmatrix}$$

where θ is the analog angle to φ in the eccentricity vector. Once again, let us analyze the linearized transformation from RKOE to this set, considering the differences δi and $\delta \Omega$. Applying the law of sines and the law of cosines for spherical trigonometry and assuming small values of δi and $\delta \Omega$, we arrive to:

$$\delta \underline{i} = \begin{Bmatrix} \delta i \\ \sin i \delta \Omega \end{Bmatrix} \approx \begin{bmatrix} 1 & 0 \\ 0 & \sin i \end{bmatrix} \begin{Bmatrix} \delta i \\ \delta \Omega \end{Bmatrix} \quad (\text{A.15})$$

where i is the inclination of the chief's orbit. Combining the results of (A.14) and (A.15) with the definitions of the remaining elements, we can easily arrive to an expression analog to (A.12):

$$\left\{ \begin{array}{l} \delta a \\ \delta e_x \\ \delta e_y \\ \delta i_x \\ \delta i_y \\ \delta \lambda \end{array} \right\} \approx \begin{bmatrix} 1 & 0 & 0 & 0 & 0 & 0 \\ 0 & \cos \omega & 0 & 0 & -e \sin \omega & 0 \\ 0 & \sin \omega & 0 & 0 & e \cos \omega & 0 \\ 0 & 0 & 1 & 0 & 0 & 0 \\ 0 & 0 & 0 & \sin i & 0 & 0 \\ 0 & 0 & 0 & 0 & 1 & 1 \end{bmatrix} \left\{ \begin{array}{l} \delta a \\ \delta e \\ \delta i \\ \delta \Omega \\ \delta \omega \\ \delta M \end{array} \right\} \quad (\text{A.16})$$

A graphical representation of this concept can be seen in figure A.5(b).

A.3.2.2 Peters-Noomen C set of relative orbital elements (CROE).

Defined by Peters & Noomen in [16], this set is also closely related with the orbit safety notion. It arises from the analysis of the Gauss Variational Equations (GVEs) applied to the relative dynamics between a deputy and a chief spacecraft, when the former performs a cotangential transfer. Without

further ado, let us define them as:

$$\left\{ \begin{array}{lll} C_1 = \delta p = \eta^2 \delta a - 2 a e \delta e & \equiv & \text{Relative parameter of the orbit} [L] \\ C_2 = e \delta p - p \delta e & \equiv & \text{unclear physical meaning} [L] \\ C_3 = -e p (\delta \omega + \cos i \delta \Omega) & \equiv & \text{unclear physical meaning} [L] \\ C_4 = a (\delta \omega + \cos i \delta \Omega + \eta^{-1} \delta M) & \equiv & \text{Modified relative mean longitude} [L] \\ C_5 = -p (\cos \omega \delta i + \sin i \sin \omega \delta \Omega) & \equiv & \text{unclear physical meaning} [L] \\ C_6 = p (\sin \omega \delta i - \sin i \cos \omega \delta \Omega) & \equiv & \text{unclear physical meaning} [L] \end{array} \right. \quad (\text{A.17})$$

For a proper geometrical and conceptual description of the elements, please see [16]. As an introduction, the first four elements essentially determine the in-plane relative motion. C_1 , C_2 & C_3 arise from a very intelligent interpretation of the GVEs, with C_4 completing the element set. On the other hand, elements C_5 and C_6 describe the out-of-plane motion.

Cartesian reference systems.

B.1 Introduction.

Cartesian states are, as mentioned in appendix A, one of the two main alternatives to describe the state of a certain spacecraft (or celestial body). Though orbital elements (OEs) are generally more intuitive and meaningful, these states are quite critical for the description of both absolute and relative motion. Ultimately, and specially considering the latter, we wish to know the relative orientation and linear distance between the involved bodies. During this appendix, a set of absolute and relative reference frames will be described and related via transformations, which have been used time and again along this thesis.

B.1.1 Inertial and rotating reference frames.

Technically, an inertial reference frame is one where Newton's law holds. Effectively, it is a frame which is not object of any acceleration whatsoever. It is then, when interpreted to the letter, an idealization, as there will always be any perturbation which disavows this assumption. Nonetheless, it is usual to neglect said perturbations up to a certain point, thus considering pseudo-inertial reference frames. From now on then, when inertial reference frames are mentioned they will be considered so, even though they are actually not. Along this thesis, both inertial and rotating frames will be considered, each bearing its different advantages and disadvantages.

B.1.2 Absolute and relative frames.

Another distinction that will be made is between absolute and relative frames. In this thesis, absolute frames are those who are centered in the Earth's center of mass, while relative frames are defined with respect to a reference orbit (the chief's generally). Again, they have different scopes, though relations between them need to be developed.

B.1.3 Time measurement.

Later it will be described how Earth's rotational state influences the dynamics of the spacecrafts, due to its non-homogeneous mass distribution. That leads to the need of precisely computing it,

which in turn requires the time elapsed since a given epoch. This section intends to briefly describe the most usual conventions for time definition, without diving in technical considerations. For further description, see [21]. These conventions are:

- I. International Atomic Time (TAI): Physical timescale which is calculated through the measurement of cesium radiation. Lacks intuitive meaning, but acts as a ultra-high precision time system and reference for other timescales.
- II. Universal Time (UT1/UT2): Civil time system, which is defined by the right ascension of the mean Sun. It is not a continuous time system, varying as time passes.
- III. Coordinated Universal Time (UTC): Civil time system, which is measured with TAI and synchronized with UT1 via leap seconds to get within 1-second range. It is then a non-continuous time system.
- IV. Terrestrial Time (TT): Civil time system, which is measured with TAI but has a delay with respect to it (32.184 seconds).

Figure B.1 shows more clearly the differences between them.

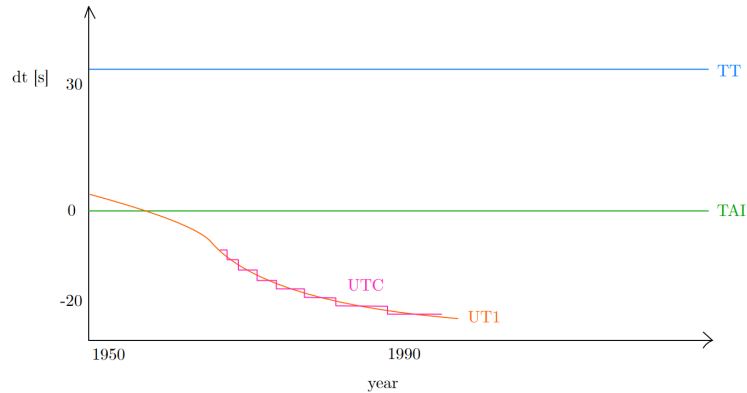


Figure B.1: Sketch of the different time systems.

B.2 Transformations between reference systems.

In this section, two approaches for reference system transformations will be presented. These will prove quite useful later on, helping to clarify how different systems relate to each other.

For the sake of generality, let us consider an inertial and absolute reference frame, and a rotating, relative reference frame (see figure B.2). In case we need to consider two absolute systems, it is enough to just nullify the displacement between both frames' origins. The notation used is described below:

- Vectors: \underline{X} refers to a vector with respect an absolute frame, while \underline{x} is used for relative reference frames. Please, note that we are not making use of any reference system (*i.e.* vector base): we are just considering the vector entity as an object.
- Subscripts: Unless specified otherwise, denote the body: \bullet_C for the chief, \bullet_D for the deputy.
- Time derivatives and superscripts: As Coriolis' Theorem states, when non-inertial reference frames are involved, it is necessary to specify the frame with respect to which the derivative is calculated. $\frac{\mathcal{F}d\bullet}{dt}$ denotes the time derivative in the frame \mathcal{F} . An equally valid yet more compact notation is $\dot{\bullet}^{\mathcal{F}}$.
- Right vertical bar subscript: Denotes the coordinate system in which one vector or matrix is described. For example, $\underline{u}|_1 = \sum_{i=1}^3 u_{xi} \hat{e}_{i1}$.

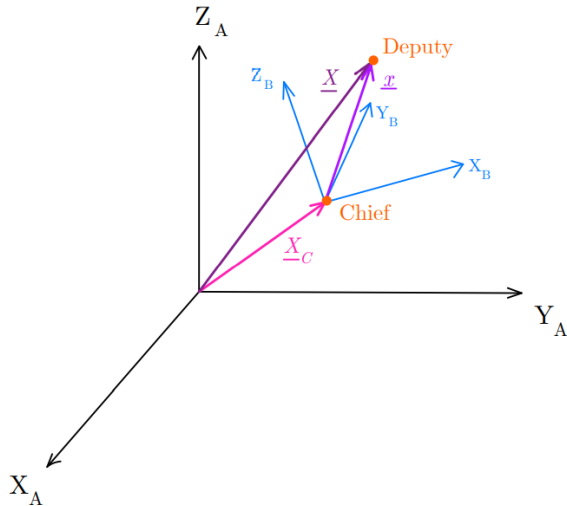


Figure B.2: Absolute and relative frames.

Consider the frames A and B from figure B.2. Let us address firstly the transformation from $A \rightarrow B$, that is, converting an absolute & inertial state vector expressed in coordinate system A to the relative, rotating frame B in its coordinates. What we would like to achieve is a relationship of the form:

$$\begin{cases} \underline{x}|_B &= \mathbf{f}_1 (\underline{X}|_A, \dots, \underline{X}_C|_A, \dots) \\ \dot{\underline{x}}^B|_B &= \mathbf{f}_2 (\underline{X}|_A, \dot{\underline{X}}^A|_A, \underline{X}_C|_A, \dot{\underline{X}}_C^A|_A) \end{cases}$$

As it turns out, this relation is actually linear on the inputs $\dot{\underline{X}}^A|_A$ and $\underline{X}|_A$. From this point on, two approaches are derived:

B.2.1 Direct analytical differentiation.

The first approach starts from the decomposition of the deputy's absolute position vector [22]:

$$\underline{X} = \underline{X}_C + \underline{x} \rightarrow \underline{x} = \underline{X} - \underline{X}_C$$

This vector can be expressed in both coordinate systems, namely $\underline{x}|_A$ and $\underline{x}|_B$. The transformation between them can be written as the following rotation:

$$\underline{x}|_B = R_{A \rightarrow B} \underline{x}|_A \quad (\text{B.1})$$

The rotation matrix $R_{A \rightarrow B}$ takes the following form:

$$R_{A \rightarrow B} = \begin{bmatrix} (\hat{e}_{xA} \cdot \hat{e}_{xB}) & (\hat{e}_{yA} \cdot \hat{e}_{xB}) & (\hat{e}_{zA} \cdot \hat{e}_{xB}) \\ (\hat{e}_{xA} \cdot \hat{e}_{yB}) & (\hat{e}_{yA} \cdot \hat{e}_{yB}) & (\hat{e}_{zA} \cdot \hat{e}_{yB}) \\ (\hat{e}_{xA} \cdot \hat{e}_{zB}) & (\hat{e}_{yA} \cdot \hat{e}_{zB}) & (\hat{e}_{zA} \cdot \hat{e}_{zB}) \end{bmatrix}$$

where each column is the coordinates of each base vector of the “origin” coordinate system expressed in the “final” one. This fact is specially useful when such vectors are characteristic of the problem at hand, as it is the case for the two body problem. In order to transform the velocity vector, let us just take the time derivative of B.1, yielding:

$$\dot{\underline{x}}|_B = \dot{R}_{A \rightarrow B} \underline{x}|_A + R_{A \rightarrow B} \dot{\underline{x}}|_A \quad (\text{B.2})$$

whose first derivative $\dot{R}_{A \rightarrow B}$ can be calculated by columns, simplifying the task at hand if we have been able to obtain the origin base $(\hat{e}_{xA}, \hat{e}_{yA}, \hat{e}_{zA})$ in terms of the final one. For the sake of completeness, let us remind that [22]:

$$\frac{d}{dt} \hat{u} = \frac{1}{u} [\dot{u} - (\hat{u} \cdot \dot{u}) \hat{u}] \quad (\text{B.3})$$

A final, more compact form of both B.1 and B.2 can be reached by rearranging terms:

$$\begin{Bmatrix} \underline{x}|_B \\ \dot{\underline{x}}^B|_B \end{Bmatrix} = \begin{bmatrix} R_{A \rightarrow B} & 0_{3 \times 3} \\ \dot{R}_{A \rightarrow B} & R_{A \rightarrow B} \end{bmatrix} \begin{Bmatrix} \underline{X}|_A - \underline{X}_C|_A \\ \dot{\underline{X}}^A|_A - \dot{\underline{X}}_C^A|_A \end{Bmatrix} \quad (\text{B.4})$$

and the inverse transformation can be expressed as:

$$\begin{Bmatrix} \underline{\underline{X}}|_A \\ \dot{\underline{\underline{X}}}^A|_A \end{Bmatrix} = \begin{bmatrix} R_{B \rightarrow A} & 0_{3 \times 3} \\ \dot{R}_{B \rightarrow A} & R_{B \rightarrow A} \end{bmatrix} \begin{Bmatrix} \underline{\underline{x}}|_B \\ \dot{\underline{\underline{x}}}^B|_B \end{Bmatrix} + \begin{Bmatrix} \underline{\underline{X}}_C|_A \\ \dot{\underline{\underline{X}}}_C^A|_A \end{Bmatrix} \quad (\text{B.5})$$

An example of this approach will be developed later on in [B.4.2.2](#).

B.2.2 Classical motion composition.

This approach, rather on pure derivation, is based on the grounds of motion composition and Coriolis' Theorem. This theorem states that the derivative of a vector in an inertial frame is equivalent to the derivative in a rotating frame plus another contribution due to the rotation of this reference frame:

$$\frac{^A d\underline{u}}{dt} = \frac{^B d\underline{u}}{dt} + \underline{\omega}_{B||A} \times \underline{u}$$

The first term of the right-hand side is associated to the temporal variation of the coordinates of \underline{u} in the rotating frame, whereas the second one is purely related to the relative rotation between both frames. If we apply this to [B.1](#):

$$\begin{aligned} \frac{^A d\underline{X}}{dt} &= \frac{^A d\underline{X}_C}{dt} + \frac{^A d\underline{x}}{dt} = \frac{^A d\underline{X}_C}{dt} + \frac{^B d\underline{x}}{dt} + \underline{\omega}_{B||A} \times \underline{x} \\ \Rightarrow \dot{\underline{\underline{X}}}^A &= \dot{\underline{\underline{X}}}_C^A + \dot{\underline{x}}^B + \underline{\omega}_{B||A} \times \underline{x} \end{aligned} \quad (\text{B.6})$$

As before, let us first go from the inertial frame towards the rotating. For that purpose, let us substitute [\(B.1\)](#) into [\(B.6\)](#), solving for $\dot{\underline{x}}^B$:

$$\dot{\underline{x}}^B = \dot{\underline{\underline{X}}}^A - \dot{\underline{\underline{X}}}_C^A - \underline{\omega}_{B||A} \times (\underline{X} - \underline{X}_C) \quad (\text{B.7})$$

Now, expressing every vector in its proper frame:

$$\dot{\underline{x}}^B|_B = R_{A \rightarrow B} \left[\dot{\underline{\underline{X}}}^A|_A - \dot{\underline{\underline{X}}}_C^A|_A + \underline{\omega}_{A||B}|_A \times (\underline{X}|_A - \underline{X}_C|_A) \right] \quad (\text{B.8})$$

Let's make use now of the axial-dual vector form, leading to:

$$\dot{\underline{x}}^B|_B = R_{A \rightarrow B} \left[\dot{\underline{\underline{X}}}^A|_A - \dot{\underline{\underline{X}}}_C^A|_A + \Omega_{A||B}|_A (\underline{X}|_A - \underline{X}_C|_A) \right] \quad (\text{B.9})$$

where $\Omega_{A||B}$ is the matrix dual form of $\underline{\omega}_{A \rightarrow B}$, that is:

$$\Omega_{A||B} = \begin{bmatrix} 0 & -\omega_z & \omega_y \\ \omega_z & 0 & -\omega_x \\ -\omega_y & \omega_x & 0 \end{bmatrix}$$

We can now express the conversion in a far more compact form as:

$$\begin{Bmatrix} \underline{x}|_B \\ \dot{\underline{x}}^B|_B \end{Bmatrix} = \begin{bmatrix} R_{A \rightarrow B} & 0_{3 \times 3} \\ R_{A \rightarrow B} \Omega_{A||B}|_A & R_{A \rightarrow B} \end{bmatrix} \begin{Bmatrix} \underline{X}|_A - \underline{X}_C|_A \\ \dot{\underline{X}}^A|_A - \dot{\underline{X}}_C^A|_A \end{Bmatrix} \quad (\text{B.10})$$

and its inverse can be easily derived, leading to:

$$\begin{Bmatrix} \underline{X}|_A \\ \dot{\underline{X}}^A|_A \end{Bmatrix} = \begin{bmatrix} R_{B \rightarrow A} & 0_{3 \times 3} \\ R_{B \rightarrow A} \Omega_{B||A}|_B & R_{B \rightarrow A} \end{bmatrix} \begin{Bmatrix} \underline{x}|_B \\ \dot{\underline{x}}^B|_B \end{Bmatrix} + \begin{Bmatrix} \underline{X}_C|_A \\ \dot{\underline{X}}_C^A|_A \end{Bmatrix} \quad (\text{B.11})$$

Comparing (B.4) and (B.10), we extract an interesting property of \dot{R} , namely:

$$\dot{R}_{A \rightarrow B} = R_{A \rightarrow B} \Omega_{A||B}|_A$$

which is in turn quite useful, as time derivation of the rotation matrix itself might be quite costly and symbolically dense. This requires though to know the angular velocity vector, whose calculation might not be easy.

B.3 Absolute reference systems.

B.3.1 Earth-Centered-Inertial reference system (ECI).

As previously stated, any Earth-centered reference system will in turn be non-inertial. That leads to the need of defining a common baseline, *i.e.* an epoch at which the reference system is known. The chosen epoch is denoted as J2000.0¹, which translates to January 1st, at 12:00:00.000 (midday) in Julian years [see 21, glossary]. Effectively, the ECI reference system, is geometrically defined as

¹J2000 denotes a reference frame, being analog to ECI. J2000.0 refers to the mentioned epoch.

follows [23]:

$$ECI \equiv \begin{cases} \text{Origin} & \equiv \text{Earth's COM} \\ \text{X-axis} & \equiv \text{Earth's COM} \longrightarrow \text{Mean vernal equinox at epoch J2000.0} \\ \text{Z-axis} & \equiv \text{Normal to the mean equatorial plane at epoch J2000.0,} \\ & \quad \text{pointing towards the Northern Hemisphere} \\ \text{Y-axis} & \equiv \text{Perpendicular to the X and Z axes forming a right-handed system} \end{cases}$$

The main reason behind using this system is that it considerably simplifies the dynamics equation of any spacecraft. It is then the most adequate frame on which dynamics can be solved. Furthermore, when considering relative motion, the reference axis are not a critical axis, as we are rather focused on the motion between spacecrafts. On the other hand, this frame is not able to describe the position relative to Earth's surface, thus being useless in communications or visibility analysis.

B.3.2 Earth-Centered, Earth-Fixed reference system (ECEF).

Due to the formerly mentioned concerns, another Earth-centered reference frame must be defined. In this case, that will be ECEF. Geometrically, it is defined as [23]

$$ECEF \equiv \begin{cases} \text{Origin} & \equiv \text{Earth's COM} \\ \text{X-axis} & \equiv \text{Earth's COM} \longrightarrow \text{Intersection of prime meridian and true equatorial plane} \\ \text{Z-axis} & \equiv \text{Earth's true angular velocity vector (rotation axis)} \\ \text{Y-axis} & \equiv \text{Perpendicular to the X and Z axes forming a right-handed system} \end{cases}$$

Once defined, it is turn to evaluate how ECI and ECEF frames differ.

B.3.2.1 Conversion from ECI to ECEF.

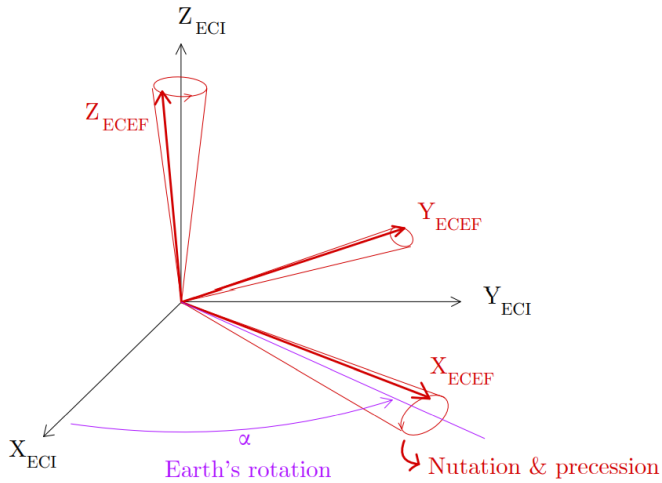


Figure B.3: ECI and ECEF reference frames.

Decomposition of the conversion.

There are four essential differences between ECI and ECEF frame, due to four motions that ECEF include due to it being fixed to Earth:

1. Precession of the equinoxes.
2. Nutations (small oscillations) of the equinoxes.
3. Earth's rotation around its axis.
4. Spin axis motion.

Each of this motions can be characterized by a rotation to an associated frame. That is, we can decompose the conversion between ECI and ECEF in four rotations, which will now be analyzed.

Involved intermediate frames & rotations.

ECI(J200) to Mean of Date.

The equinoxes rotate at a slow, but relevant rate. That means that the vernal equinox today differs considerably from the one at J2000.0. The Mean of Date (MOD) frame arises from this notion, being defined as [23]:

$$MOD \equiv \begin{cases} \text{X-axis} & \equiv \text{Earth's COM} \longrightarrow \text{Mean vernal equinox at current epoch} \\ \text{Z-axis} & \equiv \text{Perpendicular to the mean equatorial plane at current epoch} \\ \text{Y-axis} & \equiv \text{Perpendicular to the X and Z axes forming a right-handed system} \end{cases}$$

The rotation matrix from J200 to MOD results:

$$R_{ECI \rightarrow MOD} = \begin{bmatrix} C\zeta_A C\theta_A Cz_A - S\zeta_A S z_A & -S\zeta_A C\theta_A Cz_A - C\zeta_A S z_A & -S\theta_A Cz_A \\ C\zeta_A C\theta_A S z_A + S\zeta_A Cz_A & -S\zeta_A C\theta_A S z_A + C\zeta_A Cz_A & -S\theta_A S z_A \\ C\zeta_A S\theta_A & -S\zeta_A S\theta_A & C\theta_A \end{bmatrix} \quad (\text{B.12})$$

where the precession angles ζ_A , θ_A and z_A , which are functions of the epoch, are shown in [23], page 519. S and C are abbreviations of the sine and cosine functions.

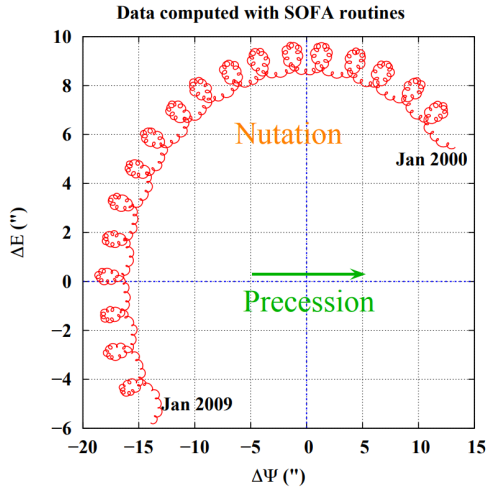


Figure B.4: Nutation and precession motion.

Mean of Date to True of Date

Besides the “long-term” precession motion, equinoxes suffer also short-period, small oscillations, which are denoted as nutations. For more clarity, see figure B.4. The True of Date (TOD) frame is thus defined as:

$$TOD \equiv \begin{cases} \text{X-axis} & \equiv \text{Earth's COM} \rightarrow \text{True vernal equinox at current epoch} \\ \text{Z-axis} & \equiv \text{Perpendicular to the true equatorial plane at current epoch} \\ \text{Y-axis} & \equiv \text{Perpendicular to the X and Z axes forming a right-handed system} \end{cases}$$

The rotation matrix now has the following shape:

$$R_{MOD \rightarrow TOD} = \begin{bmatrix} C\Delta\psi & -C\epsilon_m S\Delta\psi & -S\epsilon_m S\Delta\psi \\ C\epsilon_t S\Delta\psi & C\epsilon_m C\epsilon_t C\Delta\psi + S\epsilon_m S\epsilon_t & S\epsilon_m C\epsilon_t C\Delta\psi - C\epsilon_m S\epsilon_t \\ S\epsilon_t S\Delta\psi & C\epsilon_m S\epsilon_t C\Delta\psi - S\epsilon_m C\epsilon_t & S\epsilon_m S\epsilon_t C\Delta\psi + C\epsilon_m C\epsilon_t \end{bmatrix} \quad (\text{B.13})$$

where four angles appear. Firstly, the mean obliquity, which is the angle between the mean ecliptic and the mean equatorial plane ($\approx 23.5^\circ$). For an analytic expression, see [23], page 519. Moreover, two nutations arise: one in longitude and one in obliquity ($\Delta\psi$ and $\Delta\epsilon$, respectively). These angles are computed by a summation of a large number of sinusoidal functions, whose construction and coefficients are shown in [24]. Lastly, the true obliquity is simply the addition of its mean counterpart and the nutation ($\epsilon_t = \epsilon_m + \Delta\epsilon$).

True of Date to Pseudo-Body-Fixed

Perhaps the biggest and most intuitive difference between ECI and ECEF is Earth's rotation around its axis. The pseudo-body-fixed is simply a clockwise rotation (seen from north pole towards the Earth's COM) around said axis from the True of Date frame:

$$PBF \equiv \begin{cases} \text{X-axis} & \equiv \text{Earth's COM} \rightarrow \text{Intersection between prime meridian and true equatorial plane} \\ & \quad (\text{without accounting for the axis' displacement}). \\ \text{Z-axis} & \equiv \text{Perpendicular to the true equatorial plane at current epoch} \\ \text{Y-axis} & \equiv \text{Perpendicular to the X and Z axes forming a right-handed system} \end{cases}$$

The rotation matrix is now as simple as:

$$R_{TOD \rightarrow PBF} = \begin{bmatrix} C\alpha_G & S\alpha_G & 0 \\ -S\alpha_G & C\alpha_G & 0 \\ 0 & 0 & 1 \end{bmatrix} \quad (\text{B.14})$$

where α_G is referred to as the Greenwich Mean Sidereal Time (GMST). $\dot{\alpha}_G$ is then the rotation rate of the Earth. An analytical expression for this angle is provided in [23], page 520 (eq. H.4.3).

Pseudo-Body-Fixed to Body-Fixed (ECEF)

The last, and surely most subtle transformation, is the one that accounts for the displacement in Earth's axis of rotation. This displacement is parametrized with the polar angles x_p and y_p , which can again be found at [24]. As these angles are sufficiently small, the rotation matrix from PBF to ECEF is:

$$R_{PBF \rightarrow BF} = \begin{bmatrix} 1 & 0 & x_p \\ 0 & 1 & -y_p \\ -x_p & y_p & 1 \end{bmatrix} \quad (\text{B.15})$$

Full rotation matrix $R_{ECI \rightarrow ECEF}$.

By simply successively composing rotations, the full rotation matrix from ECI to ECEF is computed as:

$$R_{ECI \rightarrow ECEF} = R_{PBF \rightarrow ECEF} R_{TOD \rightarrow PBF} R_{MOD \rightarrow TOD} R_{ECI \rightarrow MOD}$$

B.3.3 Perifocal (PQW) reference frame.

B.3.3.1 Definition.

The perifocal reference frame is defined as:

$$PQW \equiv \left\{ \begin{array}{lcl} \text{Origin} & \equiv & \text{Central body's COM} \\ \text{X-axis} & \equiv & \text{Origin} \longrightarrow \text{Periapsis.} \\ \text{Z-axis} & \equiv & \text{Perpendicular to the osculating orbital plane (out-of-plane)} \\ \text{Y-axis} & \equiv & \text{Perpendicular to the X and Z axes forming a right-handed system} \end{array} \right.$$

This frame takes advantage of the motion being contained in the orbital plane (when using osculating elements, see **CITE MEAN2OSC**). That means that usually, the problem reduces to evaluating two components of the position and velocity. It also allows for a quite straightforward description of the motion in terms of the Keplerian OEs, assuming elliptical motion. In this case, and

using \underline{q} and $\dot{\underline{q}}$ to denote perifocal position and velocity, the perifocal state vector is expressed as:

$$\underline{q} = \begin{Bmatrix} r \cos \theta \\ r \sin \theta \\ 0 \end{Bmatrix} = \begin{Bmatrix} a(\cos E - e) \\ a \sin E \\ 0 \end{Bmatrix} \quad \dot{\underline{q}} = \frac{na}{\sqrt{1-e^2}} \begin{Bmatrix} -\sin \theta \\ e + \cos \theta \\ 0 \end{Bmatrix}$$

where E is the eccentric anomaly, r is the orbital radius, n is the mean orbital rate and the remaining parameters are the regular Keplerian OEs. r and n can be expressed as a function of them as:

$$r = \frac{a(1-e^2)}{1+e \cos \theta} = a(1-e \cos E); \quad n = \sqrt{\frac{\mu}{a^3}}$$

with $\mu = GM$ being the gravitational parameter of the central body.

B.3.3.2 State vector transformation.

Our target is to get an expression analogous to (B.10). As both frames are Earth-centered, $\underline{X}_C = 0$, so that only the rotation and angular velocity matrices are to be found.

Rotation matrix from & to ECI.

As done with the ECI to ECEF transformation, this one can also be decomposed in three rotations, each associated with one Keplerian angle.

The first rotation is associated to Ω , being done around the Z ECI axis. The resulting frame will be named I1 (intermediate 1), and the rotation matrix from ECI is:

$$R_{ECI \rightarrow I1}(\Omega) = \begin{bmatrix} \cos \Omega & \sin \Omega & 0 \\ -\sin \Omega & \cos \Omega & 0 \\ 0 & 0 & 1 \end{bmatrix}$$

Afterwards, a rotation around X axis of I1 (nodal line) of value i is performed, leading to frame I2. The rotation matrix is simply:

$$R_{I1 \rightarrow I2}(\Omega) = \begin{bmatrix} 1 & 0 & 0 \\ 0 & \cos i & \sin i \\ 0 & -\sin i & \cos i \end{bmatrix}$$

Finally, a rotation around Z axis of I2 (out-of-plane direction) of value ω is done, yielding the desired perifocal frame (which we will denote as PQW):

$$R_{I2 \rightarrow PQW}(\Omega) = \begin{bmatrix} \cos \omega & \sin \omega & 0 \\ -\sin \omega & \cos \omega & 0 \\ 0 & 0 & 1 \end{bmatrix}$$

By composition, the matrix $R_{ECI \rightarrow PQW}$ can easily be calculated:

$$R_{ECI \rightarrow PQW} = R_{I2 \rightarrow PQW} R_{I1 \rightarrow I2} R_{ECI \rightarrow I1} = \begin{bmatrix} C\Omega C\omega - S\Omega C i S\omega & S\Omega C\omega + C\Omega C i S\omega & S i S\omega \\ -C\Omega S\omega - S\Omega C i c\omega & C\Omega C i C\omega + S\Omega S\omega & S i C\omega \\ S\Omega S i & -C\Omega S i & C i \end{bmatrix}$$

Angular velocity.

In order to fully transform the system, it is necessary to calculate the relative angular velocity between both frames. Again, that can be done by composing the angular movements:

$$\underline{\omega}_{PQW||ECI} = \dot{\Omega} \hat{k}_{I1} + i \hat{i}_{I2} + \dot{\omega} \hat{k}_{PQW}$$

Expressing everything in PQW frame:

$$\underline{\omega}_{PQW||ECI}|_{PQW} = \begin{Bmatrix} \omega_x \\ \omega_y \\ \omega_z \end{Bmatrix} = \dot{\Omega} R_{ECI \rightarrow PQW} \begin{Bmatrix} 0 \\ 0 \\ 1 \end{Bmatrix} + i R_{I2 \rightarrow PQW} R_{I1 \rightarrow I2} \begin{Bmatrix} 1 \\ 0 \\ 0 \end{Bmatrix} + \dot{\omega} R_{I2 \rightarrow PQW} \begin{Bmatrix} 0 \\ 0 \\ 1 \end{Bmatrix}$$

In virtue of the axial dual form principle, there exists one matrix that, when applied to a certain vector, yields the same result as doing the cross product between $\underline{\omega}$ and that vector. This matrix has the following shape:

$$\Omega_{PQW||ECI}|_{PQW} = \begin{bmatrix} 0 & -\omega_z & \omega_y \\ \omega_z & 0 & -\omega_x \\ -\omega_y & \omega_x & 0 \end{bmatrix}$$

Transformation matrices $\mathbf{T}_{PQW \rightarrow ECI}$, $\mathbf{T}_{ECI \rightarrow PQW}$.

The transformation matrices can easily be built as in (B.10):

$$\mathbf{T}_{PQW \rightarrow ECI} = \begin{bmatrix} R_{PQW \rightarrow ECI} & 0_{3 \times 3} \\ R_{PQW \rightarrow ECI} \Omega_{PQW \parallel ECI} |_{PQW} & R_{PQW \rightarrow ECI} \end{bmatrix}$$

whose inverse counterpart can be obtained in terms of the same components, as:

$$\mathbf{T}_{ECI \rightarrow PQW} = \begin{bmatrix} R_{PQW \rightarrow ECI}^T & 0_{3 \times 3} \\ -\Omega_{PQW \parallel ECI} |_{PQW} R_{PQW \rightarrow ECI}^T & R_{PQW \rightarrow ECI}^T \end{bmatrix}$$

It is important to note that, as the rotation angles are Keplerian OEs, the unperturbed assumption leads to a null angular velocity (as the orbital plane remains unchanged along time). That greatly simplifies the transformation, turning into a trivial rotation of the position and velocity vectors.

B.4 Relative reference systems.

It is time now to address relative reference frames. For each of them, a description is provided, followed by a conversion to and from the ECI reference frame.

B.4.1 RTN reference frame.

B.4.1.1 Definition.

The Radial-Tangential-Normal (RTN) reference frame is defined as [18]:

$$RTN \equiv \left\{ \begin{array}{lcl} \text{Origin} & \equiv & \text{Chief SC COM} \\ \text{X-axis}(\underline{e}_R) & \equiv & \text{Radial direction (positive outwards)} \\ \text{Z-axis}(\underline{e}_N) & \equiv & \text{Normal to the orbit plane (positive with orbit momentum)} \\ \text{Y-axis}(\underline{e}_T) & \equiv & \text{Perpendicular to the X and Z axes forming a right-handed system} \\ & & (\approx \text{tangent to the trajectory}) \end{array} \right.$$

A graphical representation of this frame is shown in figure B.5.

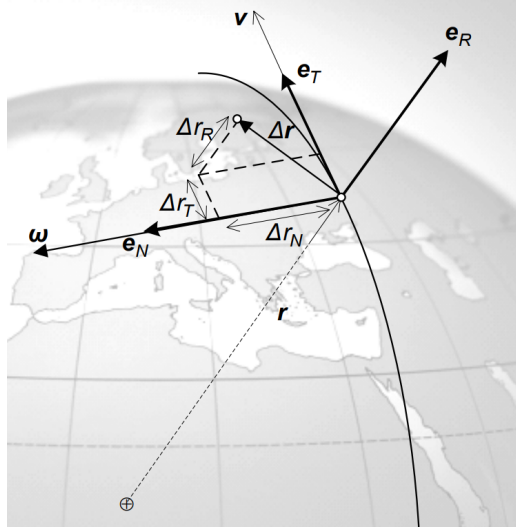


Figure B.5: RTN frame [18].

B.4.1.2 State vector transformation.

As before, we need to build two matrices: The rotation matrix and the angular velocity matrix.

Rotation matrix from ECI.

If we pay close attention to both PQW and RTN frames, it arises that the rotation matrix is virtually the same, only changing the value of the last rotation from ω to $u = \theta + \omega$. That is:

$$R_{I2 \rightarrow RTN} = R_{I2 \rightarrow RTN}|_{\omega \rightarrow u} \Rightarrow R_{ECI \rightarrow RTN} = R_{ECI \rightarrow PQW}|_{\omega \rightarrow u}$$

which leads to the following expression:

$$R_{ECI \rightarrow RTN} = \begin{bmatrix} C\Omega Cu - S\Omega Ci Su & S\Omega Cu + C\Omega Ci Su & Si Su \\ -C\Omega Su - S\Omega Ci Cu & -S\Omega Su + C\Omega Ci Cu & Si Cu \\ S\Omega Si & -C\Omega Si & Ci \end{bmatrix}$$

Angular velocity.

Assuming unperturbed motion, the only time-varying angle is u through the true anomaly. Its rate is in fact:

$$\dot{\theta} = \dot{M} \frac{\rho^2}{\eta^3} = \frac{n\rho^2}{\eta^3}$$

where $\rho = 1 + e \cos \theta$ and $\eta = \sqrt{1 - e^2}$. With this in mind, the angular velocity matrix takes the following form:

$$\Omega_{RTN||ECI}|_{RTN} = \begin{bmatrix} 0 & -\dot{\theta} & 0 \\ \dot{\theta} & 0 & 0 \\ 0 & 0 & 0 \end{bmatrix}$$

Transformation matrices $T_{RTN \rightarrow ECI}$, $T_{ECI \rightarrow RTN}$.

The transformation matrices are composed as follows:

$$T_{ECI \rightarrow RTN} = \begin{bmatrix} R_{ECI \rightarrow RTN} & 0_{3x3} \\ -\Omega_{RTN||ECI}|_{RTN} R_{ECI \rightarrow RTN} & R_{ECI \rightarrow RTN} \end{bmatrix}$$

whose inverse counterpart can be obtained in terms of the same components, as:

$$T_{RTN \rightarrow ECI} = \begin{bmatrix} R_{ECI \rightarrow RTN}^T & 0_{3x3} \\ R_{ECI \rightarrow RTN}^T \Omega_{RTN||ECI}|_{RTN} & R_{ECI \rightarrow RTN}^T \end{bmatrix}$$

B.4.2 LVLH reference frame.

B.4.2.1 Definition.

The Local Vertical-Local Horizontal frame (LVLH) may be understood as a different interpretation of the RTN frame. It basically differs from it in the naming and direction of the axis, namely:

$$LVLH \equiv \left\{ \begin{array}{lcl} \text{Origin} & \equiv & \text{Chief SC COM} \\ \text{Z-axis}(-\underline{e}_R) & \equiv & \text{Radial direction (positive inwards)} \\ \text{Y-axis}(-\underline{e}_N) & \equiv & \text{Normal to the orbit plane (cross-track)} \\ & & \text{(negative with orbit momentum)} \\ \text{X-axis}(\underline{e}_T) & \equiv & \text{Perpendicular to the Y and Z axes (along-track)} \\ & & \text{forming a right-handed system (\approx tangent to the trajectory)} \end{array} \right.$$

B.4.2.2 State vector transformation.

There are two main ways to obtain the ECI to LVLH frame transformation:

A) Using reference orbit's Keplerian OEs.

This method is the one we have used for the PQW and the RTN frame. It is as easy as performing yet another rotation from the RTN frame, being consistent with the angular velocity.

Rotation matrix from ECI.

The additional rotation from RTN to LVLH is:

$$R_{RTN \rightarrow LVLH} = \begin{bmatrix} 0 & 1 & 0 \\ 0 & 0 & -1 \\ -1 & 0 & 0 \end{bmatrix}$$

leading to the full rotation matrix:

$$R_{ECI \rightarrow LVLH} = R_{ECI \rightarrow RTN} R_{RTN \rightarrow LVLH} = \begin{bmatrix} -C\Omega Su - S\Omega Ci Cu & C\Omega Ci Cu - S\Omega Su & Cu Si \\ -S\Omega Si & C\Omega Si & -Ci \\ -C\Omega Cu + S\Omega Ci Su & -C\Omega Ci Su - S\Omega Cu & -Su Si \end{bmatrix}$$

Angular velocity.

Although one could rotate either the vector or the matrix itself, it is actually easier to graphically derive the angular velocity (assuming of course unperturbed motion). Doing this, we can easily see that the only angular velocity component is the one in Y-axis, of value $-\dot{\theta}$. The angular velocity matrix then becomes:

$$\Omega_{LVLH||ECI}|_{LVLH} = \begin{bmatrix} 0 & 0 & -\dot{\theta} \\ 0 & 0 & 0 \\ \dot{\theta} & 0 & 0 \end{bmatrix}$$

B) Using reference ECI state vector.

This approach is based on [22], and was introduced in B.2.1. For this transformation to be performed, we need to calculate the rotation matrix and its derivative. With this approach, that is analogous to get the unitary vectors expressed in ECI frame. As our inputs are actually the ECI coordinates and velocity of the chief spacecraft, this is almost already done. The unitary vectors of the rotating frame

in this case are:

$$\left\{ \begin{array}{l} \hat{\underline{e}}_z = -\hat{\underline{r}} \\ \hat{\underline{e}}_y = -\hat{\underline{h}} \\ \hat{\underline{e}}_x = \hat{\underline{e}}_y \times \hat{\underline{e}}_z \end{array} \right. \quad (\text{B.16})$$

where $\hat{\underline{h}} = \frac{\underline{r} \times \underline{v}}{|\underline{r} \times \underline{v}|}$. \underline{r} and \underline{v} are respectively the position and velocity of the chief spacecraft.

Rotation matrix from ECI.

The rotation matrix $R_{ECI \rightarrow LVLH}$ is then:

$$R_{ECI \rightarrow LVLH} = \begin{bmatrix} \hat{\underline{e}}_x^T \\ \hat{\underline{e}}_y^T \\ \hat{\underline{e}}_z^T \end{bmatrix}$$

that is, each unitary vector is transposed into one row of the matrix.

Rotation matrix derivative.

By using equation (B.3) we can easily get the vectors' time derivatives:

$$\left\{ \begin{array}{lcl} \frac{d}{dt}(\hat{\underline{e}}_z) & = & \frac{d}{dt}(-\hat{\underline{r}}) \\ \frac{d}{dt}(\hat{\underline{e}}_y) & = & \frac{d}{dt}(-\hat{\underline{h}}) \\ \frac{d}{dt}(\hat{\underline{e}}_x) & = & \frac{d}{dt}(\hat{\underline{e}}_y \times \hat{\underline{e}}_z) \end{array} \right. \begin{array}{lcl} & = & -\frac{1}{r} [\underline{v} - (\hat{\underline{r}} \cdot \underline{v}) \hat{\underline{r}}] \\ & = & -\frac{1}{h} [\dot{\underline{h}} - (\hat{\underline{h}} \cdot \dot{\underline{h}}) \hat{\underline{h}}] \\ & = & \frac{d}{dt}(\hat{\underline{e}}_y) \times \hat{\underline{e}}_z + \hat{\underline{e}}_y \times \frac{d}{dt}(\hat{\underline{e}}_z) \end{array}$$

where all entities are known except for $\dot{\underline{h}}$, which is in turn:

$$\dot{\underline{h}} = \frac{d}{dt}(\underline{r} \times \underline{v}) = \underline{r} \times \underline{a}$$

Hence, the acceleration of the chief spacecraft needs to be provided when it is not radial. As that is the case with the unperturbed two-body problem, the rotation matrix is significantly simplified:

$$\left\{ \begin{array}{lcl} \frac{d}{dt}(\hat{\underline{e}}_z) & = & -\frac{1}{r} [\underline{v} - (\hat{\underline{r}} \cdot \underline{v}) \hat{\underline{r}}] \\ \frac{d}{dt}(\hat{\underline{e}}_y) & = & 0 \\ \frac{d}{dt}(\hat{\underline{e}}_x) & = & -\hat{\underline{h}} \times \frac{d}{dt}(\hat{\underline{e}}_z) \end{array} \right.$$

The construction of $\dot{R}_{ECI \rightarrow LVLH}$ is identical to its primitive. The transformation matrices can now be built, following equations B.4 and B.5.

B.4.3 TAN reference frame.

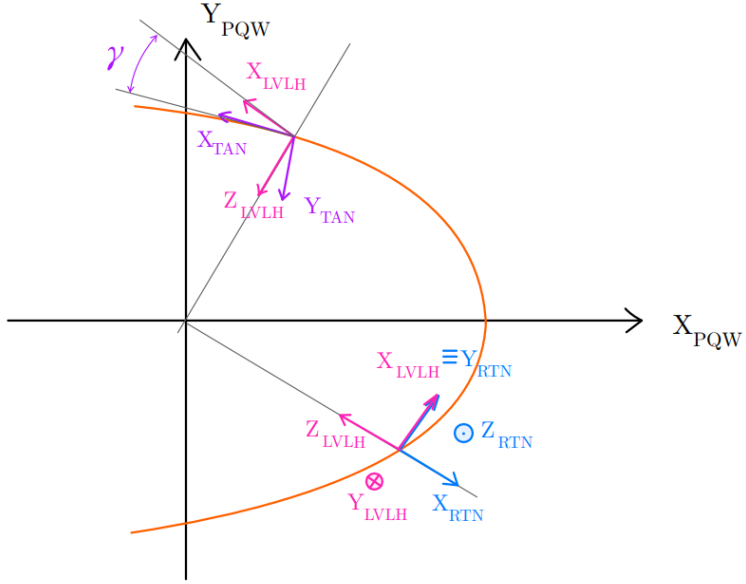


Figure B.6: Relative reference frames.

B.4.3.1 Definition.

The Tangent reference frame (TAN) is quite similar to the LVLH frame, but instead of featuring an axis pointing towards *nadir* (Earth), this frame includes an axis pointing always in the velocity direction. This involves a simple rotation from the LVLH frame, of an angle γ called flight path angle (see figure B.6). It is then unsurprisingly defined as the angle between the horizon (local horizontal) and the velocity vector. Let us then analyze the transformation from the LVLH frame.

B.4.3.2 State vector transformation.

Rotation matrix from LVLH.

In this case, it is a simple clockwise rotation around LVLH Y-axis, that is:

$$R_{LVLH \rightarrow TAN} = \begin{bmatrix} \cos \gamma & 0 & -\sin \gamma \\ 0 & 1 & 0 \\ \sin \gamma & 0 & \cos \gamma \end{bmatrix}$$

Angular velocity.

As it has been explained before, let us just write the angular velocity matrix as:

$$\Omega_{LVLH \rightarrow TAN}|_{LVLH} = \begin{bmatrix} 0 & 0 & -\dot{\gamma} \\ 0 & 0 & 0 \\ \dot{\gamma} & 0 & 0 \end{bmatrix}$$

There is something remaining: γ and its derivative must be calculated. Starting with the angle itself, its sine and cosine satisfy:

$$\begin{cases} \sin \gamma = \frac{e \sin \theta}{\Theta} \\ \cos \gamma = \frac{\rho}{\Theta} \end{cases}$$

where $\Theta = \sqrt{2\rho - \eta^2}$. γ is simply calculated as:

$$\gamma = \text{atan2}(\sin \gamma, \cos \gamma)$$

On the other hand, $\dot{\gamma}$ can be calculated as:

$$\dot{\gamma} = n \frac{\rho^2 (\rho - \eta^2)}{\eta^3 \Theta^2}$$

Therefore, the transformation is complete.

B.5 Conversions from OEs to cartesian coordinates.

B.5.1 Keplerian OEs to ECI and vice versa.

B.5.1.1 KOE to ECI transformation.

Let us start with the simpler, unambiguous transformation. By considering the perifocal coordinates (q, \dot{q}) (see B.3.3), we can easily derive an explicit relation from Keplerian OEs to the ECI state vector:

$$\begin{cases} x = (\cos \Omega \cos u - \sin \Omega \cos i \sin u) & r \\ y = (\sin \Omega \cos u + \cos \Omega \cos i \sin u) & r \\ z = (\sin i \sin u) & r \\ \dot{x} = (\cos \Omega \cos u - \sin \Omega \cos i \sin u) v_R - (\cos \Omega \sin u + \sin \Omega \cos i \cos u) v_T & v_T \\ \dot{y} = (\sin \Omega \cos u + \cos \Omega \cos i \sin u) v_R - (\sin \Omega \sin u - \cos \Omega \cos i \cos u) v_T & v_T \\ \dot{z} = (\sin i \sin u) v_R + (\cos u \sin i) & v_T \end{cases}$$

where v_R and v_T are the radial and tangential velocities, namely:

$$\begin{cases} v_R = \dot{r} = \frac{h}{p} e \sin \theta \\ v_T = r\dot{\theta} = \frac{h}{p} \rho \end{cases}$$

B.5.1.2 ECI to KOE transformation.

This transformation is considerably more complex. For that reason, the relations will not be entirely justified. These are the following:

- Semimajor axis: Directly from energy equation:

$$a = \frac{r}{2 - \frac{rv^2}{\mu}}$$

- Eccentricity: Prior relations arise from (a) the dot product of velocity and position and (b) the polar equation of the ellipse:

$$\begin{cases} e \sin \theta = \frac{h}{\mu r} \mathbf{r} \cdot \mathbf{v} \\ e \cos \theta = \frac{p}{r} - 1 \end{cases} \Rightarrow e = \sqrt{(e \sin \theta)^2 + (e \cos \theta)^2}$$

where p is the orbit parameter.

- Inclination From the orientation of the angular momentum vector:

$$i = \text{atan2}(h_{xy}, h_z)$$

$$\text{where } h_{xy} = \sqrt{h_x^2 + h_y^2}$$

The remaining elements (Ω , ω and M) depend on the type of the orbit. As we know, if the orbit is equatorial ($i = 0$), Ω and ω are not defined by themselves. Furthermore, if the orbit is circular, not even ω is defined, and therefore we have to make some adjustments. In the first case, we will assume $\varpi = \omega + \Omega$ as our fifth element, and the fourth will be null. In the second case, we will merge all values into the mean anomaly, assuming both ω and Ω to be null.

Case A) Non-singular eccentricity or inclination.

$$\begin{cases} \Omega = \text{atan2}(h_x, -h_y) \\ u = \text{atan2}(h \cdot z, y \cdot h_x - x \cdot h_y) \\ \theta = \text{atan2}(e \sin \theta, e \cos \theta) \\ \omega = u - \theta \end{cases}$$

Case B) Null inclination, non-singular eccentricity.

$$\begin{cases} \Omega = 0 \\ u = \text{atan2}(y, x) \cdot \text{sign}(h_z) \\ \theta = \text{atan2}(e \sin \theta, e \cos \theta) \\ \omega = u - \theta \end{cases}$$

Case C) Null eccentricity, non-singular inclination.

Auxiliary definitions:

$$\begin{cases} \underline{N} = \underline{\hat{e}_z} \times \underline{h} \\ N_{xy} = \sqrt{N_x^2 + N_y^2} \\ S = \text{sign}((\underline{e} \times \underline{r}) \cdot \underline{h}) \end{cases}$$

Element computation:

$$\begin{cases} \Omega = \text{atan2}(h_x, -h_y) \\ \omega = 0 \\ \theta = S \cdot \arccos\left(\frac{\underline{r}}{r}, \frac{\underline{N}}{N_{xy}}\right) \end{cases}$$

Case D) Null eccentricity and inclination.

$$\begin{cases} \Omega = 0 \\ \omega = 0 \\ \theta = \text{atan2}(y, x) \cdot \text{sign}(h_z) \end{cases}$$

B.5.2 Relative Keplerian OEs to RTN.

Although one can technically go from RKOEs to RTN coordinates in several steps already described, there is a direct mapping between them, developed by H. Schaub [19]. Without further

ado, the position mapping is expressed as follows:

$$\begin{cases} x \approx \frac{r}{a} \delta a + \frac{ae \sin \theta}{\eta} \delta M - a \cos \theta \delta e \end{cases} \quad (\text{B.17a})$$

$$\begin{cases} y \approx \frac{r \rho^2}{\eta^3} \delta M + r \delta \omega + \frac{r \sin \theta}{\eta^2} (\rho + 1) \delta e + r \cos i \delta \Omega \end{cases} \quad (\text{B.17b})$$

$$\begin{cases} z \approx r (\sin u \delta i - \cos u \sin i \delta \Omega) \end{cases} \quad (\text{B.17c})$$

Nonetheless, the mapping for the velocity is expressed in terms of relative quasi-non-singular OEs [25]. For the conversion from RKOEs to these, please see [A](#):

$$\begin{cases} \dot{x} \approx -\frac{V_r}{2a} \delta a + \left(\frac{1}{r} - \frac{1}{p} \right) h \delta u \end{cases} \quad (\text{B.18a})$$

$$\begin{cases} \dot{x} \approx + (V_r a q_1 + h \sin u) \frac{\delta q_1}{p} + (V_r a q_2 - h \cos u) \frac{\delta q_2}{p} \end{cases} \quad (\text{B.18b})$$

$$\begin{cases} \dot{y} \approx -\frac{3V_t}{2a} \delta a - V_r \delta u + (3V_t a q_1 + 2h \cos u) \frac{\delta q_1}{p} \end{cases} \quad (\text{B.18c})$$

$$\begin{cases} \dot{y} \approx + (3V_t a q_2 + 2h \sin u) \frac{\delta q_2}{p} + V_r \cos i \delta \Omega \end{cases} \quad (\text{B.18d})$$

$$\begin{cases} \dot{z} \approx (V_t \cos u + V_r \sin u) \delta i \end{cases} \quad (\text{B.18e})$$

$$\begin{cases} \dot{z} \approx + (V_t \sin u - V_r \cos u) \sin i \delta \Omega \end{cases} \quad (\text{B.18f})$$

The mapping represented by equations (B.17) and (B.18) is a linear approximation, in which it is assumed that the relative distance between spacecrafts is much smaller than the chief's orbital radius. For more in-depth content about this transformation, please see [19, 25].

Bibliography

General

Books

- [1] K. T. Alfriend and Srinivas. SPACECRAFT FORMATION FLYING. 1st ed. Oxford, United Kingdom: Elsevier, 2010 (cit. on pp. [3](#), [4](#)).
- [2] W. E. Wiesel. MODERN ASTRODYNAMICS. 2nd ed. Beavercreek, Ohio: Aphelion Press, 2010 (cit. on pp. [4](#), [56](#), [57](#)).
- [3] W. Fehse. AUTOMATED RENDEZVOUS AND DOCKING OF SPACECRAFT. Cambridge Aerospace Series. Cambridge: Cambridge University Press, 2003. doi: [10.1017/CBO9780511543388](https://doi.org/10.1017/CBO9780511543388) (cit. on p. [9](#)).
- [4] O. Montenbruck and E. Gill. SATELLITE ORBITS: MODELS, METHODS AND APPLICATIONS. 1st ed. Wessling, Germany: Springer, 2001 (cit. on p. [11](#)).
- [10] R. H. Battin. AN INTRODUCTION TO THE MATHEMATICS AND METHODS OF ASTRODYNAMICS, REVISED EDITION. 1st ed. Reston, Virginia: American Institute of Aeronautics and Astronautics, 1999 (cit. on p. [25](#)).
- [21] P. K. S. Dennis D. McCarthy. TIME: FROM EARTH ROTATION TO ATOMIC PHYSICS. Wiley-VCH, 2009. ISBN: 3527407804; 9783527407804 (cit. on pp. [68](#), [72](#)).
- [23] B. D. Tapley, B. E. Schutz, and G. H. Born. STATISTICAL ORBIT DETERMINATION. 1st ed. Amsterdam, Netherlands: Elsevier, 2004 (cit. on pp. [73–77](#)).
- [26] D. Brouwer and G. M-Clemence. METHODS OF CELESTIAL MECHANICS. Brackley Square House, London: Academic Press, 1961.
- [27] H. Schaub and J. L. Junkins. ANALYTICAL MECHANICS OF SPACE SYSTEMS. Reston, VA: AIAA Education Series, Oct. 2003. doi: [10.2514/4.861550](https://doi.org/10.2514/4.861550).

Articles

- [8] O. Montenbruck, M. Kirschner, and S. D'Amico. E/I-VECTOR SEPARATION FOR SAFE SWITCHING OF THE GRACE FORMATION. In: *Aerospace Science and Technology* 10 (2006), pp. 628–635. doi: [10.1016/j.ast.2006.04.001](https://doi.org/10.1016/j.ast.2006.04.001) (cit. on pp. [24](#), [29](#)).

- [12] J. Sullivan, S. Grimberg, and S. D'Amico. COMPREHENSIVE SURVEY AND ASSESSMENT OF SPACECRAFT RELATIVE MOTION DYNAMICS MODELS. In: *Journal of Guidance, Control & Dynamics* 40.8 (2017), pp. 1837–1859. DOI: [10.2514/1.G002309](https://doi.org/10.2514/1.G002309) (cit. on p. 33).
- [19] H. Schaub. RELATIVE ORBIT GEOMETRY THROUGH CLASSICAL ORBIT ELEMENT DIFFERENCES. In: *Journal of Guidance, Control & Dynamics* 27.5 (2004), pp. 839–848. DOI: [10.2514/1.12595](https://doi.org/10.2514/1.12595) (cit. on pp. 59, 63, 64, 88, 89).
- [25] H. Schaub and K. T. Alfriend. HYBRID CARTESIAN AND ORBIT ELEMENT FEEDBACK LAW FOR FORMATION FLYING SPACECRAFT. In: *Journal of Guidance, Control & Dynamics* 25.2 (2002), pp. 387–393. DOI: [10.2514/2.4893](https://doi.org/10.2514/2.4893) (cit. on p. 89).
- [31] N. Capitaine. THE CELESTIAL POLE COORDINATES. In: *Celestial Mechanics and Dynamical Astronomy* 48 (1990), pp. 127–143.

Eccentric Dynamics

Articles

- [7] M. Eckstein, C. Rajasingh, and P. Blumer. COLOCATION STRATEGY AND COLLISION AVOIDANCE FOR THE GEOSTATIONARY SATELLITES AT 19 DEGREES WEST. In: *CNES International Symposium on Space Dynamics*. Vol. 25. Oberpfaffenhofen, Germany: DLR GSOC, Nov. 1989, pp. 60–66 (cit. on pp. 23, 24, 57, 58).
- [9] S. D'Amico and O. Montenbruck. PROXIMITY OPERATIONS OF FORMATION-FLYING SPACECRAFT USING AN ECCENTRICITY/INCLINATION VECTOR SEPARATION. In: *Journal of Guidance, Control & Dynamics* 29.3 (2006), pp. 554–563. DOI: [10.2514/1.15114](https://doi.org/10.2514/1.15114) (cit. on p. 24).
- [13] J. Tschauner and P. Hempel. OPTIMALE BESCHLEUNIGUNGSPROGRAMME FÄR DAS RENDEZVOUS-MANÖVER. In: *Astronautica Acta* 10 (1964), pp. 296–307 (cit. on p. 33).
- [14] T. Carter. STATE TRANSITION MATRICES FOR TERMINAL RENDEZVOUS STUDIES: BRIEF SURVEY AND NEW EXAMPLE. In: *Journal of Guidance Control and Dynamics* 21 (Jan. 1998), pp. 148–155. DOI: [10.2514/2.4211](https://doi.org/10.2514/2.4211) (cit. on p. 33).
- [15] K. Yamanaka and F. Ankersen. NEW STATE TRANSITION MATRIX FOR RELATIVE MOTION ON AN ARBITRARY ELLIPTICAL ORBIT. In: *Journal of Guidance, Control & Dynamics* 25.1 (2002), pp. 60–66. DOI: [10.2514/2.4875](https://doi.org/10.2514/2.4875) (cit. on pp. 33, 36, 42).

- [16] T. Vincent Peters and R. Noomen. LINEAR COTANGENTIAL TRANSFERS AND SAFE ORBITS FOR ELLIPTIC ORBIT RENDEZVOUS. In: *Journal of Guidance, Control & Dynamics* 44.4 (2021), pp. 732–748. DOI: [10.2514/1.G005152](https://doi.org/10.2514/1.G005152) (cit. on pp. 34, 47–49, 51, 65, 66).
- [32] R. Broucke. ON THE MATRIZANT OF THE TWO-BODY PROBLEM. In: *Astronomy and Astrophysics* 6 (June 1970), p. 173.

Perturbations

Books

- [28] A. H. Nayfeh. PERTURBATION METHODS. Weinheim, Germany: Wiley-VCH, 2004.
- [29] W. M. Kaula. THEORY OF SATELLITE GEODESY. Mineola, New York: Dover Publications, 2013.
- [30] F. Tisserand. TRAITÉ DE MÉCANIQUE CÉLESTE. Vol. 1. Paris, 1889.

Articles

- [17] D.-W. Gim and K. T. Alfriend. SATELLITE RELATIVE MOTION USING DIFFERENTIAL EQUINOCTIAL ELEMENTS. In: *Celestial Mechanics and Dynamical Astronomy* 92.4 (2005), pp. 295–336. DOI: [10.1007/s10569-004-1799-0](https://doi.org/10.1007/s10569-004-1799-0) (cit. on p. 59).
- [18] S. D'Amico. RELATIVE ORBITAL ELEMENTS AS INTEGRATION CONSTANTS OF HILL'S EQUATIONS. TN 05-08. Oberpfaffenhofen, Germany: Deutsches Zentrum für Luft- und Raumfahrt (DLR), 2005 (cit. on pp. 59, 63, 80, 81).
- [20] G. Gaias, C. Colombo, and M. Lara. ACCURATE OSCULATING/MEAN ORBITAL ELEMENTS CONVERSIONS FOR SPACEBORNE FORMATION FLYING. In: (Feb. 2018). https://www.researchgate.net/publication/340378956_Accurate_OsculatingMean_Orbital_Elements_Conversions_for_Spaceborne_Formation_Flying (cit. on p. 60).
- [33] D.-W. Gim and K. Alfriend. STATE TRANSITION MATRIX OF RELATIVE MOTION FOR THE PERTURBED NONCIRCULAR REFERENCE ORBIT. In: *Journal of Guidance Control and Dynamics* 26 (Nov. 2003), pp. 956–971. DOI: [10.2514/2.6924](https://doi.org/10.2514/2.6924).
- [34] G. Gaias, J.-S. Ardaens, and C. Colombo. PRECISE LINE-OF-SIGHT MODELLING FOR ANGLES-ONLY RELATIVE NAVIGATION. In: *Advances in Space Research* 67.11 (2021). Satellite Constellations and Formation Flying, pp. 3515–3526. DOI: [10.1016/j.asr.2020.05.048](https://doi.org/10.1016/j.asr.2020.05.048).
- [35] G. Gaias, C. Colombo, and M. Lara. ANALYTICAL FRAMEWORK FOR PRECISE RELATIVE MOTION IN LOW EARTH ORBITS. In: *Journal of Guidance, Control, and Dynamics* 43.5 (2020), pp. 915–927. DOI: [10.2514/1.G004716](https://doi.org/10.2514/1.G004716).

- [36] D. Brouwer. SOLUTION OF THE PROBLEM OF ARTIFICIAL SATELLITE THEORY WITHOUT DRAG. In: *Astronomical Journal* 64.5 (Nov. 1959), p. 378. doi: [10.1086/107958](https://doi.org/10.1086/107958).
- [37] R. H. Lyddane. SMALL ECCENTRICITIES OR INCLINATIONS IN THE BROUWER THEORY OF THE ARTIFICIAL SATELLITE. In: *Astronomical Journal* 68 (Oct. 1963), p. 555. doi: [10.1086/109179](https://doi.org/10.1086/109179).

Matlab Exchange libraries

- [40] F. G. Nievinski. SUBTIGHTPLOT. <https://www.mathworks.com/matlabcentral/fileexchange/39664-subtightplot>. 2013.
- [41] J. C. Lansey. LINSPECER. <https://www.mathworks.com/matlabcentral/fileexchange/42673-beautiful-and-distinguishable-line-colors-colormap>. 2015.
- [42] Jan. WINDOWAPI. <https://www.mathworks.com/matlabcentral/fileexchange/31437-windowapi>. 2013.
- [43] T. Davis. ARROW3. <https://www.mathworks.com/matlabcentral/fileexchange/14056-arrow3>. 2022.

Websites

- [5] Mathworks. CONVERT COMPLEX DIAGONAL FORM INTO REAL DIAGONAL FORM. 2022. URL: <https://www.mathworks.com/help/matlab/ref/cdf2rdf.html>.